

Vehicle Model-Based Filtering for Spacecraft Attitude Determination

by

Christopher W. Dever

B.S., Mechanical Engineering (1996)
University of Kentucky

Submitted to the Department of Mechanical Engineering
in partial fulfillment of the requirements for the degree of

MASTER OF SCIENCE

at the

MASSACHUSETTS INSTITUTE OF TECHNOLOGY

September 1998

©Christopher W. Dever 1998. All rights reserved.

The author hereby grants to MIT permission to reproduce and to distribute publicly paper and electronic copies of this thesis document in whole or in part.

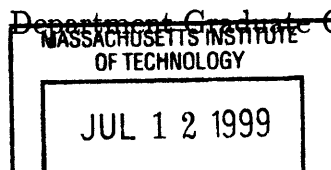
Author.....
Department of Mechanical Engineering
8 August, 1998

Certified by.....
Dr. Rami S. Mangoubi
Senior Member of the Technical Staff, C.S. Draper Laboratory
Thesis Supervisor

Certified by.....
Mr. Roger M. Hain
Senior Member of the Technical Staff, C.S. Draper Laboratory
Thesis Supervisor

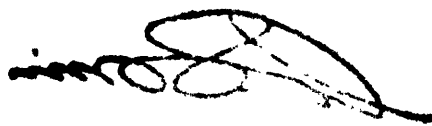
Certified by.....
Professor Zaichun Feng
Assistant Professor of Mechanical Engineering
Thesis Supervisor

Accepted by.....
Professor Ain A. Sonin
Chairman, Department Graduate Committee



ENG

1000 1000 1000

A handwritten signature or scribble consisting of several overlapping loops and a horizontal line at the end, rendered in black ink.

Vehicle Model-Based Filtering for Spacecraft Attitude Determination

by

Christopher W. Dever

Submitted to the Department of Mechanical Engineering
on 8 August, 1998, in partial fulfillment of the
requirements for the degree of
MASTER OF SCIENCE

Abstract

This thesis investigates the use of vehicle model-based filtering for spacecraft attitude determination. Whereas traditional navigation filters typically rely only on the kinematic relations between body rate and attitude in their filter designs, the state estimator presented here expands the plant model to include rigid body effects and disturbance torques. When rate sensing gyroscope measurement error components are large, as is anticipated in the new generation of micromechanical inertial sensors, the model-based approach provides superior performance to the standard kinematic designs. The estimation performance gains, which include enhanced attitude tracking of several tenths of a degree and closed-loop control stabilization, are most apparent when external attitude data becomes sparse. Even if the gyroscope measurement quality were to improve, for some satellite missions the possibility of an external measurement outage still necessitates vehicle dynamic modeling for greater gyro bias observability. The thesis also gives insight into robustness measures to compensate for model uncertainty, disturbance torque estimation, and GPS multipath error mitigation.

Thesis Supervisor: Dr. Rami S. Mangoubi

Title: Senior Member of the Technical Staff, C.S. Draper Laboratory

Thesis Supervisor: Mr. Roger M. Hain

Title: Senior Member of the Technical Staff, C.S. Draper Laboratory

Thesis Supervisor: Professor Zaichun Feng

Title: Assistant Professor of Mechanical Engineering

Acknowledgments

The thanks should begin with the folks who deserve it most: Roger Hain and Rami Mangoubi. Serving as my thesis technical advisors at C.S. Draper Laboratory, Roger and Rami formed an excellent duo helping me out in academic and research matters. Even when the discussions became rigorous and intense, they always maintained a friendly and free atmosphere critical for learning. I must confess some envy of Roger's working style. His patience, courtesy, level-headedness, and professionalism are qualities that most of us can only aspire to. Roger, I wish you the best of luck at the Smithsonian and with your growing family. Rami's drive, stamina, and intellectual curiosity are also qualities I hope have rubbed off, at least a little. Thanks for the inspiration *and* for providing excellent editorial comments. I look forward to seeing you around the lab in the future.

I'd like to express my sincere gratitude to the staff of the Control and Dynamical Systems Directorate, especially Neil Adams and Susan Carr, the staff of the Draper Education Office, especially John Sweeney and Arell Mcguire, and the MIT Mechanical Engineering Graduate Office, especially Leslie Regan and Joan Kravit. These are the people who make every detail of graduate life possible through their patience, diligence, spirit of cooperation, and smiling faces.

Professor Feng of the Mechanical Engineering Department graciously served as MIT thesis reader, despite his own busy schedule.

My fondest memories of this epoch spent at MIT and Draper Laboratory will always belong to the group of comrades who coalesced into one of the most jovial, charismatic, clandestine, adventuresome, witty, goofy, genuine, and often sketchy gangs ever assembled in such an otherwise respectable place as Cambridge. Whether it was smacking billiard balls around on a red-felted table, exploring/exploiting and nocturnal personality of Boston and Cambridge, camping in the foggy womb of the Maine woods, jetting to San Francisco for a little R&R while the rest of town suffered through a Northeast January, staying more local to hurtle uncontrollably down a Massachusetts mountain, cycling around through the roundabout-saturated byways of Eastern Mass., yucking it up for a weekend on Martha's Vineyard, or just having the usual fun times around the lab, home, and Hub, these guys never forgot that regardless of what you are doing, you had better make it a good time. To Beau, I must bestow the greatest honor, since he had to endure me not only as a tag-along friend but as a roommate too. Beau, even though you were an inspiration in many ways, none of us will ever remember anything but your last hurrah at Tony's party. I'll see you out west some day, my friend. I can thank Chad for my clinical addiction to Maxim magazine. I recently figured out how it's going to work in the future, Chad. You'll have your place in the Caribbean, I'll have mine in Kentucky, and

we can convene every summer at our jointly-owned place on Thames Street. I hope that sounds as good to you as it does to me. To Alexi, er-, Gordon all I can say this: next time we're both in the need (which seems to be most of the time), I'll meet you at The Burren. Actually I can something else. You're my hero, tough guy. Who's next? Well, since I'm getting the urge to head up to Grendel's right now, it must be Tony. Best of luck with the fighters, man. You'll always be my top gun. You win the award for always keeping things lively and tongue-in-cheek. Rudy, on your behalf, I'll hereby declare today official "oh-yaah" day. Remember, L.A.'s a big town but I have confidence that you'll know it all by the time I make my first visit. Don't forget the kneepads when you strap on those rollerblades. Nhut, you came through where all these other guys failed miserably - in supporting the NY Jets. I look forward to a few more years of talking trash and generally breaking the hearts of UCLA and Patriots fans. To Ramses, I wish you a great time out in California and around these fifty states. Maybe you can pick up the mantle where Ansel Adams left it. As far as I'm concerned, you took your best picture ever on a pier in Newport. Maybe you can stop by and see Andy in New Mexico. He's the one who introduced me to stout and club dancing. That's not too bad for a otherwise mild-mannered OR-head. I hope it's a lot dryer in the Southwest than up here. By the way, I believe you win the award for the first among us to "cross over to the other side". Congratulations to you and Barbara.

I wish to express my sincerest affection to Tina, whose companionship has made New England an extra special place. Since neither one of us is moving away, I plan on having many more great times with you, as always.

My love goes out to the people who are my greatest inspiration: my mother, father, sister and grandfather. It is you all that I think of every day and constantly look forward to seeing again. Without your love behind me, I cannot move forward.

This thesis is dedicated to my mother, Karen.

8 August, 1998

This thesis was prepared at the Charles Stark Draper Laboratory, Inc., under Independent Research and Development Project Number 13299.

Publication of this thesis does not constitute approval by Draper Laboratory of the findings or conclusions contained therein. It is published for the exchange and stimulation of ideas.

Permission is hereby granted by the author to the Massachusetts Institute of Technology to reproduce any or all of this thesis.

/

Contents

1	Introduction	16
1.1	Navigation with the Kinematic and Dynamic Approaches	17
1.2	Gyroscopes for Inertial Rate Sensing	22
1.3	Global Positioning System for Attitude Sensing	26
1.4	Satellite Control	28
1.5	Thesis Objective	30
2	Truth Dynamics, Environment, and Measurements	32
2.1	Rigid Body Dynamics and Reference Frames	33
2.2	Torques	39
2.2.1	Control Torques	39
2.2.2	Gravity Gradient Torque	44
2.2.3	Solar Radiation Pressure Torque	45
2.2.4	Magnetic Dipole Torque	46
2.2.5	Atmospheric Drag Torque	47
2.3	Measurements	48
2.3.1	Gyroscopes	49
2.3.2	GPS Attitude	49
2.4	Summary	51
3	Filter Designs	53
3.1	Model Filter Design	54
3.1.1	State and Covariance Propagation	54

3.1.2	Measurement Update	60
3.1.3	Summary	70
3.2	Nonmodel Filter Design	71
3.2.1	State and Covariance Propagation	71
3.2.2	Measurement Update	74
4	Simulation Results	76
4.1	Measures of Performance	77
4.2	LVLH-Aligned Performance	79
4.3	Tumbling Performance	87
4.4	Maneuver Performance	99
4.5	Gyro-Free Operation	113
4.6	Summary	125
5	Conclusions	126
5.1	Conclusions	127
5.2	Directions for Continued Investigation and Implementation . . .	129
A	First Order Gauss-Markov Stochastic Processes	132
A.1	Continuous Scalar Processes	133
A.2	Simulation Considerations	138
A.3	Classical Gyro Error Modeling	140
B	Attitude Representations	143
B.1	A Generic Rotation	143
B.2	Euler Angles	144
B.3	Direction Cosine Matrices	146
B.4	Quaternions	149
C	Kalman and Extended Kalman Filtering	155
C.1	The Kalman Filter	155
C.2	The Extended Kalman Filter	160

Bibliography	166
Index	171

List of Figures

1-1	Particle Motion on a 1-D Path	18
1-2	Gimballed Gyroscope	24
1-3	GPS Interferometry for Attitude	27
2-1	Inertial and Satellite Body Frames	34
2-2	Orbital Configuration with Inertial, Local, and Body Frames . .	36
2-3	Control Loop Including Dynamics and Filter	40
4-1	Attitude Error, Nonmodel Filter, Trivial Motion, No GPS . . .	81
4-2	Attitude Error, Model Filter, Trivial Motion, No GPS	82
4-3	Gyro Bias Error, Nonmodel Filter, Trivial Motion, No GPS . . .	84
4-4	Gyro Bias Error, Model Filter, Trivial Motion, No GPS	84
4-5	Attitude Error, Model Filter, Trivial Motion, With GPS	85
4-6	Attitude Error, Nonmodel Filter, Trivial Motion, With GPS . .	85
4-7	Truth Rate Profile During Tumbling	89
4-8	Truth Attitude Profile During Tumbling	89
4-9	Nonmodel Filter - Tumbling With High GPS Rate	91
4-10	Model Filter - Tumbling With High GPS Rate	91
4-11	Model Filter with 10% Inertia Errors - Tumbling With High GPS Rate	93
4-12	Nonmodel Filter - GPS Multipath Estimation Error	95
4-13	Nonmodel Filter Attitude Error During Tumbling - Low Fre- quency GPS	97

4-14 Model Filter Attitude Error During Tumbling - Low Frequency GPS	98
4-15 Robustified Model Filter Attitude Error During Tumbling - Low Frequency GPS	99
4-16 Nonmodel Filter Gyro Bias Error During Tumbling	100
4-17 Model Filter Gyro Bias Error During Tumbling	100
4-18 Commanded Attitude Profile for Maneuver, Expressed as a Local to Body Transformation	103
4-19 Nonmodel Filter - Attitude Estimation Error During Maneuver - Worst Case Torque	104
4-20 Model Filter - Attitude Estimation Error During Maneuver - Worst Case Torque	106
4-21 Nonmodel & Model Filters - Attitude Control Error During Ma- neuver - Worst Case Torque	108
4-22 Nonmodel & Model Filters - Attitude Control Error During Ma- neuver - Mild Torque	110
4-23 True Total Disturbance Torques	111
4-24 Disturbance Torque Estimates With Gyro Biases Present, Model Filter	111
4-25 Disturbance Torque Estimates With Bias-Free Gyros, Model Filter	112
4-26 Nonmodel Filter - Attitude Error Without Gyros	117
4-27 Nonmodel Filter - True Attitude Without Gyros	117
4-28 Model Filter - Attitude Error Without Gyros	118
4-29 Model Filter - True Attitude Without Gyros	119
4-30 Robustified Model Filter - Attitude Error Without Gyros	120
4-31 GPS Receiver Solution - Attitude Error Without Gyros	121
4-32 Model Filter - Attitude Error Without Gyros	123
4-33 Model Filter - True Attitude Without Gyros	123
4-34 GPS Receiver Solution - Attitude Error Without Gyros	124

B-1	Generic Frame Transformation from A to B	144
B-2	Vector v Expressible In Two Frames	147
B-3	Euler Axis Rotation From XYZ to xyz	149

List of Tables

1.1	Classification of Gyro Quality by Error Parameters	25
2.1	Key Truth Simulation Relations	52
4.1	Description for LVLH-Aligned Simulation	80
4.2	Attitude Performance Statistics - No GPS Updating	83
4.3	Attitude Performance Statistics - With GPS Updating	86
4.4	Description for Satellite Tumble Simulation	88
4.5	Attitude Performance - Tumbling With High Frequency GPS Updates	92
4.6	Truth and Erroneous Filter Satellite Inertia Matrices and Their Eigenproperties - Tumbling Scenario	93
4.7	Attitude Performance - Tumbling With High Frequency GPS Updates	94
4.8	GPS Multipath Performance - Tumbling With High Frequency GPS Updates	95
4.9	Attitude Performance Statistics - Tumbling with Infrequent GPS Updating	98
4.10	System Description for Controller Maneuver Simulation	101
4.11	Attitude Estimation Error During Maneuver - Worst Case Torque	106
4.12	Attitude Estimation Error During Maneuver - Mild Torque	109
4.13	Disturbance Torque Estimation Error - All Units 10^{-7} N*m	113
4.14	System Description for Gyro-Free Simulation	115

4.15 Truth and Erroneous Filter Satellite Inertia Matrices and Their Eigenproperties - Gyro-Free Scenario	119
4.16 Attitude Error Performance - No Gyros and Frequent GPS . . .	121
4.17 Attitude Error Performance - No Gyros and Infrequent GPS . .	124

Chapter 1

Introduction

Estimator design for vehicle navigation is rarely straightforward. Although only one truth process exists, many navigation filters may be implemented to wring information from sensor measurements. The variety of designs is made possible by the curious aspects of real physical and engineering systems: nonlinearities, unmodeled dynamics, unaccountable errors, high order effects, and others.

This thesis is concerned with extended Kalman filter design for small satellite attitude determination. Competing filter design models are proposed and compared. The fundamental goal is to suggest estimation strategies useful for mitigating the ill effects of low grade inertial instruments. Although the nonlinear nature of vehicle attitude dynamics forbids an implementable optimal solution, we can study the effectiveness of realistic suboptimal filters.

Towards this end, Chapter 1 begins by introducing the system of interest. Chapter 2 gives qualitative and quantitative models of the truth plant and environment. Chapter 3 continues by describing the competing estimator designs. Chapter 4 provides specific test examples and Chapter 5 draws conclusions and illuminates further points of interest. The Appendices are included to give meaningful tutorials on special topics without interrupting the flow of the main document. Appendix A treats first order statistical models and gyroscopic error model terminology. Appendix B discusses the dominant attitude representations and their interrelationships. Finally, Appendix C gives the Kalman

filter and extended Kalman filter algorithms and some of their properties.

Within this first chapter, Section 1.1 discusses two competing approaches to navigation estimator design. Sections 1.2 and 1.3 introduce the sensors employed to observe satellite motion. The control system actuators are considered in Section 1.4 and Section 1.5 concludes by outlining the research objectives.

1.1 Navigation with the Kinematic and Dynamic Approaches

The problem of Kalman filtering for aerospace navigation is well founded. It is often a matter of combining relevant information from a variety of sources. Inertial sensors give rate or acceleration data; altimeters, radars, and star trackers measure position-like quantities; Doppler mechanisms and position differencing techniques give velocity updates. Given the relatively simple first order differential relations between position and velocity and between velocity and acceleration, the Kalman filter (KF) is well suited to synerize any and all of these sensor readings while providing a straightforward way to mitigate the effects of measurement errors. Since linear filters rely on spectral content to infer state behavior from measurement sequences, the KF traditionally has been used to correct the low-frequency biases of inertial navigation systems (see Section 1.2 below) with periodic high-frequency error content data from other instruments. The marriage of sensor measurements, Kalman filtering, and navigation requirements has indeed been a successful one.

One of the greatest strengths of Kalman filtering for navigation is the flexibility it provides. Although there may be only one truth system, comprised of vehicle, environment, and sensors, there are multiple KF designs possible for any situation. For example, in his chapter on filter design and performance, Maybeck discusses competing methodologies and introduces terminology such as *total* or *error state* formulation, and *error feedback* vs. *feedforward* design (Ch.

6, [30]). To fully outline these differences here would be a redundant attempt to convey what Maybeck and many others have eloquently expressed before [9], [17], [28], [31], [43].

Instead, we focus in this thesis on a single distinction in filter designs and in a single setting. Specifically, we consider the problem of satellite navigation with gyroscope and GPS sensors. Our distinction is over dynamic model inclusion. Most traditional attitude filters rely exclusively on kinematic and instrument error models for their filter design. We choose to compare this philosophy to one that includes not only these sources, but a dynamic realization of satellite motion as well. A simple toy example will illustrate.

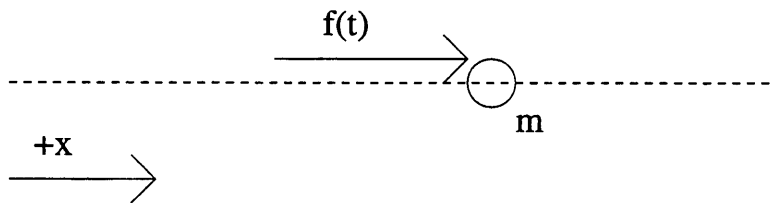


Figure 1-1: Particle Motion on a 1-D Path

Consider a single particle moving along a one-dimensional path as shown in Figure 1-1. It has mass m and responds under the action of a *stochastic* force history $f(t)$. In order to track the particle’s motion, we have available a continuous velocity sensor measurement $v_{meas}(t)$ and a continuous position measurement $x_{meas}(t)$. Unfortunately, each is perturbed from a true reading by continuous time white noise so that

$$v_{meas}(t) = v(t) + e_1(t) \tag{1.1}$$

$$x_{meas}(t) = x(t) + e_2(t),$$

where $v(t)$ and $x(t)$ are the true velocity and position and the $e_i(t)$ ’s are the stochastic measurement errors. The traditional “kinematics plus errors equals filter” approach, which is hereafter referred to as the “nonmodel” ap-

proach would look at the truth system as merely

$$\dot{x}(t) = v(t) \tag{1.2}$$

so the natural Kalman filter truth model is

$$\begin{aligned} \dot{x}(t) &= Ax(t) + Bv_{meas}(t) + Ge_1(t) \\ y(t) &= Cx(t) + De_2(t). \end{aligned} \tag{1.3}$$

where

$$A = 0, B = 1, G = -1, C = 1, D = 1. \tag{1.4}$$

The estimation then proceeds according to Equations (C.16) and (C.17) after the covariances of processes $e_1(t)$ and $e_2(t)$ have been defined.

Alternatively, the dynamically aware filter, hereafter called the “model” filter, considers relations (1.1), (1.2), *and* the underlying Newtonian dynamics

$$\begin{aligned} \dot{v}(t) &= a(t) \\ a(t) &= f(t)/m \end{aligned} \tag{1.5}$$

to arrive at the larger Kalman filter truth model:

$$\begin{pmatrix} \dot{x}(t) \\ \dot{v}(t) \end{pmatrix} = A \begin{pmatrix} x(t) \\ v(t) \end{pmatrix} + Gf(t) \tag{1.6}$$

$$y(t) = C \begin{pmatrix} x(t) \\ v(t) \end{pmatrix} + D \begin{pmatrix} e_1(t) \\ e_2(t) \end{pmatrix}, \tag{1.7}$$

with

$$A = \begin{bmatrix} 0 & 1 \\ 0 & 0 \end{bmatrix}, G = \begin{bmatrix} 0 \\ \frac{1}{m} \end{bmatrix}, C = D = I_{2 \times 2}. \tag{1.8}$$

Now to proceed with operations (C.16) and (C.17), we must define an additional process covariance for the driving term $f(t)$.

Overall, we see that the model filter considers more elements of the true system than the nonmodel filter. While the latter must directly integrate the velocity measurement (including errors) as a truth input in (1.3), the model filter appropriately treats it as a plant output, comparing it to the inertial limitations of the system captured in the $\frac{1}{m}$ term.

The strength of the model filter is the additional information it brings to the table. If the instrument error sources are large, particularly for the velocity sensor, the nonmodel filter's uncertainty in the position state $x(t)$ will grow rapidly. If position measurements are infrequent or noisy themselves, then knowledge of the true $x(t)$ may become unacceptable. However, by considering the $F = ma$ of the situation, the model filter has an edge in tracking position, since it can compare velocity measurements with the physical limitations, i.e. inertia, of the system. In situations when x_{meas} is unavailable, the model filter should experience a slower error growth rate in the uncertainty of $x(t)$. Intuitively, the model filter should possess superior performance since it supercedes the nonmodel filter by including additional inertial information.

However, the model filter is not without liabilities. By adding in additional dynamic relations to the filter design, we are claiming to know more about the real system. Hopefully this confidence is well founded; but if we add erroneous mass data, then we could potentially create a misguided filter that will undervalue the information present in the measurements. Further, in real situations $f(t)$ is partially or fully composed of stochastic process which, like the coefficient $\frac{1}{m}$, must be well modeled in order for the additional dynamics to be effective. These caveats highlight a fundamental difference between the two estimation methodologies. Specifically, the nonmodel filter is essentially *autonomous* of its constituent vehicle, which in this case is the unit mass m . It does not have to be specially tuned to consider the real plant dynamics. In contrast, the model-based filter requires additional design effort to include inertial effects and stochastic environmental disturbance models. However, if the instruments have poor error behavior, then this effort may be rewarded with vastly superior performance.

Chapter 4 is concerned with examining this tradeoff in specific test cases.

Historically, navigation and attitude filters have operated only in the kinematic, or nonmodel mode for a number of reasons. The inclusion of dynamic equations of motion entails a larger state space model and thus a greater computational burden. In fact, even obtaining useful equations of motion might involve unjustifiable time and expense. Also, the potentially deleterious effects of model uncertainty were likely deemed an unnecessary risk to take. In most cases, the vehicle's instruments, especially the gyros, were of sufficiently high quality to marginalize the model's contribution.

However, dynamic model inclusion is not without precedent. Typically, a filter designer adds it in when he feels that the measurement quality is low or when a condition of insufficient measurement *quantity* exists. In such cases, one requires an additional source of information about vehicle motion. The model's use derives from the its ability to provide a more realistic propagation of system states em between measurement updates.

Koifman and Merhav have used aerodynamic vehicle models in conjunction with angular rate, heading, velocity, and altitude measurements to estimate a whole suite of navigation states [25]. They included the model to enhance vehicle autonomy by limiting the reliance on outside navigation aids. Azor, Bar-Itzhack, and Harman have included satellite dynamic information to obtain body rate insight from vector attitude measurements [4]. Here, rate gyros were totally unavailable so an additional information source was necessary to extract useful state estimates between the vector sensor updates. Their scheme cleverly performed nonlinear tracking via linear approximations. In another study, Crassidis and Markley employed dynamic modeling for spacecraft attitude estimation in the complete absence of rate gyros [14]. Without the necessity of tracking gyro biases, they were able to estimate disturbance torques and obtain significant dynamic information. Once again, a limited sensor suite motivated the model's inclusion in the filter. In their investigations of INS/GPS integration, Puri and Giustino used satellite inertia properties to mitigate large rate

gyro error components [36], [18].

This thesis continues the collective study of model-based filtering by comparing the effects of dynamic model inclusion and exclusion in several settings. Here, we consider satellite orbital attitude dynamics in the presence of a poor quality gyro and/or the absence of external measurement aiding. If gyro quality was sufficiently high, then one could very easily design a nonmodel estimator to achieve reliable attitude estimates. However, if the gyro is poor, that is, if the gyro output contains significant error components, then the satellite dynamic model should intuitively improve estimation performance.

The next two sections introduce the measurement systems at our disposal. The first describes generic gyro operating principles and defines more precisely what is meant by a “high” or “low” quality gyroscope. The second discusses GPS interferometry, in which position readings are converted to useful attitude information.

1.2 Gyroscopes for Inertial Rate Sensing

An essential component of many flight vehicles’ guidance and navigation suites is the inertial navigation system, or INS. This term typically denotes a collection of accelerometers and gyroscopes arranged with a known orientation to the vehicle body.

An accelerometer is an instrument which monitors specific force along a particular axis, typically using some elastic effect, and reports the corresponding linear acceleration. To obtain linear velocity from an accelerometer, the output is integrated once. The position follows from an additional integration of velocity [31], [34].

A gyroscope monitors angular velocity about a particular input axis. This instrument typically functions by measuring the effects of angular rate on a mass already moving or spinning in some known fashion. Examples include tuning fork gyroscopes that track the motion of vibrating beams and fiber optic

gyroscopes that check phase shifts of counterrotating light beams. Regardless of the particular phenomena that governs their operation, all gyroscopes output an angular rate or accumulated angle signal [12], [31], [34].

As spatial bodies typically possess at least six degrees of freedom, a minimal INS contains three orthogonally mounted accelerometers and three orthogonally mounted gyroscopes (or “gyros” for short). A reliable flight system would likely contain even more instruments for redundancy and additional motion observability [15]. Although accelerometers are often employed in satellites for orbit tracking, we focus here on gyros and rotational kinematics since translational and attitude dynamics can often be decoupled in astrodynamical settings. Our interest is filtering for satellite attitude, which is crudely expressed as the first integral of angular rate.

It is important to keep in mind that, as the name implies, gyroscopic inertial instruments measure angular velocity with respect to an *inertial* frame. Therefore if we desire angular information in some other reference frame, we must introduce coordinate transformations. For example, we often wish to define motion relative to an accelerating/noninertial frame like the Earth, since this frame often has the most practical meaning in engineering settings. The need to relate the inertial frame to other frames leads to the additional coordinate definitions and mathematics, as seen in Chapters 2 and 3.

The distinction between reference frames has also spawned different approaches to constructing gyros themselves. One family of designs endeavors to keep the gyro input axes, i.e. the axes about which angular rate is to be measured, constantly aligned with an arbitrary inertial frame. Naturally, no flight vehicle maintains this inertial alignment at all times and hence, the gyros must be mounted on a moving *gimballed* platform. Figure 1-2 shows a simplified schematic of a gimballed gyro.

As the vehicle rotates, inertial rate measurements come in from the gyros. These rates are integrated into angles and the vehicle motion with respect to inertial space is tracked. Acting to oppose the gyro-reported body rates, actua-

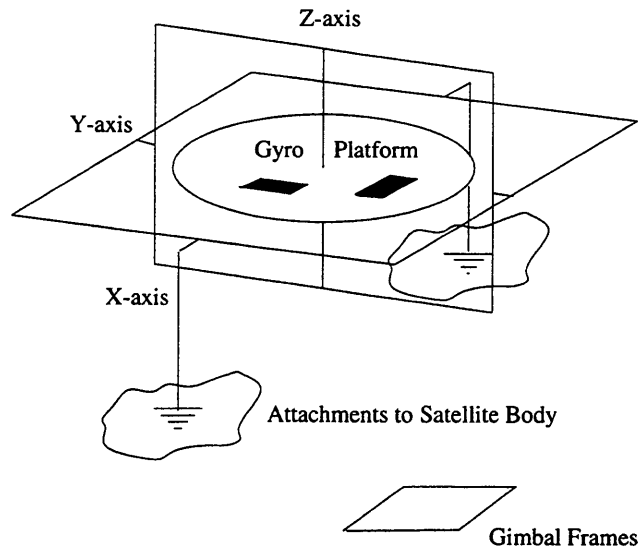


Figure 1-2: Gimballed Gyroscope

tors simultaneously rotate the gimbals to keep the gyro platform in its original inertially-fixed alignment. The orientation between the vehicle and its onboard gyro platform changes as long as the the former undergoes angular motion.

The alternative design methodology prefers to keep the gyros rigidly mounted to the vehicle body frame. (The body frame is defined precisely in Section 2.1). No hardware or control logic exists to maintain the original instrument orientation. Instead, the instruments are rigidly attached to the vehicle body so that the inertial input axes are constantly changing. The computational effort now goes to tracking what the input axes are. They are constant with respect to the body, but are time varying with regards to any external environment. Because these systems essentially piggyback the vehicle, they are termed *strapdown* inertial systems.

Even within these two broad classes of gyros, there are still numerous physical bases for computing angular rate. Hence gyros come in many forms. Examples include spinning mass gyros, ring laser gyros, fiber optic gyros, and tuning fork gyros. Reference [31] is one of several sources on the subject.

If gyros operated continuously, gave perfect high-bandwidth measurements,

	Gyro Quality		
Sensor Parameter	High	Medium	Low
Gyro Bias	≤ 0.01 deg/hr	0.1 to 1.0 deg/hr	≥ 10 deg/hr
Gyro ARW	≤ 0.0018 deg/rt-hr	0.06 deg/rt-hr	≥ 0.06 deg/rt-hr

Table 1.1: Classification of Gyro Quality by Error Parameters

and were not prohibitively expensive or bulky, then the vehicle navigation problem would be permanently solved. One could simply start with a sufficiently accurate initial condition and numerically integrate the gyro output to maintain a complete vehicle attitude history. However, inertial instruments are known for introducing many different errors into their outputs [9], [30], [31]. Some of these effects have zero mean and are not time-correlated. Others, start small, but generally grow in time until their impact on the measurement becomes unignorable. Examples include biases, nonorthogonality effects g-sensitive terms, g-squared-sensitive terms, and quantization distortion.

For ease of modeling, gyro errors are typically divided into two coarse categories: bias (or bias drift) and white noise. Their terminology and basic math models are saved for Appendix A to prevent the discussion here from becoming too long. However it suffices to say for now that gyro quality is often classified by the rate at which the bias term drifts and the intensity, or magnitude, of the white errors. Reference [9] presents the gyro classification chart in Table 1.1. The units of angle random walk (ARW) have been converted from their original form and their meaning should be evident from the Appendix discussion. The bias statistics refer the standard deviation of the bias *drift* over a one hour period. A “high” quality gyro is very self-sufficient and can provide reliable rate data for long periods. For example, a commercial airliner on a ten hour trans-Atlantic flight would only accumulate a 0.31 degree net error ($1\text{-}\sigma$) while integrating a gyro’s ARW error at the level indicated in the Table. During that same period the gyro bias would drift only 0.1 deg/hr ($1\text{-}\sigma$). In contrast, a “low” quality gyro requires frequent external aiding to prevent unacceptable

error buildup. Continuing the example, if the airliner employed a low quality gyro for the same flight, the angle random walk buildup would be on the order of 10 degrees and the bias would typically wander 100 deg/hr or more.

At present, the Charles Stark Draper Laboratory is developing a micromechanical gyroscopic instrument for aerospace and defense applications. Information on its operating principles, design, and performance are available in reference [26]. One of this research effort's intentions is to create a small size, low cost, low power consumption strapdown inertial instrument appropriate for small, low budget spacecraft missions. Since micromechanical sensors historically entail significant error characteristics, this thesis research performs a preliminary investigation of attitude determination filter design for INS error mitigation.

1.3 Global Positioning System for Attitude Sensing

Seeking a reliable method for determining location at any point on earth, the U.S. Department of Defense, in cooperation with academic and commercial organizations, developed the Global Positioning System, or GPS [21]. Its heart is a constellation of twenty-four high orbit satellites with time-correlated output signals. Receivers on earth, whether held by individual persons or vehicles, take in specially coded transmissions from the satellites, determine the time they took to travel from space to the surface, convert this time to a distance, and then "triangulate" the earth-bound position.

Although originally intended for military use, the extraordinary success of GPS technology is now available for commercial and civilian benefit. Private corporations and ordinary citizens are exploring GPS positioning for applications as diverse as airline navigation and outdoor recreation.

One of the useful applications of GPS is satellite tracking and attitude de-

termination. Here, tracking refers to orbital position (translational motion), the computation of which is similar to earth-bound positioning. For attitude determination, interferometric techniques are employed. The basic principle is to place several GPS receivers in a rigid array mounted to the satellite body. As each receiver is capable of producing a position output, *relative* position information is available to compute spacecraft orientation, or attitude. Figure 1-3 gives a two-dimensional illustration of this technique, known as GPS “interferometry”.

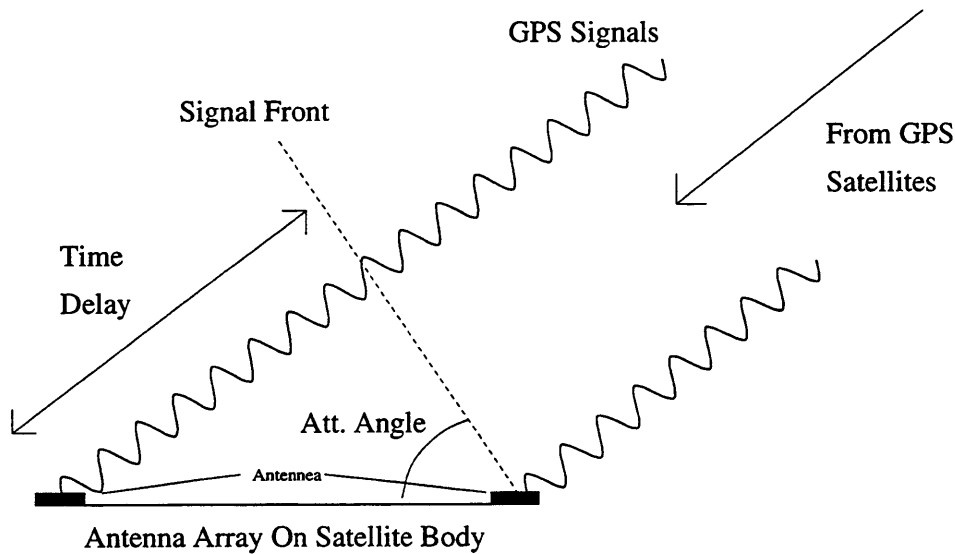


Figure 1-3: GPS Interferometry for Attitude

The National Aeronautic and Space Administration (NASA) has performed on-orbit GPS interferometry proof-of-concept experiments [11]. Further earth-bound experimentation and extensive simulation is ongoing at several research institutions, including Stanford University [33], the University of Colorado at Boulder [5], [6], and the Charles Stark Draper Laboratory [18], [36].

For the purposes of this research, GPS interferometry provides the simulated on-orbit attitude sensor. Of course, like any real engineering sensor, GPS attitude is not an error-free measurement. First of all, the measurement might be totally unavailable at times. During satellite tumbling or installation, the

algorithms that convert individual antennae position information to attitude may be still be preprocessing as it can take many iterations to resolve the number of integer wavelengths that make up the time delay in Figure 1-3. Puri and Giustino treat this wavelength computation issue under the heading of “integer ambiguity” [18], [36]. Further, during high orbit periods, a receiver-bearing satellite may not observe enough GPS satellites to compute a meaningful attitude.

Even when a sufficient number of GPS satellites are in view and attitude solutions are available, there are still unignorable errors. As with virtually all sensors, present will be a time-uncorrelated white noise which perturbs every measurement from truth. This white noise exists at every update epoch; knowledge of the previous white noise value is useless in predicting the next. Another perturbation may also be present, this one low-frequency and time-correlated. It arises from a multitude of sources such as antenna line biases, phase center variation, antenna array flexibility, and the reflected signal phenomenon known as GPS multipath [36], [41]. Models for both white and time-correlated errors are provided in Section 2.3. Their magnitudes as well as the GPS update interval depends on the particular test.

1.4 Satellite Control

Virtually all orbiting spacecraft have mission objectives which require some sort of attitude and motion control mechanisms. Sometimes we desire a satellite to point constantly at a fixed spot on the earth for communication or surveillance. Later on, we might wish to slowly sweep a given geographic area rather than hold a stationary posture. Still other times the desired state might be an inertially constant attitude as employed in astronomical studies.

Whatever the control objective, the satellite must contain some method of actuation that a control law can utilize. Without going into unnecessary details, it suffices to say that many alternatives exist. Examples include reaction wheels, control moment gyros, magnetic coils, gravity gradient stabilization, spin stabi-

lization, and gas thrusters [10], [43]. The choice of the best actuation method depends fundamentally on the mission objective and operating constraints. In *this* study we choose to employ thrusters for simulated attitude control. The reasoning is this: thrusters provide a mathematically simple way to obtain full three-axis spacecraft attitude control. An elementary gas thruster system for each body axis allows a series of three independent, clean control signals without the additional dynamic modeling seen in rotating mass controllers. For the purposes of mathematical simulation, thrusters do not require environment interaction modeling or de-spin maneuvering. Further, many satellite control algorithms are written with generic three-axis control in mind and thrusters provide a simple method of realizing such laws. Of course, gas thrusting naturally does entail certain practical challenges such as fuel and weight budget satisfaction but those aspects will be brushed over here as secondary to our attitude estimation objective. If specific engineering designs require alternative actuators, then the filtering techniques presented in later chapters can be appropriately modified. References [10], [27], and [43] should provide further insight.

Simple linear momentum conservation is the fundamental operating principle for spacecraft gas thrusters. Gas molecules ejected at high velocity from a satellite orifice will produce a reaction force in the opposite direction. Commercial jets come in hot gas and cold gas varieties. The former gets its energy from an exothermic chemical reaction and typically produces larger reaction forces (5 N or greater). The cold jets are powered instead by thermodynamic processes, such as matter phase change or compression/expansion phenomena. These actuators produce smaller thrusts (approx. 1 N or less) and are best employed for fine control. In subsequent simulations, we will not worry about the specific jet type but instead monitor the control torque magnitudes and make sure they stay at or below 2.5 N-m. Larger torques might be unreasonable for small spacecraft that necessarily have small thruster moment arms. If we assume a moment arm length of half a meter (0.5 m), then the thrust magnitude should

remain below 5 newtons, which is reasonable based on the above discussion.

Of course, given a capable actuator, the choice of control law is an important matter. Alternative control laws are presented in Section 2.2.1 and their relative merits given. Actuator dynamics that govern behavior between command input and thruster steady-state are neglected to prevent overcomplication of the truth and filter models.

1.5 Thesis Objective

The objective of this thesis is to explore the usefulness of dynamic modeling in satellite attitude determination. Inclusion of the vehicle model is motivated by the advent of small, inexpensive, inertial sensors with possibly significant error components. Whereas a purely kinematic, or nonmodel approach was once sufficient for mission requirements, gyros with high bias drift rates and large noise intensities may require additional aiding in the form of dynamic modeling. This model information should prove especially useful when external attitude sensors, such as GPS, are unavailable.

Sections 1.1 and 1.2 outlined in greater detail the specific differences between the model and nonmodel filter designs. The former section also gave a summary of research into the benefits of vehicle model inclusion. Whereas some previous studies have included inertia information in satellite attitude filters, this thesis designs both a model and nonmodel filter specifically in the context of poor quality inertial sensing. As such, we bring forth new quantitative knowledge about the strengths and weaknesses of the competing filter designs in various test settings.

The contributions of this research include the demonstration of dynamic modeling's effect on attitude performance, the development of a high-fidelity simulation applicable to this and future research, the explicit discussion of competing filter designs, and a series of Appendix of tutorials on related topics, the first of which gives the clearest explanation of Gauss-Markov based gyro error

model vocabulary and term dimensions seen yet by this author.

Chapter 2 continues by discussing the truth system in greater detail. Here, the equations of motion are stated, the sensor and actuator models are completed, and the disturbance environment is described. Chapter 3 gives the exact model and nonmodel filters in the context of satellite attitude determination. Chapter 4 demonstrates filter performance in a variety of sections and Chapter 5 draws conclusions and points the way for further investigation.

The Appendices are included to allow a thorough introduction to relevant side topics. Appendix A discusses the related items of Gauss-Markov process statistics, a technique for simulating white disturbances numerically, and terminology of gyro error modeling in the context of Gauss-Markov processes. Appendix B outlines the three dominant attitude representations, their relative merits, and their interrelationships. Appendix C finishes by giving the Kalman and extended Kalman filter algorithms and some of their properties.

Chapter 2

Truth Dynamics, Environment, and Measurements

In any sort of filtering or estimation study, it is necessary to have a “truth” system where the “real” dynamics take place and “real” measurements are generated. As the filter processes the available data, the state estimates are compared to the simulated truth counterparts to gauge the actual performance of the filter.

There are advantages and disadvantages of using a real, physical system as a truth model in the filter design study. The obvious benefits include the opportunity to fairly test the estimator, the satisfaction of seeing an abstract algorithm work in actual hardware, and the peace of mind that one is not relying on a naive or overly simplified model of the real world. The disadvantages are the large effort and cost involved in performing experiments and the slow turn-around time for studying the effects of parameter variation. With the advent of what some call the “third paradigm” [20] of science (analysis and experimentation being the first two), engineers can employ computer simulation to emulate a real system with a desktop workstation. Not only does simulation avoid the time and financial burdens of full blown experimentation, it also provides easy access to the truth states so that filter performance can be accurately computed.

For the problem of satellite attitude determination, computer simulation

allows large scale investigation that would be absolutely infeasible with real hardware. This chapter lays out the mathematical assumptions used to simulate the dynamics and measurement processes for a real satellite. This truth model is then coupled with competing filter designs to assess their relative merits. In some cases there will be close agreement between truth model and filter design; in others, we will introduce deliberate errors. Specific numerical values for truth parameters will be given in subsequent chapters as needed; only the generic mathematical formulae are given here.

Section 2.1 begins by defining the necessary reference frames and giving the dynamics equations for satellite rigid body motion. Appendix B provides further discussion of the kinematic relations. Here, it is important to note that although the fixed inertial frame is critical to define both the dynamics and gyro measurement processes, we never need to compute its specific orientation relative to the satellite.

Section 2.2 continues by describing the control and environmental torques that excite the truth system. Since most of them are hard to characterize mathematically and are stochastic in nature, there will be considerable assumption underlying their corresponding filter models.

Section 2.3 describes the truth measurement processes. Just as with the truth dynamics, these models are convenient and tractable concepts of the “real world”. The measured quantities and their typical error sources are described.

Finally, Section 2.4 summarizes the chapter.

2.1 Rigid Body Dynamics and Reference Frames

In this thesis, we assume that a satellite can be represented accurately by a rigid body in circular orbit. Of course, real satellites are in fact complex interconnections of numerous engineering subsystems and are not true rigid bodies. Solar

arrays and flexible panels can certainly introduce oscillatory modes invisible in a simple lumped parameter model. However, the rigid body assumption is a convenient starting point for analysis and captures significant features of orbital motion, such as gravity field interaction and Euler coupling.

To mathematically study rigid body motion, we traditionally begin with two frames of reference. They are the inertial reference frame and the rigid body frame. The former is an abstract entity that never accelerates and provides an environment in which to express the usual laws of motion. Knowledge of its specific orientation is not always necessary for analysis; it is sufficient to assume that it exists and that we could define it more specifically should the need arise. Alternatively, the body frame is permanently attached to the satellite center of mass with fixed body orientation and accelerates with it under the action of applied forces and torques. It is often important to know its exact orientation with respect to the surrounding environment to compute such disturbance values. Figure 2-1 illustrates these two frames, showing an arbitrary orientation between the two.

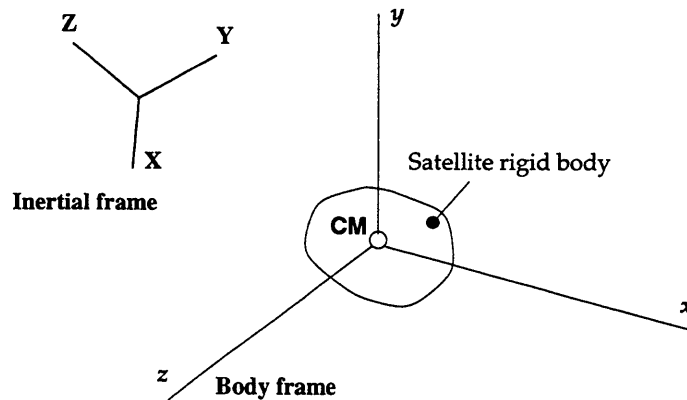


Figure 2-1: Inertial and Satellite Body Frames

With the inertial and body frames defined, we can give the general Newtonian equation of rigid body rotation as

$$\frac{d}{dt}(H) = \Sigma T. \quad (2.1)$$

The variable H is the total rigid body momentum and ΣT is the sum of applied torques, both resolved in the inertial frame.

By finding analytical expressions for the momentum of a rigid body in terms of its mass distribution and angular velocity and by carefully computing the time derivatives of quantities relative to moving reference frames, it is possible to derive the following general equation for rigid body rotation: [13], [32]

$$\frac{d}{dt}(I\omega_{bi}) + \omega_{bi} \times I\omega_{bi} = T. \quad (2.2)$$

This fundamental relation is known as Euler’s equation of motion and is the starting point of virtually all rigid body dynamics [13]. Unlike Equation (2.1), the quantities here, including the applied torque T , are all resolved in the *body frame*. The matrix I is the moment of inertia tensor and ω_{bi} is the angular velocity of the body frame with respect to the inertial frame. That is, the subscript bi should be read “body with respect to inertial”. The $(.) \times (.)$ denotes the usual vector cross product operator.

To study satellite orbital motion, we will need to introduce an additional reference frame. Although the inertial and body frames are sufficient to describe rigid body rotation (Equation (2.2)), they do not capture the fact that in orbit, some of the applied torques are actually attitude dependent. By “attitude”, we mean the orientation of the satellite body with respect to its environment. In the orbital setting, gravity must always act towards the center of the earth and its effect on the satellite will vary, depending on its attitude with respect to the gravity field. Therefore, we define an intermediate frame whose origin corresponds exactly with the body frame origin. We choose it with the z axis trained on the nadir (earth pointing) direction, the x axis pointing in the orbital velocity direction, and the y axis pointing normal to the orbital plane, consistent with a right-handed system. Figure 2-2 illustrates this intermediate “local vertical-local horizontal” frame and its relationship to the inertial and body frames. We typically shorten the expression “local vertical-local horizontal” to

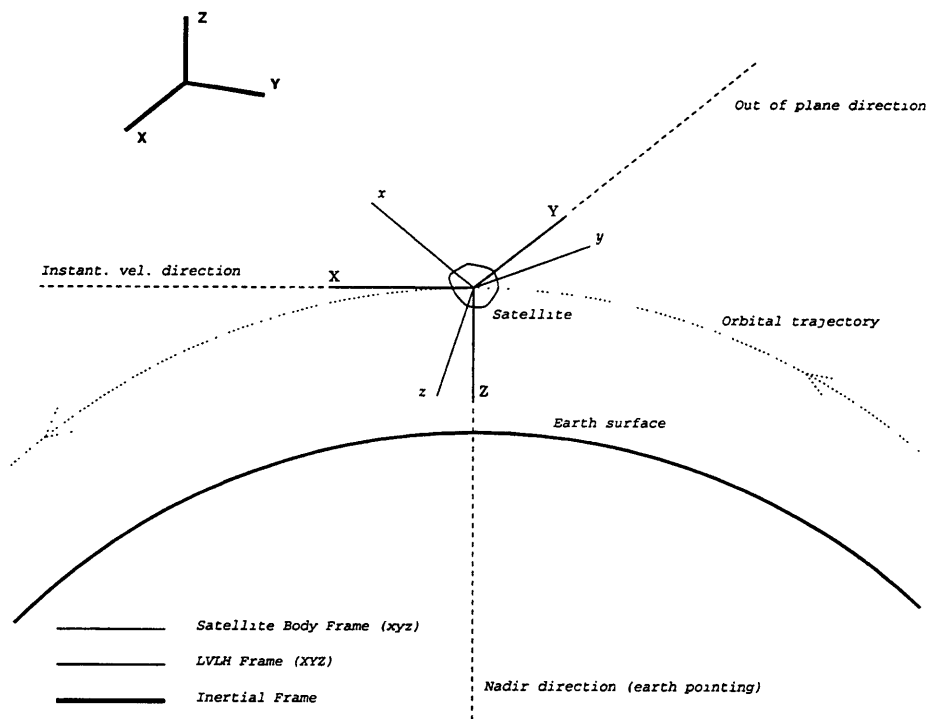


Figure 2-2: Orbital Configuration with Inertial, Local, and Body Frames

local, LVLH, or abbreviate with the symbol l . Alternate names exist in orbital mechanics literature; examples include “orbital”, “earth-referenced”, and “navigation” frame [36]. Since this frame is always aligned with its z axis pointing parallel to gravity, knowing the body frame’s attitude with respect to LVLH is equivalent to knowing the satellite’s orientation with respect to the earth. Therefore, the LVLH frame is necessary and useful for two reasons. First, it allows us to compute analytically the affect of gravity on satellite motion. Secondly, it gives us a convenient and physically meaningful frame with which to define satellite attitude.

It is important to distinguish between the local frame and the classic earth-centered inertial frame used in so many dynamics studies. The local frame, as we have defined it here, is a rotating and therefore *noninertial* frame. The earth frame, whose origin lies at the planet’s center, may be considered as stationary for the scope of this research and is therefore a candidate for an inertial frame.

However, since we do not need to declare a specific inertial frame for the purposes of computation, the earth-centered frame will not be introduced formally.

Since the *local* frame x and z axes must track the velocity vector and nadir directions, respectively, the local frame actually rotates with respect to the inertial frame as orbit progresses. Making reference to Figure 2-2, we see that the x and z axes always remain in the orbit plane, i.e. the plane of the paper. During orbit, the y axis remains invariant, always pointing *into* the paper. Not coincidentally, this is the exact rotation axis for x and z . Therefore, we can give the angular velocity of the local frame with respect to the inertial frame *expressed* in the local frame as

$$\omega_{li}^l = \begin{bmatrix} 0 \\ -\omega_{orb} \\ 0 \end{bmatrix}. \quad (2.3)$$

The li subscript should be read “local with respect to inertial”. The l superscript indicates that the vector is expressed in the local frame. Here, ω_{orb} is the orbit rate. The negative sign comports with the right hand rule; the y axis is directed into the paper in Figure 2-2 while the other axes rotate counterclockwise about it. In the remainder of this thesis, rate quantities appearing *without* superscripts are automatically expressed in the *body* frame.

Since we choose to study the alignment relationship between the body and local frames, we will work primarily with the quantities q_{bl} and ω_{bl} . The former, q_{bl} , is the quaternion that describes the instantaneous attitude transformation from the local frame to the body frame. (See Appendix B for a detailed discussion of quaternions and attitude fundamentals). The vector ω_{bl} is the angular velocity of body frame relative to local expressed in the body frame. By analogy to nonrotational dynamics, q_{bl} plays the role of position while ω_{bl} is essentially a velocity. As seen in Appendix B, the differential relationship between the

quaternion and the angular velocity is

$$\dot{q}_{bl} = \frac{1}{2}\Omega(\omega_{bl})q_{bl}. \quad (2.4)$$

where $\Omega(\omega_{bl})$ is defined by Equation (B.18).

So far, we have defined three different angular velocities: ω_{bi} , which appeared in Equation (2.2); ω_{li}^l , which described the motion of the orbital frame; and ω_{bl} which relates the body and local frames. These three vectors are of course related according to

$$\begin{aligned} \omega_{bi} &= \omega_{bl} + \omega_{li} \\ &= \omega_{bl} + T_{bl}(q_{bl})\omega_{li}^l. \end{aligned} \quad (2.5)$$

Here T_{bl} is a direction cosine matrix that transforms vectors in the local frame to their body frame representation. Its information content is identical to that of q_{bl} .

By differentiating Equation (2.5) with respect to time while accounting for the motion of noninertial unit vectors and *then* substituting the result into Equation (2.2), we can obtain the following relation

$$\dot{\omega}_{bl} = I^{-1}(T - \omega_{bl} \times I \omega_{bl}) + \omega_{bl} \times \omega_{li}. \quad (2.6)$$

This effort merely substitutes ω_{bl} for ω_{bi} since the “*bl*” quantities are of more interest to us than the “*bi*” quantities. Note that the inertia matrix I is assumed constant in Equation (2.6).

Equations (2.4) and (2.6) govern the truth dynamics. The next section gives further insight into components of the torque term T .

2.2 Torques

The T appearing on the right hand side of Equation (2.6) includes any and all torques that might act on the the satellite during orbit. We will generally split this term into two components, torques due to control inputs and torques due to disturbances:

$$T = T_{cont} + T_{dist}. \quad (2.7)$$

The control torque represents all deliberate efforts to dictate satellite motion. Typically, feedback control is employed: relevant quantities portraying satellite motion are measured or inferred and then fed to a *controller* that decides how to reconcile the current state of the system with the desired objectives. Controller design is obviously a major field unto itself and the engineering community has produced volumes on satellite control alone [10], [27], [43]. Section 2.2.1 below gives three elementary laws for attitude control.

The disturbance torque term T_{dist} represents basically every torque *other* than control torque. It has many possible components but we choose to treat only four of them in our truth model. They are gravity gradient torque, solar radiation pressure torque, magnetic dipole torque, and atmospheric drag torque. These components act independently in general and can thus be combined additively:

$$T_{dist} = T_{gg} + T_{solar} + T_{mag} + T_{aero}. \quad (2.8)$$

Subsequent subsections describe each disturbance component in greater detail. References [27] and [43] are good starting points for further investigation of these and other disturbance phenomena, such as third body effects and unintentional forces and torques arising from satellite internal motion.

2.2.1 Control Torques

On any given satellite or spacecraft, there can be many different possible controllers. Some transfer orbits or provide periodic reboosting. Others govern

the experimental apparatus or deploy and position solar arrays. The controllers considered here focus on attitude. Their objectives are to point the satellite in a commanded direction. Three-axis thrusters provide actuation.

Naturally, feedback controllers are limited by the quality of information available. If the objective is to point in a given direction, then the satellite needs to know how the current attitude compares to the commanded one. In the case of perfect measurements of all system states, the controller acts on “truth” and knows the exact relation between the current state and the goal state. However, since perfect measurements do not exist and sensors rarely observe all the desired quantities we must drive the controller with *estimates* instead of truth quantities. In this configuration, the system operates in a true feedback loop: the controller drives the satellite, whose motion is measured. The measurements are input to the estimator, or filter, to obtain state estimates. The controller acts on these estimates and the loop is closed. Figure 2-3 illustrates one possible closed-loop system configuration.

Three different controllers are described briefly below. They differ in their inputs, methods of actuation, and dynamic models.

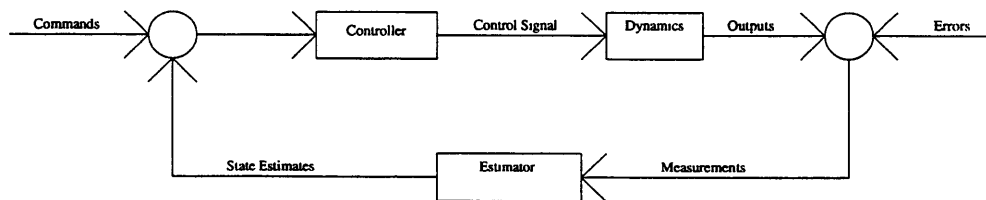


Figure 2-3: Control Loop Including Dynamics and Filter

Proportional Angle and Rate Feedback Control

When satellite motion is sufficiently slow and the control torques are strong compared to the disturbances, it is possible to assume that the Euler dynamics are approximately decoupled about the three rigid body principal axes [10], [13].

In such cases, one can operate independent controllers about each principal axis and ignore spillover effects. We think of the overall control torque vector being composed of three principal axis components:

$$T_{cont} = \begin{bmatrix} T_x \\ T_y \\ T_z \end{bmatrix}. \quad (2.9)$$

A specific control law is now declared for each axis. If both attitude and rate information are available and thrusters actuate, Bryson [10] suggests the following simple proportional feedback law for each axis:

$$T_i = -D_i\dot{\theta}_i - K_i(\theta_i - \theta_{ic}) \quad i = x, y, z. \quad (2.10)$$

Here, the D_i and K_i are control design parameters. If both are positive, then the motion is stable. The angle θ_i represents the estimated Euler angle component about principal axis i when rotating from the local to body frame. Naturally, $\dot{\theta}_i$ is the time rate of change of this angle. The commanded value of the Euler angle is θ_{ic} .

Since the θ_i are Euler angles and depend on hard nonlinear trigonometric computations (see Appendix B), this control law works best when the actual and commanded attitudes are “near” each other. That is, this linear law is better suited for local regulation and should not be used to execute large-angle motion, when nonlinear effects are significant.

If these caveats are heeded and the satellite motion is indeed slow and decoupled, then each principal axis obeys Newton’s second law in angular form: $I_i\ddot{\theta}_i = T_i$. Combining this fundamental relation with Equation (2.10) gives the following closed-loop expression:

$$I_i\ddot{\theta}_i + D_i\dot{\theta}_i + K_i\theta_i = K_i\theta_{ic}. \quad (2.11)$$

As a final comment, Bryson warns that such proportional feedback laws are often unrealistic for thruster control. The explanation is that thrusters often clog or fail when asked to provide a continuous range of output values; it is more realistic to request a fixed discrete thrust value. The section on bang-bang control is meant to provide more realistic control alternative. However, since computer simulations are ideally suited for continuous outputs, this proportional controller and the following quaternion-based scheme can be useful for analysis purposes.

Quaternion Feedback Control

Extending the above Euler angle feedback law to quaternions, Wie, Weiss, and Arapostathis [44] provide the following control law:

$$T_{cont} = -\omega \times I \omega - D\omega - K\bar{q}_e. \quad (2.12)$$

Here, T_{cont} is the full dimension control vector, expressed in the body frame, I is the estimated satellite inertia, and ω is the estimated angular rate. The parameters D and K are now full 3x3 matrices. The attitude error is now expressed by \bar{q}_e , which is the three component partition of the error quaternion q_e between the current attitude estimate q and the commanded attitude q_c :

$$q_e = q \otimes q_c^{-1}. \quad (2.13)$$

Appendix B explains the relationship between Euler angles and the first three quaternion elements.

Unlike the previous feedback control expression, this law is ideally suited for large angle attitude maneuvers since the $-\omega \times I \omega$ term counteracts Euler coupling effects and thus eliminates the principal axis restriction.

Wie, et.al. give several stability, performance, and robustness results for control law (2.12) with proper selection of the parameter matrices D and K .

When used For example, if we choose the parameters as scaled inertia matrices:

$$D = dI \qquad K = kI, \qquad (2.14)$$

with $d > 0$ and $k > 0$, then the control law becomes

$$T_{cont} = -\omega \times I \omega - dI\omega - kI\bar{q}_e. \qquad (2.15)$$

This choice generally revolves the satellite about its eigenaxis for large-angle maneuvers. The eigenaxis is the shortest possible angular path between two given orientations.

If the body rates and error angles are both small, expression (2.15) reduces cleanly to the angle-based law (2.10).

Bang-Bang Control

From a control point of view, the above angle and quaternion feedback laws have two liabilities. The first was already mentioned; continuous-valued action is not always feasible for thrusters. Secondly, control law tuning requires knowledge of the satellite inertia properties, knowledge which may actually be in error. Of course, feedback is a natural robustness measure but at times we may desire a completely model-ignorant controller. Bryson [10] provides a bang-bang control law:

$$T_i = -T_i^* \operatorname{sgn}(\theta_i - \theta_{ic} + \tau_i \dot{\theta}_i) \qquad i = x, y, z. \qquad (2.16)$$

The quantities T_i , θ_i , θ_{ic} , and $\dot{\theta}_i$ have been previously defined. Bang-bang control allows only a single magnitude of thrust; the only decision is when to fire and in which direction. Here, the thrust magnitude is given by T_i^* , sgn is the sign function, and τ_i is a design parameter. If rate is more tolerable than pointing error, we choose τ to be small. Similarly, τ should be chosen large if motion is more harmful than attitude deviation.

With bang-bang controllers, it is often desirable, if not critical, to build

in a “deadband”. A deadband is a region where, should the decision variable magnitude, in this case $|\theta_i - \theta_{ic} + \tau_i \dot{\theta}_i|$, fall below a certain value, the thrusters stay mute. Otherwise, the actuators will operate continuously, wasting fuel, fighting each other, and possibly disrupting the spacecraft mission. In subsequent simulations we will specify a deadband limit α_i , typically between 0.1 and 2 degrees.

The thrust magnitude T_i^* depends on the specific satellite equipment. We typically assume cold gas jets with output of less than one newton.

Note that like the angle feedback controller, this bang-bang algorithm acts on each body axis independently. Therefore, it is advisable to keep the same restrictions: use the law only for smaller angle corrections and in near-principal axis mass distributions.

2.2.2 Gravity Gradient Torque

The first disturbance component is the gravity gradient torque, T_{gg} . It is unique among the four components considered here in that it is wholly deterministic. That is, assuming that both the satellite altitude and attitude are known, this vector disturbance torque is given exactly by a closed-form analytical expression. The other three torque components are stochastic, depending on many independent and unpredictable phenomena and can not be computed analytically.

Gravity gradient torque arises, as the name implies, from the dropoff in gravitational field strength with increasing altitude. That is, the difference in pull on satellite elements that are at unequal distances from the earth’s center can actually create enough moment about the center of mass to induce rotation. Although not a relevant consideration in atmospheric flight, this torque’s magnitude is significant compared to other torques in the relatively benign space environment. In fact, with careful design, the engineer can use gravity gradient torque as an effective control mechanism.

For an orbiting rigid body, one can give a mathematical formula for this torque, expressed in the body frame. Discussions and derivations are available in [10], [27], and [43] so we give the final result here. Essentially, the torque can be computed by integrating a force times moment arm expression across the entire rigid body. A compact expression for this body integral is given by

$$\begin{aligned}
T_{gg} &= T_{gg}(\text{altitude}, q_{bl}) \\
&= 3\omega_{orb}^2 (r_{zenith} \times I r_{zenith}) \\
&= 3\omega_{orb}^2 (T_{bl}(q_{bl})i_z \times I T_{bl}(q_{bl})i_z).
\end{aligned} \tag{2.17}$$

We see the dependence on altitude in the orbit rate term ω_{orb} and the attitude dependence in the local to body transformation $T_{bl}(q_{bl})$. The satellite mass distribution is captured in the inertia matrix I . Here, r_{zenith} is the zenith-pointing unit vector resolved in the body frame. It can be computed by premultiplying its local frame resolution, $i_z = [0, 0, -1]^T$, by the local to body transformation matrix $T_{bl}(q_{bl})$. The exact functional relationship $T_{bl}(q_{bl})$ is given by Equation (B.26).

Equation (2.17) is the formula used to compute the gravity gradient torque in all subsequent numerical simulations.

2.2.3 Solar Radiation Pressure Torque

Unfortunately, the remaining three disturbances are stochastic and cannot be predicted with compact analytical expressions, as was the case with gravity gradient torque. Solar radiation pressure occurs as electromagnetic waves impact the satellite body. The response to radiation of the specific spacecraft materials greatly influence the torque magnitudes. For a multi-material, complex geometry body, it is very difficult to predict the response to a given radiation field, especially if the attitude is uncertain. Further, the local radiation environment will be constantly varying since it depends on factors such as orbit position and solar flare activity. Therefore, in order to simplify analysis, Larson and

Wertz [27] give the following formula to compute the *worst case* solar radiation pressure torque magnitude:

$$|T_{solar}| \leq |T_{solar}|_{max} = \frac{F_s}{c} A_s (1 + q) (\cos(\theta_{inc})) (c_{ps} - c_g) \quad (2.18)$$

where

$$F_s = \text{solar constant} = 1358 \text{ W/m}^2$$

$$c = \text{speed of light} = 3(10)^8 \text{ m/s}$$

$$A_s = \text{satellite surface area in m}^2$$

$$q = \text{reflectance factor} \simeq 0.6$$

$$\theta_{inc} = \text{solar incidence angle, assumed 0 degrees}$$

$$c_{ps} - c_g = \text{distance from center of solar pressure to center of gravity in m}$$

With the quantities in the specified units, the magnitude upper bound is in Newton-meters. Since the bound is in fact a magnitude bound while we need to drive the truth simulation with three-component disturbance vectors, the simulation generates vector components each with a three-sigma value of $(1/\sqrt{3})|T_{solar}|_{max}$.

In order to reasonably approximate the orbit rate frequency content of true solar radiation pressure torque, white noise inputs are processed through a sixth-order bandpass filter (third-order rolloff at low and high frequencies) centered around the satellite orbital frequency. Each torque component is generated independently.

2.2.4 Magnetic Dipole Torque

Another relevant disturbance in satellite attitude dynamics is magnetic dipole torquing. Everything in a satellite from instruments to payload to electrical wiring can create electromagnetic fields, which in turn must interact with the

Earth's own magnetic field. Naturally, such interactions can produce significant forces compared to the satellite inertia, resulting in net disturbance torques. Because of its strength, one may consider the magnetic dipole torque as either a significant disturbance or a useful control mechanism. Focusing on the former consideration, Larson and Wertz give the following formula to estimate the worst case disturbance torque magnitude [27]:

$$|T_{mag}| \leq |T_{mag}|_{max} = DB = \frac{2DM}{R^3} \quad (2.19)$$

where

- D = vehicle residual dipole, typically 1 A-m²
- B = Earth magnetic field in Tesla
- M = Earth magnetic moment = 7.96×10^{15} Tesla-m³
- R = orbit radius in m²

Again, the dimensions of the torque upper bound are Newton-meters.

Just as with the solar radiation pressure torque, we expect the magnetic torque to vary at approximately orbit rate since the satellite will revisit the same local magnetic environment roughly every period. Therefore, we apply the same bandpass filter used to shape the solar torque and tune each torque component to have a three-sigma value of $(1/\sqrt{3})|T_{mag}|_{max}$.

2.2.5 Atmospheric Drag Torque

The final disturbance component we consider is aerodynamic drag due to interactions between the satellite and Earth's atmosphere. Detailed computations of this torque would naturally require extensive fluid dynamics considerations and knowledge of prevailing atmospheric conditions. Since this kind of effort is beyond the scope of this thesis, we again make use of a Larson and Wertz [27]

worst case approximation. The torque magnitude upper bound is

$$|T_{aero}| \leq |T_{aero}|_{max} = \frac{1}{2}\rho C_d A V^2 (c_{pa} - c_g) \quad (2.20)$$

where

ρ = atmospheric density in kg/m^3

C_d = drag coefficient, taken as 2

A = satellite surface area normal to velocity in m^2

V = satellite velocity magnitude in m/s

$c_{pa} - c_g$ = distance from center of aerodynamic pressure to center of gravity in m

As with the other formulae, the torque magnitude is computed in Newton-meters.

Note that there are two parameters, ρ and V , in Equation (2.20) that depend on orbit altitude. Not surprisingly, it turns out that of the three stochastic torques just considered, atmospheric drag torque is the most sensitive to orbit radius. At lower altitudes, say around 300 km, it has the dominant magnitude, while at altitudes of around 800 km, it has fallen off and is comparable to the other two.

Since the drag torque does not depend on orbit position as much as satellite bandwidth, we obtain simulation disturbances by low pass filtering white noise through a fourth order filter that cuts off around orbit frequency. Again, the component magnitudes are scaled by $1/\sqrt{3}$.

2.3 Measurements

With the truth dynamics described, we can now discuss how the sensors observe truth quantities. Each outputs a reading of the truth quantity corrupted by one or more error signals.

2.3.1 Gyroscopes

Strapdown gyroscopes are body mounted inertial sensors and as such, measure body relative to inertial frame angular velocity. However, as real engineering instruments, gyros introduce measurement errors. Typically, there is a time-correlated low frequency component b_g called a “gyro bias”. Time variation in this error signal is termed “gyro drift”. There is an additional white, or time-uncorrelated, noise component v_g . In continuous time models, this term is known as “angle random walk”. See Section A.3 for a detailed discussion of these error terms with a numerical example. In equation form, we express the gyro measurement as

$$\begin{aligned}\omega_{gyro} &= \omega_{bi} + b_g + v_g \\ &= \omega_{bl} + T_{bl}\omega_{ii}^l + b_g + v_g.\end{aligned}\tag{2.21}$$

The second relation merely restates Equation (2.5) and will be highly relevant to the dynamic filter design covered in the next chapter.

Although gyro bias behavior is very mysterious and without exact truth models, the navigation community often considers the truth bias to generally follow a Gauss-Markov stochastic process

$$\dot{b}_g = A_g b_g + G_g w_g.\tag{2.22}$$

Again, consult Section A.3 for a discussion of the terms and units in Equation (2.22).

2.3.2 GPS Attitude

For the purposes of this research, we assume the attitude (GPS) measurement is of the spacecraft orientation with respect to the local frame. That is, GPS measures q_{bl} , not q_{bi} . Of course, GPS has its own error sources which prevent us from taking the GPS receiver output as truth. Conceptually, the attitude error

consists of two components, just as in the gyro case. There is a time correlated error and an independent white error which we envision as combining in an additive fashion to form a total error E_{GPS} :

$$E_{GPS} = E_{correlated} + E_{white}. \quad (2.23)$$

The correlated error can derive from antennae line biases, antennae array flexure, phase center variation, and signal transmission reflection effects [36]. This latter phenomenon is labeled “GPS multipath error” and like the other error sources, is a subject of ongoing research.

The combined correlated and white errors perturb a perfect measurement of q_{bl} by an error quaternion q_{err} , which is conceptually representative of the combined error in Equation (2.23):

$$E_{GPS} \mapsto q_{err}. \quad (2.24)$$

In this setting it is inappropriate to think of the error as entering the quaternion measurement in as strict additive sense, as in (2.21) for gyros, since the GPS receiver output must be a feasible attitude. Therefore, the measurement is an attitude perturbation of the true attitude q_{bl} :

$$q_{GPS} = q_{err} \otimes q_{bl}. \quad (2.25)$$

(See Appendix B for a discussion of attitude fundamentals, including quaternion composition). Mathematically, we generate simulated attitude errors by creating correlated and white Euler angle sequences which perturb the measurement from truth. These angle sequences are then combined into an error quaternion according to Equation (B.19) and then combined with q_{bl} as in Equation (2.25) to form a “truth” GPS measurement.

Just as with the gyro bias, the GPS time correlated error may follows a

Gauss-Markov stochastic process for approximation purposes

$$\dot{b}_{GPS} = A_{GPS}b_{GPS} + G_{GPS}w_{GPS}, \quad (2.26)$$

where b_{GPS} is the time correlated error, and (A_{GPS}, G_{GPS}) is a linear system that shapes a white noise input w_{GPS} .

2.4 Summary

This chapter has laid out the concepts, terminology, and relations necessary to generate a reasonable truth model of satellite motion. When generating truth data in numerical simulation form, the core attention goes to integrating the kinematic and dynamics equations of motion, Equations (2.4) and (2.6), respectively. Other than arbitrary initial conditions, the only other input to these relations is the torque term T . Depending on the desired scenario, T can have two components as expressed in Equation (2.7). If a controller is active, then T_{cont} must be computed in real time according one of the laws described in Section 2.2.1. If the disturbance term T_{dist} is to be used, then Sections 2.2.2 through 2.2.5 give the appropriate methods. It is important to note that of the four disturbance torque components, only gravity gradient torque must be computed in real time; the other three and be precomputed and stored for later use.

The only remaining task is to form the truth measurements, which will serve as filter inputs. If rate gyro outputs are available to the filter, then we employ Equation (2.21). This shows the corruption of the true body-to-inertial rate by a time-correlated bias term, given in (2.22), and a white angle random walk term. Appendix B gives a more complete gyro background. The alternative measurement is a GPS attitude reading. Like the gyro output, the truth quantity is corrupted, according to relation (2.25), with a time-correlated component and a white component. The former is typically described by Equation (2.26).

Dynamics	
$\dot{q}_{bl} = \frac{1}{2}\Omega(\omega_{bl})q_{bl}$	Eqn. (2.4)
$\dot{\omega}_{bl} = I^{-1}(T - \omega_{bl} \times I \omega_{bl}) + \omega_{bl} \times \omega_{li}$	Eqn. (2.6)
$T = T_{cont} + T_{dist}$	Eqn. (2.7)
T_{cont} from control law	Eqn. (2.10), (2.12), or (2.16)
$T_{dist} = T_{gg} + T_{solar} + T_{mag} + T_{aero}$	Eqn. (2.8)
$T_{gg} = 3\omega_{orb}^2(T_{bl}(q_{bl})i_z \times I T_{bl}(q_{bl})i_z)$	Eqn. (2.17)
T_{solar} from bandpass filter	Magnitude from Eqn. (2.18)
T_{mag} from bandpass filter	Magnitude from Eqn. (2.19)
T_{aero} from lowpass filter	Magnitude from Eqn. (2.20)
Measurements	
$\omega_{gyro} = \omega_{bl} + T_{bl}\omega_{li}^l + b_g + v_g$	Eqn. (2.21)
$\dot{b}_g = A_g b_g + G_g w_g$	Eqn. (2.22)
$q_{GPS} = q_{err} \otimes q_{bl}$	Eqn. (2.25)
$\dot{b}_{GPS} = A_{GPS} b_{GPS} + G_{GPS} w_{GPS}$	Eqn. (2.26)

Table 2.1: Key Truth Simulation Relations

Table 2.1 summarizes the key truth model relations.

Chapter 3

Filter Designs

We now lay out the specific estimator design differences previewed in Section 1.1. The filter algorithms are obtained by taking the principles of that section, extending them to fit the truth dynamics as explained in Chapter 2, and applying the extended Kalman filter methodology of Section C.2.

Throughout the estimation process, attitude is maintained in quaternion form. Appendix B is included to give a complete introduction to the dominant attitude representations, their relative merits, and their interrelations. The quaternion is specifically chosen in this setting because of its low order compared to direction cosine matrices and its singularity-free propagation (unlike Euler angles). The consequence of this choice is a modified covariance scheme that will apply to both model and nonmodel filters.

Throughout this chapter, references are made to Appendices B and C. Although many authors choose to include this material in the body of their research, they have been separated here to maintain the flow of the material and enable a more complete treatment of these topics. Also, many of the equations presented here are excerpted directly from or inspired by Lefferts, Markley, and Shuster's landmark paper on quaternions for attitude determination [28]. These expressions will be impossible to verify without consulting this reference and/or the Appendices.

Section 3.1 begins by giving the full state, covariance, and update relations

for the model filter. Recall that this estimator is centered around the vehicle dynamic equations of motion and provides periodic gyro and GPS updating. Section 3.2 continues by describing the competing nonmodel filter. Since this approach does not employ the Euler equations or disturbance modeling, it must rely solely on the system measurements to estimate attitude. Here, gyro outputs will be taken as a truth-like system input with GPS offering a periodic update.

3.1 Model Filter Design

This section presents the relations describing the model filter algorithm. It is obtained by merging the truth model of Chapter 2 with the generic filter algorithm of Section C.2.

3.1.1 State and Covariance Propagation

With the satellite equations of motion presented in the previous chapter, we review the model filter design first. Its state vector consists of the body relative to local attitude, the body relative to local angular rate, and the time-correlated measurement errors for the gyros and GPS:

$$x(t) \equiv \begin{bmatrix} q_{bl}(t) \\ \omega_{bl}(t) \\ b_b(t) \\ b_{GPS}(t) \end{bmatrix}. \quad (3.1)$$

The nonlinear filter plant model equations are given by citing Equations (2.4), (2.6), (2.17), 2.22), and (2.26), and take the generic form $\dot{x}(t) = f(x(t), t) + g(t)w(t)$:

$$\begin{aligned} \dot{q}_{bl} &= \frac{1}{2}\Omega(\omega_{bl})q_{bl} \\ \dot{\omega}_{bl} &= I^{-1}(T_{gg} - \omega_{bl} \times I \omega_{bl}) + \omega_{bl} \times \omega_{li} + I^{-1}T_{cont} + I^{-1}T_{dist} \end{aligned} \quad (3.2)$$

$$\begin{aligned}\dot{b}_g &= A_g b_g + G_g w_g \\ \dot{b}_{GPS} &= A_{GPS} b_{GPS} + G_{GPS} w_{GPS}.\end{aligned}$$

Note that the general torque term T in Equation (3.2), has been expanded according to $T = T_{gg} + T_{cont} + T_{dist}$ and that we have distributed out the control T_{cont} and stochastic disturbance T_{dist} to obviate the *total* system control input T_{cont} and disturbance input $[T_{dist}^T, w_g^T, w_{GPS}^T]^T$. The analytical gravity gradient disturbance term T_{gg} is not pulled out, as it contributes to the deterministic system evolution.

The equations of (3.2) comprise the filter's truth model. Propagation between measurements is accomplished numerically integrating the noise-free dynamics:

$$\begin{aligned}\dot{\hat{q}}_{bl} &= \frac{1}{2}\Omega(\hat{\omega}_{bl})\hat{q}_{bl} \\ \dot{\hat{\omega}}_{bl} &= I^{-1}(T_{gg}(\hat{q}_{bl}) - \hat{\omega}_{bl} \times I \hat{\omega}_{bl}) + \hat{\omega}_{bl} \times \hat{\omega}_{li} + I^{-1}T_{cont} \\ \dot{\hat{b}}_g &= A_g \hat{b}_g \\ \dot{\hat{b}}_{GPS} &= A_{GPS} \hat{b}_{GPS}.\end{aligned}\tag{3.3}$$

During state propagation the KF and EKF algorithms maintain an approximation of the state estimate error covariance matrix $P(t)$,

$$\begin{aligned}P(t) &\equiv E[\tilde{x}(t)\tilde{x}^T(t)] \\ \tilde{x}(t) &\equiv x(t) - \hat{x}(t)\end{aligned}\tag{3.4}$$

(See Appendix C for a broader discussion of KF and EKF filter methodology). Because of our choice of attitude state, we will need to modify the error covariance definition. Recall that the attitude partition q_{bl} of the state vector is a unit norm quaternion. Errors in this quantity do not act as simple arithmetic additions and subtractions but as quaternion compositions. For instance, Equation (2.25) shows measurement corruption of truth using quaternion composition,

not the traditional arithmetic addition of the form $q_{GPS} = q_{bl} + q_{err}$. Furthermore, the authors of [28] show how the unit norm constraint on quaternion objects induces singularities in what would otherwise be a positive definite matrix $P(t)$. Therefore, Lefferts, et. al. develop an EKF scheme which maintains the state vector as in (3.1) for state propagation but modifies its definition for error covariance calculation and measurement update. This redefinition effectively reduces the dimension of $P(t)$ by 1 while making its terms more physically intuitive. Since the quaternion attitude is present in both the model and non-model filters, the following filter covariance and update modifications will be used in both estimator designs.

We begin by defining a hypothetical reduced order state vector $\bar{x}(t)$ as follows:

$$\bar{x}(t) \equiv \begin{bmatrix} \delta q(t) \\ \omega_{bl}(t) \\ b_g(t) \\ b_{GPS}(t) \end{bmatrix}. \quad (3.5)$$

The departure from (3.1) is the replacement of $q_{bl}(t)$ with $\delta q(t)$. The latter is a 3x1 vector the resides in the first three elements of the estimation error quaternion q_{err} ,

$$q_{err} = \begin{bmatrix} \delta q \\ \delta q_4 \end{bmatrix}. \quad (3.6)$$

The attitude estimation error q_{err} , like the usual arithmetic error, relates the estimated attitude \hat{q}_{bl} and truth attitude q_{bl} according to,

$$q_{bl} = q_{err} \otimes \hat{q}_{bl}. \quad (3.7)$$

If the estimation error is small, say, on the order of a few degrees or less, then Equation (B.19) can be used to show that δq is basically proportional to the

error expressed as a small angle Euler sequence in radians:

$$\delta q \simeq \frac{1}{2} \begin{bmatrix} \phi_{err} \\ \theta_{err} \\ \psi_{err} \end{bmatrix}. \quad (3.8)$$

If the filter covariance considers arithmetic errors in δq instead of q_{bl} , then its interpretation as three small angles is more physically intuitive than quaternion composition. Instead of calculating second moments for the dependent and physically hard to interpret elements of q_{bl} , we calculate them for the three independent degrees of freedom, ϕ , θ , and ψ , which are sufficient to describe any attitude error. Thus, we define a reduced order covariance $\tilde{P}(t)$ whose only distinction from that in Equation (3.4) is that $\bar{x}(t)$ supplants $x(t)$. As such, the reduced covariance's formal definition is

$$\tilde{P}(t) \equiv E[(\bar{x}(t) - E[\bar{x}(t)])(\bar{x}(t) - E[\bar{x}(t)])^T]. \quad (3.9)$$

Since the uppermost partition of $\bar{x}(t)$ is in fact an error, then $E[\delta q(t)] = 0_{3 \times 1}$ in Equation (3.9) since we typically must assume an unbiased EKF. The authors of [28] demonstrate that the traditional and reduced order covariances are related by the similarity transformation

$$\begin{aligned} \tilde{P}(t) &= S^T(\hat{q}_{bl}(t))P(t)S(\hat{q}_{bl}(t)) \\ P(t) &= S(\hat{q}_{bl}(t))\tilde{P}(t)S^T(\hat{q}_{bl}(t)), \end{aligned} \quad (3.10)$$

with the following two matrix definitions:

$$S(\hat{q}_{bl}(t)) = \begin{bmatrix} \Xi(\hat{q}_{bl}(t)) & 0_{4 \times 3} & 0_{4 \times 3} & 0_{4 \times 3} \\ 0_{3 \times 3} & I_{3 \times 3} & 0_{3 \times 3} & 0_{3 \times 3} \\ 0_{3 \times 3} & 0_{3 \times 3} & I_{3 \times 3} & 0_{3 \times 3} \\ 0_{3 \times 3} & 0_{3 \times 3} & 0_{3 \times 3} & I_{3 \times 3} \end{bmatrix} \quad (3.11)$$

and

$$\Xi(q) \equiv \begin{bmatrix} q_4 & -q_3 & q_2 \\ q_3 & q_4 & -q_1 \\ -q_2 & q_1 & q_4 \\ -q_1 & -q_2 & -q_3 \end{bmatrix}. \quad (3.12)$$

Looking at the block structure of $S(\hat{q}_{bl}(t))$, we see that the only action occurs in the attitude partition (upper left corner). The invariance of the other states to transformation is consistent with their invariance between definitions (3.1) and (3.5).

Since covariance manipulation is an intimate part of filtering, the propagation and update relations must accommodate the reduced order covariance $\tilde{P}(t)$. Typically, we carry the covariance between measurements according to Equations (C.21), (C.25), and (C.26). Lefferts, et. al. show, using two independent arguments, that $\tilde{P}(t)$ evolves in a similar manner. Specifically,

$$\dot{\tilde{P}}(t) = \tilde{F}(\hat{x}(t), t)\tilde{P}(t) + \tilde{P}(t)\tilde{F}^T(\hat{x}(t), t) + \tilde{G}(t)Q(t)\tilde{G}^T(t). \quad (3.13)$$

The Jacobian matrix $\tilde{F}(\hat{x}(t), t)$ is obtained by differentiating $\dot{\hat{x}}(t)$ with respect to $\bar{x}(t)$ subject to (3.2). Note however, that the partial derivative evaluation is made at $\hat{x}(t)$, instead of $\hat{\hat{x}}(t)$, since $\hat{x}(t)$ contains our best knowledge of the current system state. That is,

$$\tilde{F}(\hat{x}(t), t) = \left. \frac{\partial \dot{\hat{x}}(t)}{\partial \bar{x}(t)} \right|_{\hat{x}(t)} \quad (3.14)$$

It is critical to keep in mind that $x(t)$ and $\hat{x}(t)$ are the actual system state and estimate, respectively. The variable $\bar{x}(t)$ is merely employed to define a reduced order covariance. As such, the partials must be taken considering the “dynamics” of $\bar{x}(t)$. Computation of these derivatives is not a simple matter and details are left to reference [28] or are omitted here.

Lefferts, et. al. computed the partial derivatives analytically, but only for

the case of a kinematic, or nonmodel filter. Puri, Giustino, and this author extended the analysis to the model filter case to obtain

$$\tilde{F}(\hat{x}(t), t) = \begin{bmatrix} [\omega_{bl}]_X & \frac{1}{2}I_{3 \times 3} & 0_{3 \times 3} & 0_{3 \times 3} \\ M_1(\hat{q}_{bl}(t)) & M_2(\hat{q}_{bl}(t)) & 0_{3 \times 3} & 0_{3 \times 3} \\ 0_{3 \times 3} & 0_{3 \times 3} & A_g & 0_{3 \times 3} \\ 0_{3 \times 3} & 0_{3 \times 3} & 0_{3 \times 3} & A_{GPS} \end{bmatrix}, \quad (3.15)$$

where the cross product matrix

$$[v]_X = \begin{bmatrix} 0 & v_3 & -v_2 \\ -v_3 & 0 & v_1 \\ v_2 & -v_1 & 0 \end{bmatrix} \quad (3.16)$$

appears in the upper left block. The M_1 and M_2 matrices are defined as follows:

$$M_1(\hat{q}_{bl}) = 6\hat{\omega}_{orb}^2([T_{bl}(\hat{q}_{bl})i_z]_X I - [IT_{bl}(\hat{q}_{bl})i_z]_X)[T_{bl}(\hat{q}_{bl})i_z]_X, \quad (3.17)$$

and

$$M_2(\hat{q}_{bl}) = I^{-1}([I\hat{\omega}_{bi}]_X - [\hat{\omega}_{bi}]_X I) - [\hat{\omega}_{li}]_X, \quad (3.18)$$

where the variables comprising M_1 are defined as in Equation (2.17).

The blocks in the first row of (3.15) come from the kinematic relationship between q_{bl} and w_{bl} as detailed in the first line of Equation (3.2). The matrix M_1 accounts for the dependence of rate evolution on attitude through gravity gradient effects. The M_2 matrix expresses rate dependence on rate. Two factors contribute to this term: Euler coupling of rigid bodies (2.2), and body rate frame transformations (2.5). The remaining A_g and A_{GPS} blocks in (3.15) are straightforward linearizations of the Gauss-Markov instrument bias error models.

The matrix $\tilde{G}(t)$ in Equation (3.13) plays the same roll as $G(t)$ in the usual covariance propagation equation; it indicates how white disturbances enter the

filter model dynamics. Since T_{dist} , w_g , and w_{GPS} all enter (3.2) in a linear fashion, $\tilde{G}(t)$ has the straightforward form

$$\tilde{G}(t) = \begin{bmatrix} 0_{3 \times 3} & 0_{3 \times 3} & 0_{3 \times 3} \\ I^{-1} & 0_{3 \times 3} & 0_{3 \times 3} \\ 0_{3 \times 3} & G_g & 0_{3 \times 3} \\ 0_{3 \times 3} & 0_{3 \times 3} & G_{GPS} \end{bmatrix}. \quad (3.19)$$

The all zero top row reflects the lack of white noise directly feeding attitude integration in (3.2).

Finally, we need a driving disturbance intensity matrix and use the usual definition as seen in Equation (C.21). For our system, we take the intensity of the vector $[T_{dist}^T, w_g^T, w_{GPS}^T]^T$ to obtain

$$Q(t) = \begin{bmatrix} Q_{dist} & 0_{3 \times 3} & 0_{3 \times 3} \\ 0_{3 \times 3} & Q_g & 0_{3 \times 3} \\ 0_{3 \times 3} & 0_{3 \times 3} & Q_{GPS} \end{bmatrix}. \quad (3.20)$$

3.1.2 Measurement Update

With state and covariance propagation covered, we turn next to the measurement update relations. Considering the gain and covariance, we note that the usual EKF algorithm employs the following relations when a measurement z_k becomes available at time t_k ,

$$\begin{aligned} K_k &= P_k^- H_k^T (H_k P_k^- H_k^T + R_k)^{-1} \\ P_k^+ &= (I - K_k H_k) P_k^- (I - K_k H_k)^T + K_k R_k K_k^T. \\ &= (I - K_k H_k) P_k^- \end{aligned} \quad (3.21)$$

Here, K_k is the filter gain, P_k^- is the error covariance estimate just prior to measurement incorporation, R_k is the discrete white noise measurement covariance matrix, and H_k , defined in Equation (C.28), results from differentiating the

nonlinear measurement equations with respect to the state vector. See Section C.2 for additional details.

Since our filter operates with a full order state but a reduced order covariance, Equations (3.21) must be modified accordingly. Lefferts, et. al. replace P_k^- with \tilde{P}_k^- to stay notationally consistent with (3.13). A matrix \tilde{H}_k is obtained by differentiating the nonlinear measurement equations with respect to \bar{x} and evaluating at \hat{x}_k^- or by differentiating with respect to x , evaluating at \hat{x}_k^- , and then performing the conversion

$$\tilde{H}_k = H_k S(\hat{q}_k^-). \quad (3.22)$$

The white noise covariance matrix R_k remains unaltered. The resulting modified update equations mirror the standard update,

$$\begin{aligned} \tilde{K}_k &= \tilde{P}_k^- \tilde{H}_k^T (\tilde{H}_k \tilde{P}_k^- \tilde{H}_k^T + R_k)^{-1} \\ \tilde{P}_k^+ &= (I - \tilde{K}_k \tilde{H}_k) \tilde{P}_k^- (I - \tilde{K}_k \tilde{H}_k)^T + \tilde{K}_k R_k \tilde{K}_k^T. \end{aligned} \quad (3.23)$$

The old and new gain, K_k and \tilde{K}_k , respectively, are related according to

$$K_k = S(\hat{q}_k^-) \tilde{K}_k. \quad (3.24)$$

Before revealing the form of the actual state update, consider the sensors available to the filter. The first is the inertial frame-referenced body rate output of the gyro. We take the gyro output as our measurement exactly. That is,

$$\omega_{meas} = \omega_{gyro}. \quad (3.25)$$

Equation (2.21) in the preceding section described this measured quantity in terms of q_{bl} and ω_{bl} . As part of the updating process, we need an *a priori* estimate of the gyro measurement. Taking expectations on the right hand side

of (2.21) and noting that q_{bl} and ω_{li}^l are independent quantities, we have

$$\begin{aligned}\hat{\omega}_{meas} &= \hat{\omega}_{bl}^- + \hat{b}_g^- \\ &= \hat{\omega}_{bl}^- + T_{bl}(\hat{q}_{bl}^-)\hat{\omega}_{li}^l + \hat{b}_g^-, \end{aligned} \quad (3.26)$$

were the filter must include a parameter that estimates ω_{orb} as part of computing ω_{li}^l . By differentiating (2.21) with respect to \bar{x} , and evaluating at \hat{x}_k^- , it can be shown that [36]

$$\tilde{H}_{gyro} = \begin{bmatrix} -2[\hat{\omega}_{li}^-]_X & I_{3 \times 3} & I_{3 \times 3} & 0_{3 \times 3} \end{bmatrix}. \quad (3.27)$$

The first block shows the effect of the current attitude in relating the body and inertial frames. The identity matrices show the presence of the body relative to local angular rate and the gyro bias.

For the white covariance matrix R_k , we use a discretized value of the continuous time gyro angle random walk (See Appendix A). This choice of R_k is standard and is not a consequence of the reduced order covariance scheme.

The other measurement is attitude reported by a GPS receiver. Equation (2.25) shows the relation between the true GPS measurement and the truth quantity q_{bl} . Rather than take q_{GPS} as our literal measurement, however, we premultiply it by the arbitrary matrix $\Xi^T(q^*(\hat{b}_{GPS}^-) \otimes \hat{q}_{bl}^-)$ to obtain the modified measurement

$$q_{meas} = \Xi^T(q^*(\hat{b}_{GPS}^-) \otimes \hat{q}_{bl}^-)q_{GPS}. \quad (3.28)$$

Here, the quaternion $q^*(\hat{b}_{GPS}^-)$ is the small angle error quaternion estimate taken by applying relation (B.19) to the GPS multipath estimate \hat{b}_{GPS}^- .

This technique is based on a combination of relations from [28] and [33]. To show the advantage of employing this pseudo-measurement, consider two arbitrary quaternions, q_1 and q_2 , that are nearly aligned but differ by a small error quaternion q_{err} :

$$q_1 = q_{err} \otimes q_2. \quad (3.29)$$

Lefferts, et. al. show that the following holds:

$$\delta q = \Xi^T(q_2)q_1 \quad (3.30)$$

where Equation (3.6) still applies.

Now recalling Equation (3.8) and the earlier interpretation of quaternion and GPS errors as small angle Euler sequences, we see that the multiplication in (3.28) exposes the measurement difference between the *a priori* attitude estimate and the *actual* GPS measurement. This difference in turn, helps to expose the measurement *error* itself, much as the standard Kalman applies its gain to the measurement innovations, defined as the difference between the actual and expected sensor outputs. We are simply expressing the measurement innovation in a quaternion error format.

Based on this discussion, we can form the necessary *a priori* estimate of the modified measurement itself:

$$\begin{aligned} \hat{q}_{meas} &= E(q_{meas}) \\ &= \Xi^T(q^*(\hat{b}_{GPS}^-) \otimes \hat{q}_{bl}^-)E(q_{GPS}) \\ &= \Xi^T(q^*(\hat{b}_{GPS}^-) \otimes \hat{q}_{bl}^-)[q^*(\hat{b}_{GPS}^-) \otimes \hat{q}_{bl}^-] \\ &= 0_{3 \times 1} \end{aligned} \quad (3.31)$$

This expectation naturally turns out to be zero, since the expected GPS measurement *error* is zero and the *a priori* GPS receiver output, $E(q_{GPS}) = q^*(\hat{b}_{GPS}^-) \otimes \hat{q}_{bl}^-$, is “expected” to be accurate. Note that in (3.31) we have employed the easily verifiable identity $\Xi^T(q)q = 0_{3 \times 1}$. The inclusion of the *a priori* multipath error estimate b_{GPS} in predicting the receiver output is completely analogous to including the *a priori* estimate of gyro bias in predicting the gyro measurement, as seen in Equation (3.26).

If we differentiate the right hand side of (3.28) with respect to the state

vector considering (2.25) and (3.8), and evaluate at \hat{x}_k^- , we obtain

$$H_{GPS} = \begin{bmatrix} \Xi^T(q^*(\hat{b}_{GPS}^-) \otimes \hat{q}_{bl}^-) & 0_{3 \times 3} & 0_{3 \times 3} & \frac{1}{2}I_{3 \times 3} \end{bmatrix}. \quad (3.32)$$

The Ξ^T block comes from the arbitrary premultiplication matrix. The half identity shows the presence of the time correlated GPS error b_{GPS} as a small Euler angle sequence. To obtain the desired \tilde{H} , matrix, we employ (3.22) to get

$$\tilde{H}_{GPS} = H_{GPS}S(\hat{q}_{bl}^-). \quad (3.33)$$

If we think of the white GPS error as another small angle Euler sequence, then we use the following discrete measurement noise covariance:

$$R_{GPS} = \frac{1}{4}\text{Cov}(v_{GPS}). \quad (3.34)$$

The $1/4$ coefficient comes from squaring the coefficient in (3.8). Here, v_{GPS} is the white component of GPS error.

Now that the measurement sensitivity calculations and gain and covariance update relations are laid out for both measurement types, we turn finally to the actual measurement update. The typical EKF update is

$$\hat{x}_k^+ = \hat{x}_k^- + K_k(z_k - h_k(\hat{x}_k^-)), \quad (3.35)$$

where z_k is the measurement and $h_k(\hat{x}_k^-)$ is its *a priori* estimate. Since our filter design uses a reduced order covariance based on the reduced state $\bar{x}(t)$, we first update $\bar{x}(t)$ itself, as shown here

$$\hat{\bar{x}}_k^+ = \hat{\bar{x}}_k^- + \tilde{K}_k(z_k - h_k(\hat{\bar{x}}_k^-)) \quad (3.36)$$

Note that we still use the full state \hat{x}_k^- in predicting z_k , however.

An alternative form of Equation (3.36) is

$$\begin{aligned}\Delta \hat{x}_k &= \tilde{K}_k(z_k - h_k(\hat{x}_k^-)) \\ \Delta \hat{x}_k &= \hat{x}_k^+ - \hat{x}_k^-, \end{aligned} \quad (3.37)$$

where the *a priori* estimate \hat{x}_k^- and the *a posteriori* estimate \hat{x}_k^+ have been combined into one Δ term.

Recall that the only difference between \bar{x} and x is the attitude error term in the first partition. The *a priori* estimate of δq is simply zero since the filter is approximately unbiased and we have no better choice then to assume that $\hat{q}_{bl,k}^-$ is accurate. Hence,

$$\hat{\delta q}_k^- \equiv 0_{3 \times 1} \quad \rightarrow \quad \Delta \hat{\delta q}_k \equiv \hat{\delta q}_k^+. \quad (3.38)$$

The other state partitions behave in the usual manner:

$$\begin{aligned}\Delta \hat{\omega}_{bl,k} &= \hat{\omega}_{bl,k}^+ - \hat{\omega}_{bl,k}^- \\ \Delta \hat{b}_{g,k} &= \hat{b}_{g,k}^+ - \hat{b}_{g,k}^- \\ \Delta \hat{b}_{GPS,k} &= \hat{b}_{GPS,k}^+ - \hat{b}_{GPS,k}^-. \end{aligned} \quad (3.39)$$

Once \hat{x}_k^+ is obtained, every state save attitude updates according to Equation (3.39). Since $\hat{\delta q}_k^+$ is an estimate of the small angle estimation error, we augment with unity to form a correction quaternion $q_{corr,k}$, recalling that small angle quaternions have a fourth element close to 1,

$$q_{corr,k} = \begin{bmatrix} \hat{\delta q}_k^+ \\ 1 \end{bmatrix}. \quad (3.40)$$

We then renormalize to form a proper, unit norm quaternion

$$\frac{q_{corr,k}}{\sqrt{q_{corr,k}^T q_{corr,k}}} \quad \rightarrow \quad q_{corr,k}. \quad (3.41)$$

The update of the full attitude estimate is then straightforward:

$$\hat{q}_{bl,k}^+ = q_{corr,k} \otimes \hat{q}_{bl,k}^- \quad (3.42)$$

and is consistent with Equation (3.7). This attitude update object $q_{corr,k}$ is perfectly analogous to the “ Δ ” states in Equation (3.39).

In the course of filter operation, we will encounter three possible update scenarios: gyro measurements alone, GPS measurements alone, or simultaneous gyro and GPS measurements:

$$z_k = \omega_{meas}, q_{meas}, \text{ or } \begin{bmatrix} q_{meas} \\ \omega_{meas} \end{bmatrix}. \quad (3.43)$$

For each case there are three corresponding *a priori* estimates:

$$h_k(\hat{x}_k^-) = \hat{\omega}_{meas}, 0_{3 \times 1}, \text{ or } \begin{bmatrix} 0_{3 \times 1} \\ \hat{\omega}_{meas} \end{bmatrix}, \quad (3.44)$$

and three corresponding measurement sensitivity matrices:

$$\tilde{H}_k = \tilde{H}_{gyro}, \tilde{H}_{GPS}, \text{ or } \begin{bmatrix} \tilde{H}_{GPS} \\ \tilde{H}_{gyro} \end{bmatrix}. \quad (3.45)$$

However, the overall update relations, formed by the union of Equations (3.23), (3.37), (3.39), and (3.42), are the same for any measurement scenario.

Disturbance Torque States

The preceding sections laid out the model filter design to estimate attitude, body rates, gyro biases, and GPS errors. However, the model-based approach is not limited to these filter states only. At times, we may wish to estimate the disturbance torque inputs to the plant dynamics. Unlike the nonmodel approach, the model filter allows a convenient method for doing so.

Consider again the second line of Equation (3.2) which shows the body rate derivative driven by two external torque terms. The first is T_{cont} , which represents the attitude controller’s system inputs. This quantity is generally known since control commands sent to the thruster actuators will also be available for estimator use. The second input term T_{dist} accounts for “everything else” that induces satellite motion and is generally unknown. As discussed in Chapter 2, we consider three stochastic disturbance torque components: solar radiation pressure, magnetic dipole effects, and atmospheric drag (gravity gradient effects are analytically modeled in the T_{gg} term).

These disturbance phenomena all represent a threat to the model-based filtering approach. They cannot be exactly represented by low order linear filters and therefore subtract from the dynamic model’s ability to provide useful information. Even worse, if the disturbance torques are significant, then these unknown system inputs might lead the estimator away from truth and induce filter divergence, an unacceptable result since the controller typically relies on the attitude estimator for accurate knowledge of the truth plant. A divergent filter jeopardizes the stability of the closed-loop control system.

Fortunately, we have a means of considering the unknown disturbance signals *other* than the angular rate filter covariance Q_{dist} . That variable is a useful design tool for limiting the estimator’s faith in its prediction of the rate dynamics. However, the assumption here is that any system disturbances are white, that is, containing all frequencies. Further, no attempt is made to estimate the exact disturbance values for vehicle propagation purposes.

Therefore, we can augment the filter state vector to include a disturbance torque vector estimate:

$$x(t) \equiv \begin{bmatrix} q_{bl}(t) \\ \omega_{bl}(t) \\ b_b(t) \\ b_{GPS}(t) \\ T_d(t), \end{bmatrix}. \quad (3.46)$$

where the new T_d partition enters the rate dynamics as follows,

$$\dot{\omega}_{bl} = I^{-1}(T_{gg} - \omega_{bl}X I \omega_{bl}) + \omega_{bl}X \omega_{li} + I^{-1}T_{cont} + I^{-1}T_d + I^{-1}T_{dist}. \quad (3.47)$$

We still represent a conceptual white disturbance T_{dist} but it simply echoes the continuing existence of the design variable Q_{dist} . However, the new player is T_d . Equation (3.47), illustrates that if T_d contained a reasonable estimate of the system disturbances, then it should enhance the propagation of ω_{bl} .

Typically, disturbance torques are low frequency, low magnitude phenomena. As explained in Chapter 2, the truth simulation employs bandpass and lowpass filtering to generate approximate disturbance signals. Therefore, it makes sense to employ a traditional first order Gauss-Markov model for the torque state:

$$\dot{T}_d = A_d T_d + G_d w_d. \quad (3.48)$$

The matrices A_d and G_d are design parameters. Using the general relations of Appendix A, we can tune these matrices to emulate suitable lowpass filters with desired steady-state characteristics. For first cut purposes, this approximation should be suitable since disturbance phenomena are typically bandlimited.

Since we are adding a system state which interacts with the rate dynamics, we must modify the filter covariance expressions appropriately. The state equation Jacobian is now larger and has a new I^{-1} term to account for the T_d state feeding the rate and a A_d term to consider the stable torque model:

$$\tilde{F}(\hat{x}(t), t) = \begin{bmatrix} [\omega_{bl}]X & \frac{1}{2}I_{3x3} & 0_{3x3} & 0_{3x3} & 0_{3x3} \\ M_1(\hat{q}_{bl}(t)) & M_2(\hat{q}_{bl}(t)) & 0_{3x3} & 0_{3x3} & I^{-1} \\ 0_{3x3} & 0_{3x3} & A_g & 0_{3x3} & 0_{3x3} \\ 0_{3x3} & 0_{3x3} & 0_{3x3} & A_{GPS} & 0_{3x3} \\ 0_{3x3} & 0_{3x3} & 0_{3x3} & 0_{3x3} & A_d \end{bmatrix}, \quad (3.49)$$

The $\tilde{G}(t)$ and $Q(t)$ terms from Equation (3.13) are now simple extensions of

their earlier versions:

$$\tilde{G}(t) = \begin{bmatrix} 0_{3 \times 3} & 0_{3 \times 3} & 0_{3 \times 3} & 0_{3 \times 3} \\ I^{-1} & 0_{3 \times 3} & 0_{3 \times 3} & 0_{3 \times 3} \\ 0_{3 \times 3} & G_g & 0_{3 \times 3} & 0_{3 \times 3} \\ 0_{3 \times 3} & 0_{3 \times 3} & G_{GPS} & 0_{3 \times 3} \\ 0_{3 \times 3} & 0_{3 \times 3} & 0_{3 \times 3} & G_d \end{bmatrix}, \quad (3.50)$$

and

$$Q(t) = \begin{bmatrix} Q_{dist} & 0_{3 \times 3} & 0_{3 \times 3} & 0_{3 \times 3} \\ 0_{3 \times 3} & Q_g & 0_{3 \times 3} & 0_{3 \times 3} \\ 0_{3 \times 3} & 0_{3 \times 3} & Q_{GPS} & 0_{3 \times 3} \\ 0_{3 \times 3} & 0_{3 \times 3} & 0_{3 \times 3} & Q_d \end{bmatrix}. \quad (3.51)$$

Here, Q_d is the estimator design covariance for the input process w_d .

In addition to the covariace relations, the sensitivity partial derivative matrices used for measurement update must now be augmented by a block matrix to keep the update relations dimensionally homogenous. Since the torque partition enters the dynamics like a disturbance and does not affect the measurement process, the sensitivities are buffered by a zero matrix $0_{3 \times 3}$. Specifically, for gyro updating,

$$\tilde{H}_{gyro} = \begin{bmatrix} -2[\hat{\omega}_i]_X & I_{3 \times 3} & I_{3 \times 3} & 0_{3 \times 3} & 0_{3 \times 3} \end{bmatrix}, \quad (3.52)$$

and for GPS updating,

$$\tilde{H}_{GPS} = \begin{bmatrix} I_{3 \times 3} & 0_{3 \times 3} & 0_{3 \times 3} & \frac{1}{2}I_{3 \times 3} & 0_{3 \times 3} \end{bmatrix}. \quad (3.53)$$

These relations conclude the technical aspects of adding a disturbance torque estimator.

However, it is important to note that in some situations, asking the model-based filter to estimate too many state simultaneously can lead to poor system observability and even filter divergence. This “overloading” is particularly a problem when all instrument errors are estimated but measurements come in

infrequently. Between updates, the filter must attempt to propagate its estimates for *all* requested states; asking it to infer the behavior of many states from too few measurements will be rewarded with totally divergent estimates after a very short period.

In general, for nonlinear estimation via the EKF, the observability of a system's filter model should be judged by computing the observability matrix from the Jacobian and sensitivity matrices ($\tilde{F}(t)$ and \tilde{H}_k), *and* by the outcomes of Monte Carlo simulations.

Obviously, the addition of a disturbance torque state has the undesirable effect of increasing the filter order and therefore incurring additional computational burdens. One should judge whether or not benefits of torque estimation can be accomplished by a simple readjustment upwards of the filter design variable Q_{dist} in a case-by-case basis.

Finally, in certain settings, the ability to estimate disturbance torques could potentially be employed for control system failure detection. If the disturbance environment is sufficiently benign, a properly tuned torque estimator can register the actual thrust level. This in turn, is compared to the *commanded* thrust. If the difference between the two is significant, then a thruster failure may be to blame. This general principle was studied in references [2] and [29] in the context of robust estimation and failure detection and isolation (FDI).

3.1.3 Summary

This section and the preceding chapter have given the origin, state equations, covariance definition, and propagation and update relations for the model filter. The only new concept aside from the truth discussion in Chapter 2 and filter discussion in Appendix C is the reduced order covariance and update to accommodate quaternion attitude representation. Otherwise, the model filter essentially copies the truth dynamics as closely as possible.

3.2 Nonmodel Filter Design

Since the model filter includes attitude kinematics as part of its total model, the kinematic filter results from a careful truncation and rearrangement.

3.2.1 State and Covariance Propagation

Since the nonmodel filter excludes any dynamic, or “ $T = I\dot{\omega}$ ”, information about the truth process, we begin by excluding the second equation from (3.2). That leaves only vehicle attitude and time correlated instrument errors in the filter state vector,

$$x(t) \equiv \begin{bmatrix} q_{bl}(t) \\ b_b(t) \\ b_{GPS}(t) \end{bmatrix}. \quad (3.54)$$

Since ω_{bl} is no longer a filter state, the gyro outputs cannot be treated as a typical filter measurement as ω_{gyro} is unformable from the remaining members of $x(t)$. Instead, we rearrange Equation (2.21), heeding (3.25) to get

$$\begin{aligned} \omega_{bl} &= \omega_{meas} - b_g - v_g \\ &= \omega_{gyro} - b_g - v_g. \end{aligned} \quad (3.55)$$

If we substitute this expression for $\omega_{bl}(t)$ into the first line of (3.2) and employ the following identity provided by Lefferts, et. al.

$$\Omega(a + b)q \equiv \Omega(a)q + \Xi(q)b, \quad (3.56)$$

we obtain the nonmodel filter state model

$$\begin{aligned} \dot{q}_{bl} &= \frac{1}{2}\Omega(\omega_{gyro} - b_g)q_{bl} - \frac{1}{2}\Xi(q_{bl})v_g \\ \dot{b}_g &= A_g b_g + G_g w_g \\ \dot{b}_{GPS} &= A_{GPS} b_{GPS} + G_{GPS} w_{GPS}, \end{aligned} \quad (3.57)$$

and propagate the state estimates according to

$$\begin{aligned}
\dot{\hat{q}}_{bl} &= \frac{1}{2}\Omega(\omega_{gyro} - \hat{b}_g)\hat{q}_{bl} \\
\dot{\hat{b}}_g &= A_g\hat{b}_g \\
\dot{\hat{b}}_{GPS} &= A_{GPS}\hat{b}_{GPS}.
\end{aligned} \tag{3.58}$$

Philosophically, this filter still accurately models the truth process. Only now the gyro is the *only* source of rate information. Instead of appearing as measurements to be filtered, the gyro output ω_{gyro} is taken as a known process input. The gyro white error v_g now enters the filter as a process disturbance. Whereas the dynamic filter treated T_{cont} and $[T_{dist}^T, w_g^T, w_{GPS}^T]^T$ as inputs, the kinematic filter replaces them with ω_{gyro} and $[v_g^T, w_g^T, w_{GPS}^T]^T$. Since the gyro bias b_g remains a filter state, the algorithm will subtract out its estimate from ω_{gyro} as the filter propagates between measurements. Unfortunately, the matrix-vector products in the first line of (3.57) are nonlinear and still necessitate an extended Kalman filter.

The nonmodel filter's advantage over the dynamic method is autonomy from the host vehicle. There is no need to know the satellite mass properties, control torques, or disturbance torque characteristics. The liability however, is that the kinematic approach relies entirely on the gyro for direct body rate information. The model no longer provides an independent check on the gyro and consequently, the gyro bias will become less observable. Of course, just as with the dynamic design, GPS-provided attitude measurements will still be available periodically.

Since we still use a quaternion to represent attitude, we again make use of the reduced order covariance scheme. The following discussion essentially mirrors that of the previous section and redundant details will be omitted.

For covariance purposes, we define a reduced state $\bar{x}(t)$ by replacing the

attitude state with the small attitude error vector $\delta q(t)$:

$$\bar{x}(t) = \begin{bmatrix} \delta q(t) \\ b_g(t) \\ b_{GPS}(t) \end{bmatrix}. \quad (3.59)$$

The transformation matrix S appearing in Equation (3.10) is now one block-dimension less in order,

$$S(\hat{q}_{bl}(t)) = \begin{bmatrix} \Xi(\hat{q}_{bl}(t)) & 0_{4 \times 3} & 0_{4 \times 3} \\ 0_{3 \times 3} & I_{3 \times 3} & 0_{3 \times 3} \\ 0_{3 \times 3} & 0_{3 \times 3} & I_{3 \times 3} \end{bmatrix}. \quad (3.60)$$

Covariance propagation between GPS updates, during which gyro outputs are injected into the filter model, follows the familiar evolution:

$$\dot{\tilde{P}}(t) = \tilde{F}(\hat{x}(t), t)\tilde{P}(t) + \tilde{P}(t)\tilde{F}^T(\hat{x}(t), t) + \tilde{G}(t)Q(t)\tilde{G}^T(t). \quad (3.61)$$

Since our nonlinear filter model has changed, we must recompute the coefficient matrices in (3.61). The system matrix \tilde{F} has a simpler form that omits any dynamic influences:

$$\tilde{F}(\hat{x}(t), t) = \begin{bmatrix} [\omega_{bl}]_X & -\frac{1}{2}I_{3 \times 3} & 0_{3 \times 3} \\ 0_{3 \times 3} & A_g & 0_{3 \times 3} \\ 0_{3 \times 3} & 0_{3 \times 3} & A_{GPS} \end{bmatrix}, \quad (3.62)$$

Note the $-\frac{1}{2}I$ that ties the gyro bias to the attitude state. This block was previously zero in Equation (3.15) because the gyro errors were accounted for during update, not filter propagation.

The \tilde{G} matrix is similarly altered to reflect the gyro white noise error term

v_g now appearing in the attitude state derivative

$$\tilde{G}(t) = \begin{bmatrix} -\frac{1}{2}I_{3 \times 3} & 0_{3 \times 3} & 0_{3 \times 3} \\ 0_{3 \times 3} & G_g & 0_{3 \times 3} \\ 0_{3 \times 3} & 0_{3 \times 3} & G_{GPS} \end{bmatrix}. \quad (3.63)$$

Recall that previously, the first block row of \tilde{G} was all zero.

The driving disturbance intensity matrix similarly must include the continuous time angle random walk covariance R_g ,

$$Q(t) = \begin{bmatrix} R_g & 0_{3 \times 3} & 0_{3 \times 3} \\ 0_{3 \times 3} & Q_g & 0_{3 \times 3} \\ 0_{3 \times 3} & 0_{3 \times 3} & Q_{GPS} \end{bmatrix}. \quad (3.64)$$

3.2.2 Measurement Update

GPS measurement update for the nonmodel filter is essentially a special case of the model filter update. The gain and covariance calculations naturally have the identical form,

$$\begin{aligned} \tilde{K}_k &= \tilde{P}_k^- \tilde{H}_k^T (\tilde{H}_k \tilde{P}_k^- \tilde{H}_k^T + R_k)^{-1} \\ \tilde{P}_k^+ &= (I - \tilde{K}_k \tilde{H}_k) \tilde{P}_k^- (I - \tilde{K}_k \tilde{H}_k)^T + \tilde{K}_k R_k \tilde{K}_k^T. \end{aligned} \quad (3.65)$$

However, this time there is only the GPS measurement available. We still feed the filter the same modified measurement

$$q_{meas} = \Xi^T (q^*(\hat{b}_{GPS}^-) \otimes \hat{q}_{bl}^-) q_{GPS}. \quad (3.66)$$

The measurement sensitivity matrix is a lower dimensioned version of (3.33) that accounts for the redefinitions of $x(t)$ and $\bar{x}(t)$,

$$H_{GPS} = \begin{bmatrix} \Xi^T (q^*(\hat{b}_{GPS}^-) \otimes \hat{q}_{bl}^-) & 0_{3 \times 3} & \frac{1}{2}I_{3 \times 3} \end{bmatrix}, \quad (3.67)$$

with

$$\tilde{H}_{GPS} = H_{GPS}S(\hat{q}_{bl}^-), \quad (3.68)$$

as before.

The discrete measurement covariance is exacty the same as before,

$$R_{GPS} = \frac{1}{4}\text{Cov}(v_{GPS}). \quad (3.69)$$

Again, the “gain times residuals” equation updates \bar{x} instead of x ,

$$\begin{aligned} \Delta \hat{x}_k &= \tilde{K}_k(z_k - h_k(\hat{x}_k^-)) \\ \Delta \hat{x}_k &= \hat{x}_k^+ - \hat{x}_k^-, \end{aligned} \quad (3.70)$$

so the actual state updates are performed just as in the dynamic case:

$$\hat{q}_{bl,k}^+ = q_{corr,k} \otimes \hat{q}_{bl,k}^- \quad (3.71)$$

for the attitude state, and

$$\begin{aligned} \Delta \hat{b}_{g,k} &= \hat{b}_{g,k}^+ - \hat{b}_{g,k}^- \\ \Delta \hat{b}_{GPS,k} &= \hat{b}_{GPS,k}^+ - \hat{b}_{GPS,k}^- \end{aligned} \quad (3.72)$$

for the instrument error states.

Chapter 4

Simulation Results

The preceding chapter laid out the algorithmic differences between the non-model and model-based filter designs. We now test their performance in a series of attitude determination experiments. Our goal is to determine how much improvement the model-based methodology offers and in what situations its use is most warranted.

Although on-orbit testing would be the best indicator of obtainable performance under real operating conditions, a natural first step to evaluating filter quality is computer simulation. This idealistic testbed produces preliminary results more rapidly than actual hardware testing. In addition, we incur minimal expense while enabling ease of parameter variation.

In the following scenarios, we expect to see superior attitude determination performance with the model-based filter, especially when the GPS update interval is large. Since a lack of external attitude verification allows more time for the gyro bias to drift unmonitored, the nonmodel filter becomes more likely to produce wandering attitude solutions as the GPS measurement interval increases. We will demonstrate that the inclusion of vehicle dynamics in estimator designs allows more accurate tracking of the satellite attitude and body rate, even when errors occur in representing the inertia matrix.

The chapter begins by defining four sample statistic measures for gauging filter performance. Since the filter covariance $P(t)$ only represents approximate

error behavior and as simulation plots can sometimes be difficult to interpret, the sample measures are included to provide additional insight.

The remaining sections compare the rival estimators in four mission scenarios. In the first, the satellite maintains a naturally stable LVLH-hold in a benign disturbance environment. Here, the model filter establishes confidence in the attitude solution. Next, the satellite tumbles after a control system failure. When the GPS update interval is large, the model filter produces superior tracking performance, even in the presence of inertia term errors. Next, the controller executes a series of attitude maneuvers; the metric of filter performance will be the agreement between the commanded and actual attitude profiles. Finally, we show that the vehicle dynamics model can prevent unstable closed-loop system behavior in the complete absence of gyro measurements. The result applies even in the case of modeling uncertainty.

4.1 Measures of Performance

In the following sections, several simulations are run for the purpose of demonstrating filter performance capabilities. As part of its algorithm, the extended Kalman filter (EKF) computes its own performance statistics, namely the *estimated* error covariance matrix $P(t)$. If this matrix were known to be exactly accurate, then we could rely heavily on it to gauge an estimator's quality. However, $P(t)$ is only an approximation of the true error covariance. As part of the EKF algorithm derivation, first order Taylor series truncations of true state dynamics were taken and the matrix $P(t)$ defined from the resulting estimation error expression. Further, if the truth and filter models do not agree, then actual performance will likely deviate from the filter's perceived performance. Therefore, it is useful to have additional performance metrics to better grasp what is actually happening. As is common in EKF studies, we look to simulation sample statistics for additional insight. An intelligent performance analysis should consider the satellite mission objectives, the filter covariance matrix $P(t)$, and

the sample measures.

In this chapter, we employ four different sample statistics. The first two are conventional; the second two are more ad hoc. In all four definitions we consider statistics of a generic sample error process $z_k; k = 1, \dots, N$.

The first statistic is the process sample *mean*, typically denoted by \bar{z} . The definition is

$$\bar{z} = \frac{1}{N} \sum_{k=1}^N z_k. \quad (4.1)$$

As might be expected, \bar{z} is a measure of the *average* or typical value of the error signal z_k . Unfortunately, the EKF, unlike the standard KF, is a biased estimator, even if there is exact truth-filter model agreement. Therefore, we do not expect $\bar{z} \equiv 0$, even if we could carry on infinite duration simulations. However, the closer \bar{z} is to zero, the better the performance, all other measures equal.

The next metric quantity is the process sample *standard deviation* σ . Ideally, this is the also the value obtained by taking the square roots of the diagonal elements of the filter covariance matrix $P(t)$. If the error distribution were perfectly normal, which is the case only for certain linear systems, then roughly sixty-three percent of the data should fall within a $\pm 1\sigma$ bound. To compute the sample value of σ , we rely on the traditional formula

$$\sigma = \sqrt{\frac{\sum_{k=1}^N (z_k - \bar{z})^2}{N - 1}}. \quad (4.2)$$

Note that whether we examine the filter or sample value of σ , it is computed about the error mean.

In order to get another handle on the overall error values without considering their dispersion, we look at the sample *mean error magnitude*. This value is computed as in Equation (4.1) but with sign dropped. In other contexts, this

metric might be termed the scaled “1-norm”. We define it here as

$$|\bar{z}| = \frac{1}{N} \|z\|_1 = \frac{1}{N} \sum_{k=1}^N |z_k|. \quad (4.3)$$

It is intended to complement \bar{z} and σ by giving an indication of what the typical error magnitude actually is. For purposes of control system design, we like to know how far from truth the average estimated quantity lies.

Finally, we harken back to the idea that for normally distributed statistics, 62.8% of the error data should fall below a 1σ magnitude. Therefore, we also compute the sample value of that percentile. Mathematically, this quantity is expressed as

$$\sigma_{62.8\%} = \{\sigma^* : 62.8\% \text{ of the sequence } |z_k| \text{ values fall below } \sigma^*\}. \quad (4.4)$$

By examining this quantity, we can get an additional “over-under” feel for how the error values are distributed.

4.2 LVLH-Aligned Performance

Intuitively, the benefits of including an accurate dynamics model in an attitude filter should be greatest when such dynamics yield significant information. That is, one might think that the model-based approach might not yield improved estimation performance when the truth dynamics are trivial, as when the satellite revolves around the Earth with constant zero angular velocity relative to the LVLH frame, i.e. $\omega_{bl}(t) = 0$, and constant trivial attitude, i.e. $q_{bl}(t) = [0, 0, 0, 1]$.

In fact, the information provided by the second member of Equations (3.2) indeed proves useful since knowledge of the motion history, albeit uninteresting, allows the filter to predict with greater confidence how the satellite body will be oriented at the next measurement. By comparison, the nonmodel filter relies only on the kinematic information, gyro outputs and GPS position measurements, to look forward. The model filter exploits the same information but

Inertia	$I = \text{diag}(40, 40, 10) \text{ kg} * \text{m}^2$
Initial body rate	$\omega_{bl}(0) = 0_{3 \times 1}$
Initial attitude	$\phi(0) = 0^\circ, \theta(0) = 0^\circ, \psi(0) = 0^\circ$
Gyro update	Every second
Bias parameter	$A_g = -1 * 10^{-5} \text{ sec}^{-1}$
Bias parameter	$G_g = 3.03 * 10^{-6} \text{ rad/sec}^{3/2}$
Angle random walk	$ARW = 0.5 \text{ deg}/\sqrt{\text{hr}}$
GPS update	First case: none., second case: every 100 sec.
GPS white error	0.3 deg 1- σ per axis
Disturbance environment	Gravity gradient only
Control	None
Orbit altitude	285 km

Table 4.1: Description for LVLH-Aligned Simulation

enriches it with an accurate dynamics model that helps counteract any erroneous trends created by less-than-perfect measurement data.

To demonstrate this principle, performance simulations were run with the parameters stipulated in Table 4.1. This table provides information for both the truth simulation and estimator designs since no mismatches were introduced. The inertia values correspond to a small cylindrical satellite and the gyro parameters are chosen to simulate an instrument with severe error characteristics. By choosing a gyro instrument with significant errors and not allowing GPS updates, we can illustrate the problematic long-term divergence of nonmodel filters.

For this run, the model filter state included only the attitude quaternion, body rates, and gyro biases. The nonmodel filter state is limited to only the attitude and gyro biases. GPS multipath effects were not included here and there was no need to estimate environmental disturbance torques.

The simulation was run for 2,000 seconds, roughly one-third of the 5,400 second orbit period. During this time, the attitude and body rate remained constant at their initial values and the gyro biases grew according to a Gauss-Markov process.

Figure 4-1 shows the attitude estimation error for the nonmodel filter. The

x-axis symmetric curves show the time-varying one-sigma bounds generated by the filter covariance. The remaining bounded signal is the actual error value.

Without periodic corrections from GPS, the gyro biases and angle random walk give rise to a constantly growing attitude uncertainty. The actual error value can become quite large, on the order of several degrees, seen especially in the second and third panels. As time goes on, the computed covariance becomes less and less valid, grossly overestimating the true error value; the small error assumption critical to EKF covariance propagation gradually becomes.

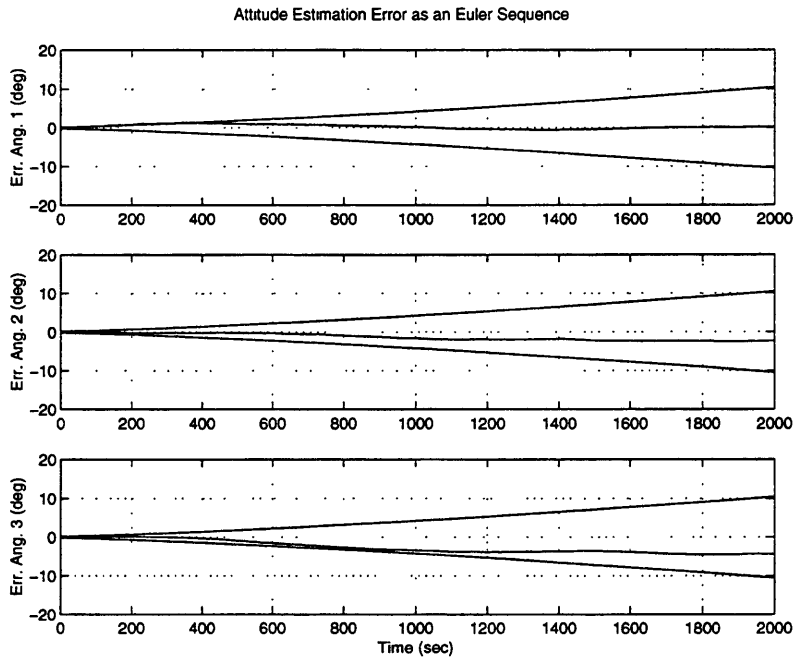


Figure 4-1: Attitude Error, Nonmodel Filter, Trivial Motion, No GPS

Figure 4-2 shows the corresponding result for the model-based filter. The lack of GPS updating still means growing uncertainty in the system states. However, the additional equations of rigid body motion allow this filter a better statistical guess of future attitudes. The consequence is a slower uncertainty growth rate in the third panel and very much enhanced, in fact nondivergent, performance the first two. Attitude estimation performance is clearly superior to that seen in Figure 4-1.

Table 4.2 presents the sample statistics from these two estimation runs. As the scaling is different between Figures 4-1 and 4-2, this data is useful as an additional judge of error behavior. We see that in every statistical category, the model filter improves the attitude tracking performance by several factors. Whereas the nonmodel filter allowed the attitude solution to diverge, reaching levels in excess of several degrees, the model filter keeps the error within more reasonable limits.

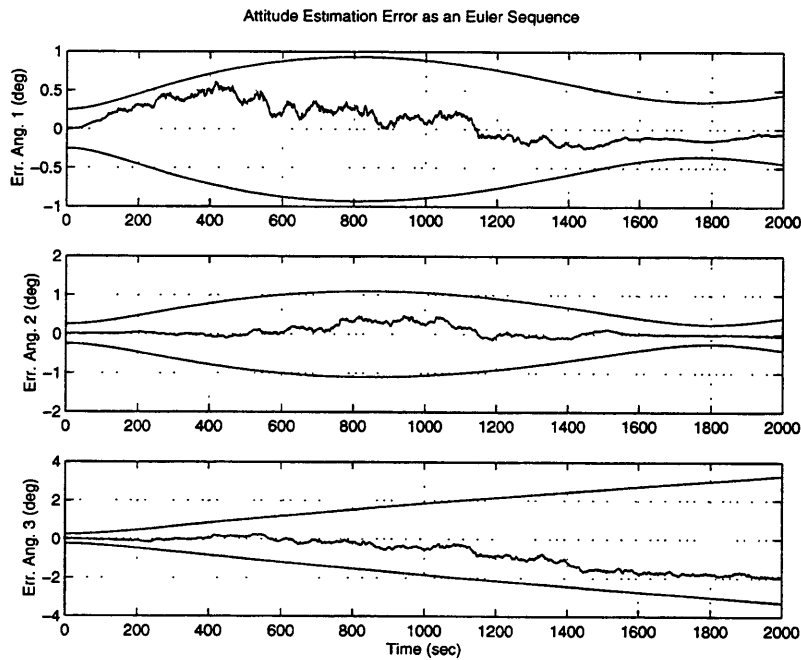


Figure 4-2: Attitude Error, Model Filter, Trivial Motion, No GPS

For this run, the common states for the model and nonmodel filter were attitude and gyro bias; the latter estimator cannot track body rate. Figures 4-3 and 4-4 show the gyro bias estimation performance for the competing filters. (Note: figure scaling is different). The story is much the same as with attitude itself; the nonmodel filter uncertainty grows continuously over time at a rate roughly two to three times that for the model filter. The interconnection is that by including the physical plant dynamics, the model-based EKF can better distinguish between the true rate and bias in the gyro measurements and thus

Axis	Mean (deg)	Std. Dev. (deg)	Mean Err. Mag. (deg)	68.2%-tile (deg)
Nonmodel Filter				
1	0.30	0.54	0.49	0.6
2	-1.30	0.91	1.3	1.9
3	-2.56	1.63	2.6	3.7
Model Filter				
1	0.09	0.22	0.2	0.22
2	0.06	0.14	0.1	0.09
3	-0.71	0.73	0.74	1.1

Table 4.2: Attitude Performance Statistics - No GPS Updating

better predict attitude.

In this performance example, the gyro-induced attitude errors grew steadily, since no external navigation aids were available to observe gyro bias growth. Thus, these runs may be considered as indicative of filter performance during orbit periods when GPS satellite are unobservable or when the receiver is turned off for cost savings. Since unintentional loss of external GPS or other attitude measurements may occur due to instrument failure, jamming, or accident, it is important that we have available navigation filters which minimize the ill effects of gyro-only operation.

Figures 4-5 and 4-6 illustrate attitude performance of the two filters operating under the exact same conditions, except this time with GPS updating every 100 sec. The GPS signal contains a white error of 0.3 deg $1\text{-}\sigma$ per axis. Time-correlated multipath error effects are deferred to later simulation tests. Table 4.3 reports the corresponding sample statistics for these runs. Note that the figure axes are scaled differently.

Referring to the figures, there are several worthwhile observations. Although the model filter takes slightly longer to reach the nonlinear equivalent of steady-state (since it has more states to sort through), its final attitude covariances are several factors less than those of the nonmodel filter. Specifically, its final values are 0.14, 0.15, and 0.25 degrees on axes 1, 2, and 3, respectively. The difference between the third axis and first two can be explained by cylindrical inertial

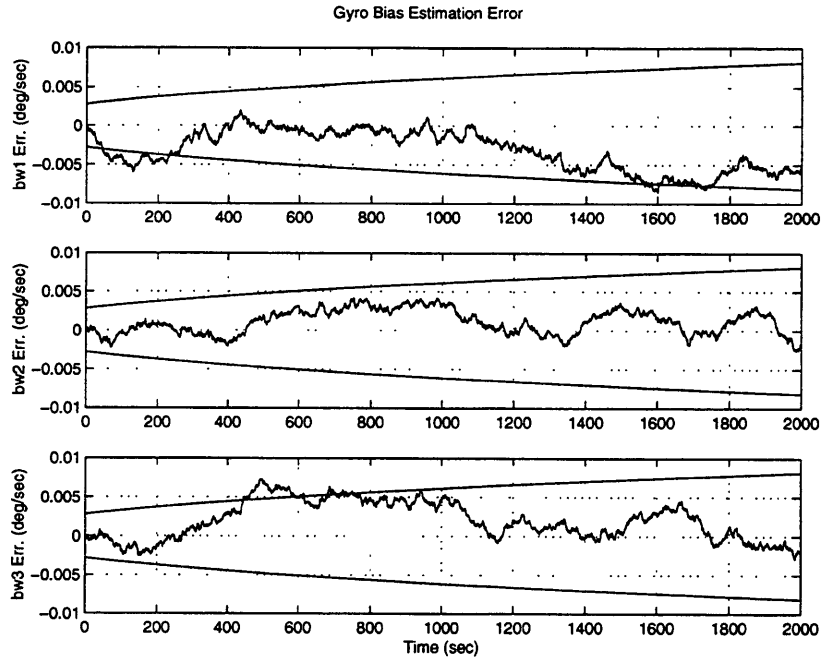


Figure 4-3: Gyro Bias Error, Nonmodel Filter, Trivial Motion, No GPS

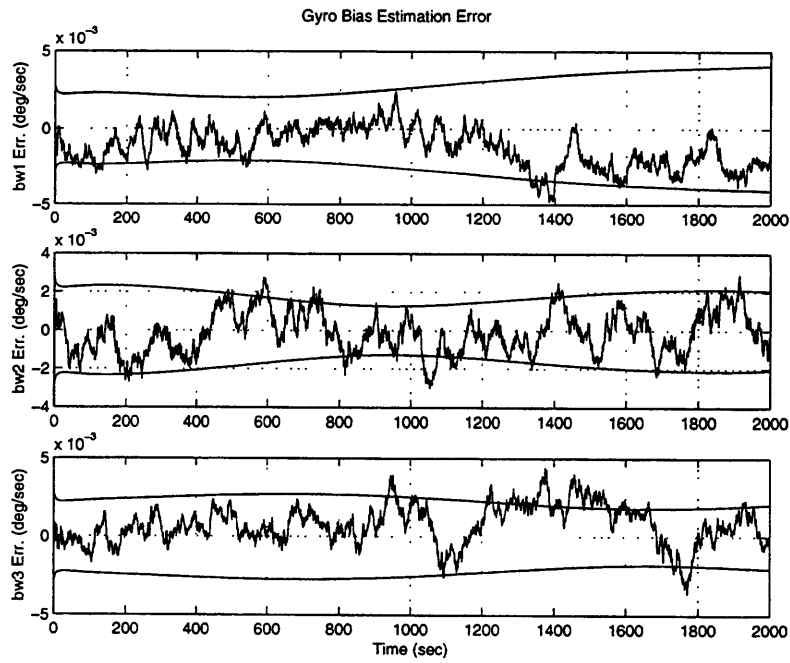


Figure 4-4: Gyro Bias Error, Model Filter, Trivial Motion, No GPS

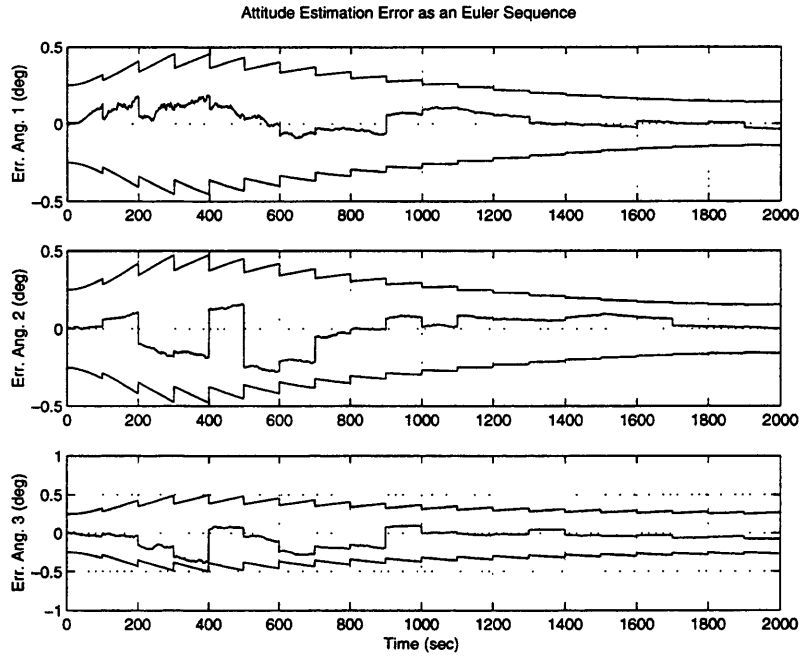


Figure 4-5: Attitude Error, Model Filter, Trivial Motion, With GPS

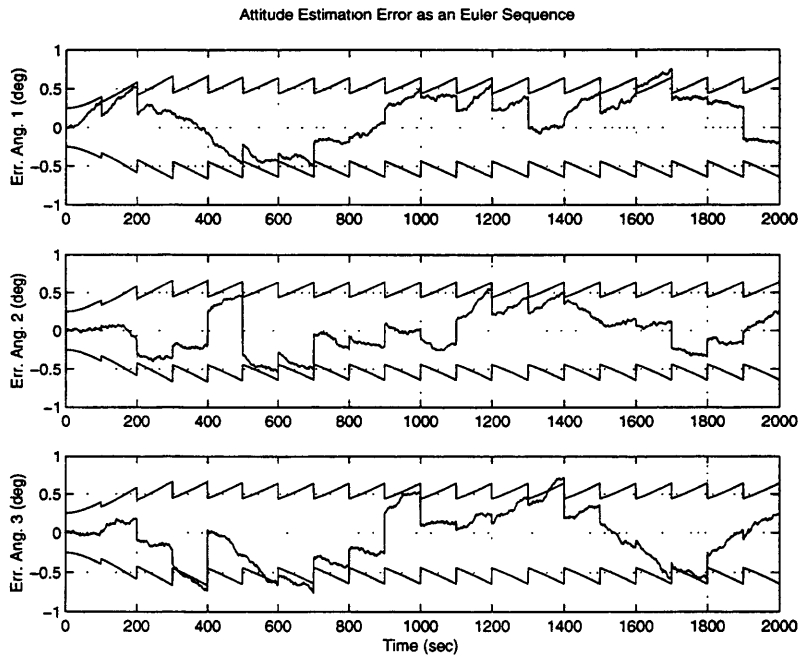


Figure 4-6: Attitude Error, Nonmodel Filter, Trivial Motion, With GPS

Axis	Mean (deg)	Std. Dev. (deg)	Mean Err. Mag. (deg)	68.2%-tile (deg)
Nonmodel Filter				
1	0.13	0.29	0.28	0.37
2	-0.02	0.26	0.22	0.30
3	-0.07	0.34	0.28	0.38
Model Filter				
1	0.03	0.06	0.05	0.07
2	0.00	0.10	0.08	0.08
3	-0.07	0.11	0.09	0.08

Table 4.3: Attitude Performance Statistics - With GPS Updating

distribution and the fact the gravity gradient torque has the least action along the yax axis, meaning that it is the most likely to drift away a nominal LVLH-aligned orientation. The corresponding nonmodel steady-state covariances are 0.44 deg after GPS update and 0.65 just prior to GPS update, equal on all three axes. Since there are no dynamic considerations in this estimator, it makes sense for all axes to behave similarly. Further, without the dynamics model for additional insight, this estimator quickly loses confidence in its attitude knowledge, accounting for the “sawtooth” covariance growth between GPS updates. The model filter has the benefit of near-constant error bounds, allowing less concern about the transient nature of filter-reported statistics.

Excluding the mean data, Table 4.3 shows consistently, across all categories, that the model-based approach offers attitude performance 2 or 3 times superior to that of estimation based exclusively on kinematic relations. Of course, these simulations perfectly match truth and filter parameters, so the model filter’s enhanced performance was vitually guaranteed.

However, even if this result was expected, we must note that traditionally, dynamics models are *not* included in attitude filter designs. They are typically excluded to reduce filter order and prevent the possible ill effects of mismodeling. However, this simulation example and those that follow indicate the value of including a sufficiently accurate vehicle dynamics model, especially when attempting to add robustness to GPS outage.

Before proceeding, we compare Figures 4-2 and 4-6. Both show attitude estimation performance for the nonmodel filter, but under different GPS circumstances. The obvious point is that periodic GPS updating was sufficient to prevent divergence. A more subtle glance shows the gap between actual and perceived performance (filter covariance) in Figure 4-2 is absent in Figure 4-6. Whereas the filter greatly overestimated error previously, the latter figure reveals a much better impression of reality. The earlier gap can be attributed to the general evils of filter divergence, especially for nonlinear systems. We recall that the filter “covariance” is no covariance at all, merely an estimate of it. When the real errors grow large, the linearization assumptions key to the EKF algorithm (See Appendix C) degrade and little of its information can be trusted.

Overall, this LVLH-aligned example has demonstrated the benefit of dynamic model inclusion. Even with stationary dynamics, the model filter significantly slows the rate of filter divergence when GPS is unavailable. In situations when external updating *is* possible, the model filter significantly estimation performance by a factor of at least two and a half.

4.3 Tumbling Performance

We now consider the case of a satellite tumbling out of control. Where the equations of rigid body motion were trivially satisfied in the previous LVLH-aligned simulations, Euler coupling effects are now relevant and we expect the model filter’s dynamic information to enhance estimation performance. Further, out of control motion represents a benchmark test case for model-based filters. Although this mode of operation is an unlikely and highly undesirable state, it is a condition in which rigid body dynamics play a dominant role in system evolution. In previous studies of model-based attitude estimation, out of control test cases have been frequently explored [25], [36].

The simulation specifications are given in Table 4.4. The satellite inertias

Inertia	$I = \begin{bmatrix} 100 & 10 & -5 \\ 10 & 200 & 40 \\ -5 & 40 & 250 \end{bmatrix}$	$kg * m^2$
Initial body rate	$\omega_{bl}(0) = \omega_{orb} \begin{bmatrix} \frac{1}{2} \\ 1 \\ -1 \end{bmatrix}$	
Initial attitude	$\phi(0) = 20^\circ, \theta(0) = 10^\circ, \psi(0) = 30^\circ$	
Gyro update	Every second	
Bias parameter	$A_g = -1 * 10^{-5} \text{ sec}^{-1}$	
Bias parameter	$G_g = 8.23 * 10^{-7} \text{ rad/sec}^{3/2}$	
Angle random walk	$ARW = 0.1 \text{ deg}/\sqrt{hr}$	
GPS update	First case: 10 sec, second case: 1,000 sec.	
Multipath parameter	$A_{GPS} = -3.7 * 10^{-4} \text{ sec}^{-1}$ (1st case only)	
Multipath parameter	$G_{GPS} = 1.3 * 10^{-4} \text{ rad/sec}^{1/2}$ (1st case only)	
GPS white error	0.3 deg 1- σ per axis	
Disturbance environment	Gravity gradient only	
Control	None	
Orbit altitude	285 km	

Table 4.4: Description for Satellite Tumble Simulation

are now increased and redistributed so that the body axes and principal axes no longer coincide. The initial attitude is not LVLH-aligned and the initial body rates are significant compared to orbit rate. These initial conditions are selected to simulate a spacecraft experiencing a severe tumble after loss of the control system. The gyro error parameters correspond exactly to the “low” quality gyro of Table 1.1.

Figures 4-7 and 4-8 illustrate the truth body rate and attitude profiles as the satellite slowly tumbles, subject only to gravity gradient torquing.

Two simulation test cases are presented. In the first, GPS updates come in every 100 seconds. This measurement rate is indicative of nominal satellite operation and the usefulness of dynamic modeling in estimator design will likely be small. In the second, the attitude measurements come in at 1,000 second intervals, roughly one-fifth of the 5,400 second orbit period. This large update period simulates a period of GPS malfunction, deactivation for power savings, or GPS satellite unobservability. In this setting, we expect the model filter’s

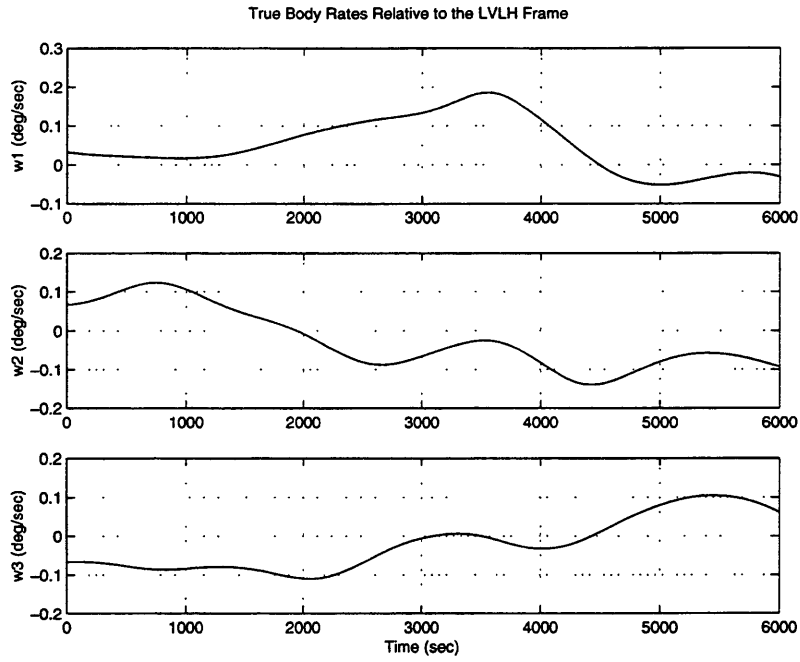


Figure 4-7: Truth Rate Profile During Tumbling

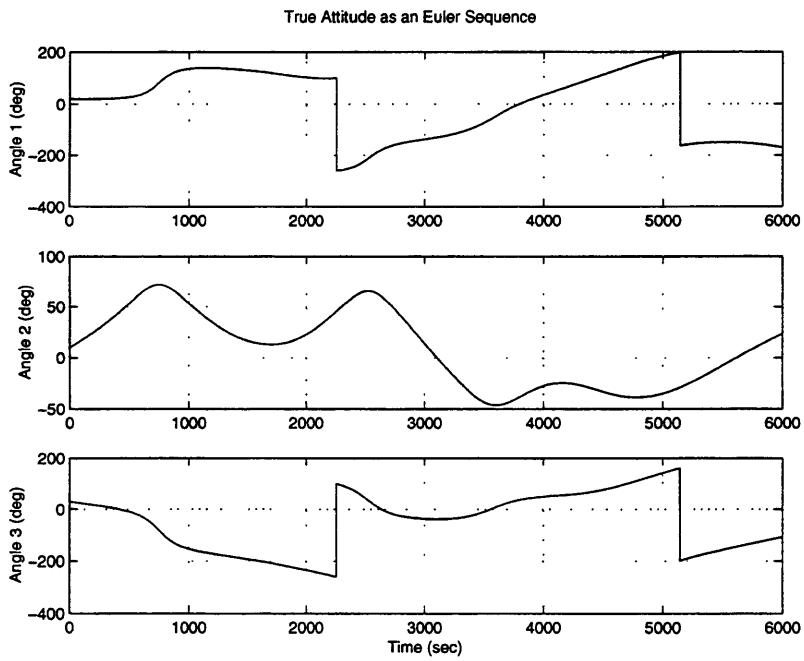


Figure 4-8: Truth Attitude Profile During Tumbling

vehicle dynamics information to provide significant system insight and therefore enhance attitude tracking. In addition, we briefly study the effect of inertia term uncertainty on model filter design and performance.

In both runs, a GPS white measurement error is included. Since time-correlated effects are more relevant with higher frequency updating, multipath errors are included only in the first run. Both filters will attempt to estimate this error source. The multipath parameters in Table 4.4 correspond to a $1\text{-}\sigma$ value of 0.28 degrees per axis and a time constant of half an orbit period [7], [36].

Tumbling with Frequent GPS Updating

Figure 4-9 shows attitude error for the nonmodel filter in the tumbling scenario with a 100 second GPS update period. Figure 4-10 shows the corresponding model filter error behavior and Table 4.5 gives the simulation sample statistics for both runs. (Note that the vertical scaling may be different in the figures).

The nonmodel estimator is designed very simply; the generic algorithm of Section 3.2 is chosen to fit the gyro and GPS error parameters of Table 4.4. In contrast, the model filter requires some degree of tuning. If the body rate process noise Q_{dist} is set too low, the algorithm will become overconfident in its imperfect state estimates and begin ignoring measurements. Filter divergence quickly results since the Euler coupling dynamics are used excessively and relevant plant information contained in the measurements is overlooked. Therefore, we tune the model filter by adding fictitious body rate process noise. The variable Q_{dist} is set numerically to $2.5 * 10^{-7} I_{3 \times 3}$. This measure suggests to the algorithm that a moderate disturbance environment is present and that the vehicle dynamics information should be slightly downweighted.

The attitude error signals in these two figures appear very similar, as are the sample statistics. The nonmodel filter has excellent observability into the gyro bias thanks to the frequent external GPS attitude measurements. Clearly, at this frequency of GPS updating, vehicle modeling does not provide significant

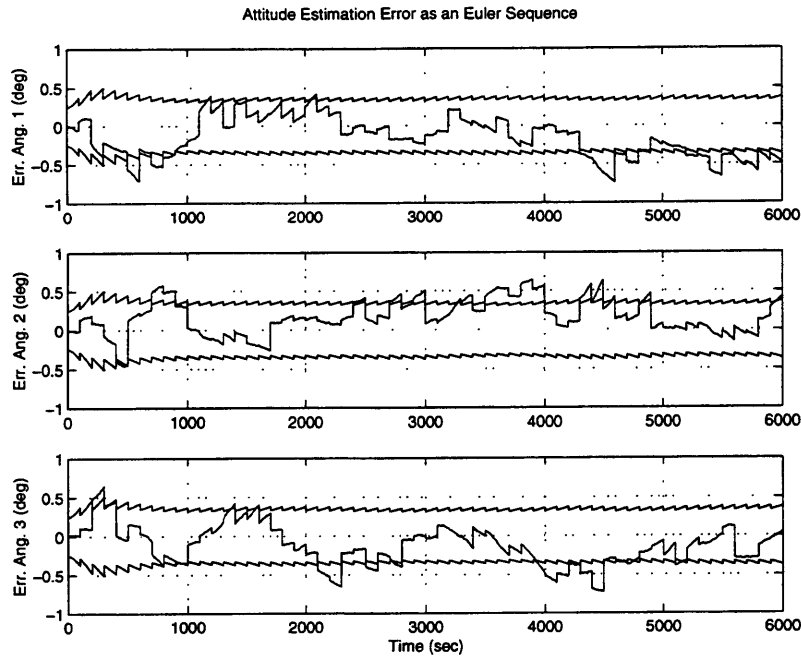


Figure 4-9: Nonmodel Filter - Tumbling With High GPS Rate

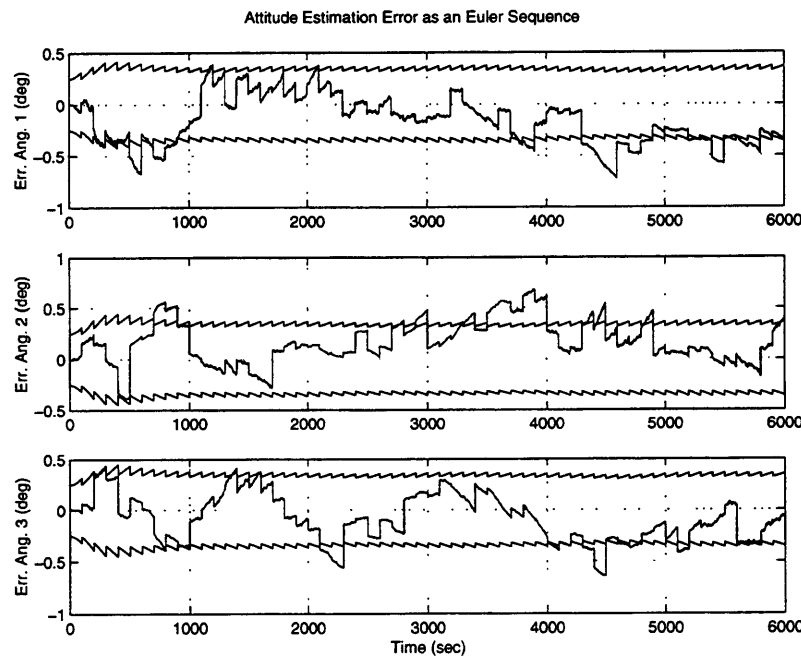


Figure 4-10: Model Filter - Tumbling With High GPS Rate

Axis	Mean (deg)	Std. Dev. (deg)	Mean Err. Mag. (deg)	68.2%-tile(deg)
Nonmodel Filter				
1	-0.16	0.26	0.25	0.32
2	0.16	0.22	0.22	0.28
3	-0.13	0.25	0.23	0.30
Model Filter - No Inertia Errors				
1	-0.17	0.24	0.24	0.33
2	0.17	0.21	0.21	0.27
3	-0.09	0.23	0.21	0.27

Table 4.5: Attitude Performance - Tumbling With High Frequency GPS Updates

additional insight into the body rate dynamics.

To test the robustness of the model-based approach, we now perturb the values of all inertia terms in the estimator design by 10% in arbitrary directions as shown in Table 4.6. These errors are introduced to represent a significant miscalculation or change in the satellite mass distribution. Since exact analytical computation of the satellite inertia matrix is impossible, in addition to the possibility of moving parts, thermal expansion, and extendable array flexibility all affecting the true mass distribution, we must test the model filter’s response to plant uncertainty.

When uncertainty occurs in any filter design, we must robustify it to maintain satisfactory estimation performance. If the filter variable Q_{dist} were kept at the same value as when the model filter contained the *correct* inertia values, the attitude solution would slowly diverge from truth. Therefore, we further reduce the filter’s confidence in its rate estimates by hiking Q_{dist} up to a numerical value of $1 * 10^{-6} I_{3x3}$. Increases in Q_{dist} have the gradual effect of invalidating the filter rate estimates, thus making the model filter behave more and more like its nonmodel counterpart. Figure 4-11 shows the resulting estimation performance.

Again, the error tracks are very similar to those of Figures 4-9 and 4-10. Table 4.7, which gives the sample statistics for the robustified model run and reiterates those of the nonmodel run, indicate when the GPS update rate is high, there is no dropoff in filter performance, even with 10% modeling error.

$I_{truth} = \begin{bmatrix} 100 & 10 & -5 \\ 10 & 200 & 40 \\ -5 & 40 & 250 \end{bmatrix} \quad kg * m^2$	$I_{filt} = \begin{bmatrix} 90 & 11 & -5.5 \\ 11 & 220 & 36 \\ -5.5 & 36 & 225 \end{bmatrix} \quad kg * m^2$
$\lambda_{i,truth} = 98.4, 180, 272$	$\lambda_{i,filt} = 88.5, 188, 259$
$v_{i,truth} = \begin{bmatrix} 0.99 \\ -0.12 \\ -0.07 \end{bmatrix}, \begin{bmatrix} -0.14 \\ -0.87 \\ 0.48 \end{bmatrix}, \begin{bmatrix} 0.00 \\ 0.49 \\ 0.87 \end{bmatrix}$	$v_{i,filt} = \begin{bmatrix} 0.99 \\ -0.10 \\ -0.07 \end{bmatrix}, \begin{bmatrix} -0.12 \\ -0.72 \\ 0.68 \end{bmatrix}, \begin{bmatrix} 0.02 \\ 0.68 \\ 0.73 \end{bmatrix}$

Table 4.6: Truth and Erroneous Filter Satellite Inertia Matrices and Their Eigenproperties - Tumbling Scenario

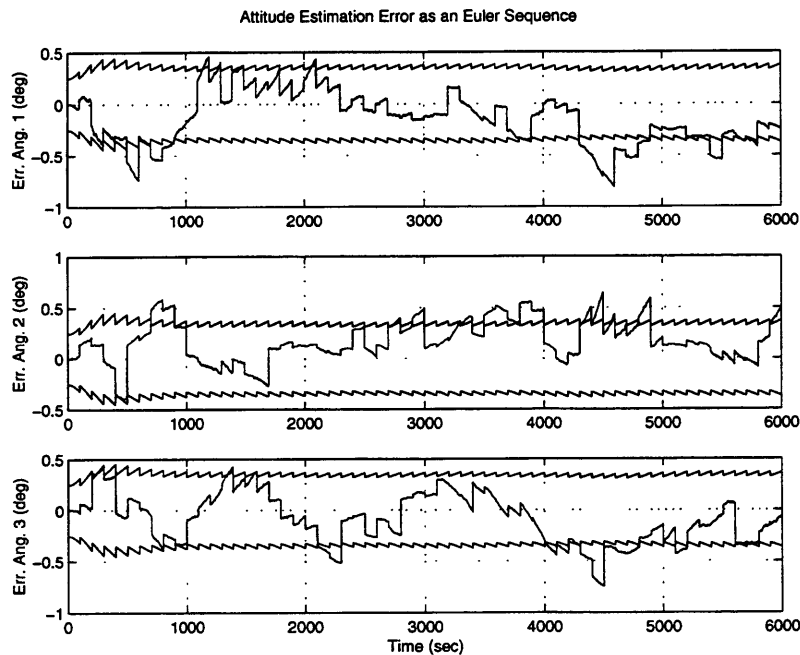


Figure 4-11: Model Filter with 10% Inertia Errors - Tumbling With High GPS Rate

Axis	Mean (deg)	Std. Dev. (deg)	Mean Err. Mag. (deg)	68.2%-tile(deg)
Nonmodel Filter				
1	-0.16	0.26	0.25	0.32
2	0.16	0.22	0.22	0.28
3	-0.13	0.25	0.23	0.30
Model Filter - 10% Inertia Errors				
1	-0.15	0.26	0.24	0.32
2	0.17	0.20	0.21	0.29
3	-0.09	0.24	0.22	0.29

Table 4.7: Attitude Performance - Tumbling With High Frequency GPS Updates

As mentioned in the introduction to this section, multipath effects are an important consideration when the GPS update interval is short. Because of time correlation, multipath errors can persist over many measurement epochs, making the white error assumption invalid. Therefore, in the previous three runs, multipath errors were added to both the truth measurements and estimator designs, following the model of Equation (2.26) and employing the parameters of Table 4.4.

Figure 4-12 shows the success of the nonmodel filter in estimating the multipath signal. The model and robustified model filters produce very similar error plots which are not given here. Performance statistics for all three are presented in Table 4.8. As with the gyro bias, it is important to estimate this quantity to minimize its corruption of the nominal measurement. Simply hiking up the filter GPS white error covariance is ineffective in mitigating multipath and other time-correlated errors.

Recall that the GPS multipath model was tuned with a steady-state variance of 0.28 degrees per axis. Since all of the sample statistics in Table 4.8 lie well below this value, we conclude that including this quantity as a filter state is an effective means of reducing its deleterious effect on attitude performance.

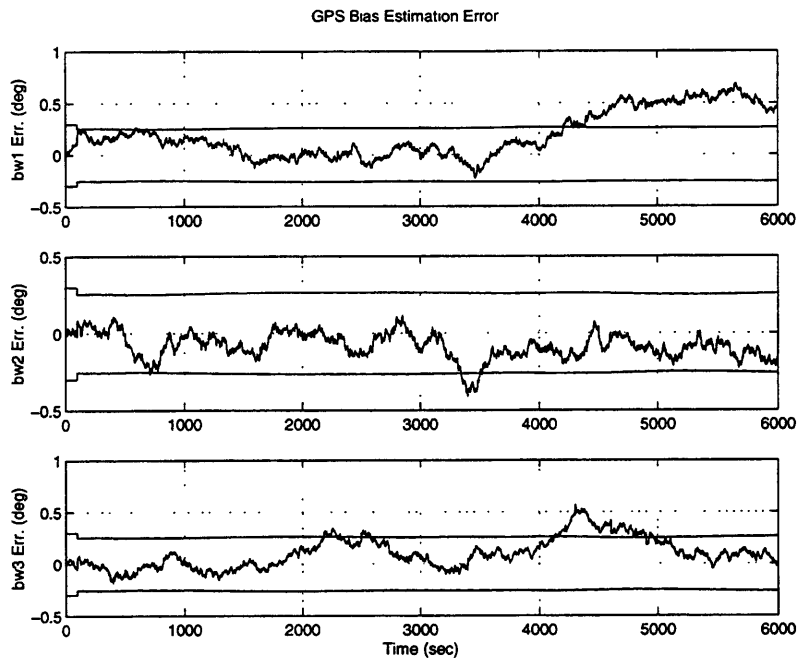


Figure 4-12: Nonmodel Filter - GPS Multipath Estimation Error

Axis	Mean (deg)	Std. Dev. (deg)	Mean Err. Mag. (deg)	68.2%-tile (deg)
Nonmodel Filter				
1	0.19	0.22	0.21	0.24
2	-0.08	0.09	0.095	0.12
3	0.10	0.14	0.13	0.14
Model Filter - No Inertia Errors				
1	0.22	0.19	0.22	0.27
2	-0.09	0.09	0.099	0.13
3	0.06	0.14	0.12	0.13
Model Filter - 10% Inertia Errors				
1	0.21	0.20	0.22	0.25
2	-0.10	0.09	0.11	0.14
3	0.06	0.15	0.12	0.14

Table 4.8: GPS Multipath Performance - Tumbling With High Frequency GPS Updates

Tumbling with Infrequent GPS Updating

In Section 4.2 on LVLH-aligned operation, we found that the performance for both model and nonmodel filters improved when the GPS rate increased. This result is not surprising since additional measurement information should only help a properly designed state estimator. We also found that the performance *difference* between the competing filter designs narrowed with more frequent GPS updates. Since the model-based filter employs the vehicle dynamics only between measurement updates, its advantage is naturally diminished as a higher GPS sample rate makes tracking the gyro bias for extended periods less important.

Therefore, as we *increase* the GPS update period in the tumbling runs, we expect both filters to degrade slightly in their quality of attitude tracking. However, the dynamic model’s usefulness should now be evident as a gap opens up between nonmodel and model performance. Figures 4-13, 4-14, and 4-15 show the attitude estimation performance of the nonmodel, model, and robustified model filters, respectively, when the GPS update interval has expanded 1,000 seconds. The underlying truth rate and attitude profiles are still the same as in Figures 4-7 and 4-8. The model filter is tuned for with $Q_{dist} = 1 * 10^{-8} I_{3x3}$ and $G_{g,filt} = 4G_{g,truth}$. The slight decrease in the variable Q_{dist} over the previous subsection is allowable since the rate covariance-contracting effects of frequent attitude updates are absent. The increase in the design variable $G_{g,filt}$ was found to produce improved performance over simply leaving $G_{g,filt} = G_{g,truth}$. The “robustified” model filter run again features an actual 10% inertia term error but with Q_{dist} tuned to $1 * (10)^{-6} I_{3x3}$ for compensation and $G_{g,filt}$ left identical to $G_{g,truth}$ to prevent undervaluation of the gyro data.

Table 4.9 presents the accompanying sample statistics. Clearly the nominal inertia model filter produces estimation performance several tenths of a degree superior to the nonmodel filter on each body axis. The robustified filter with inertia value errors beat the nonmodel on the second and third axes while the

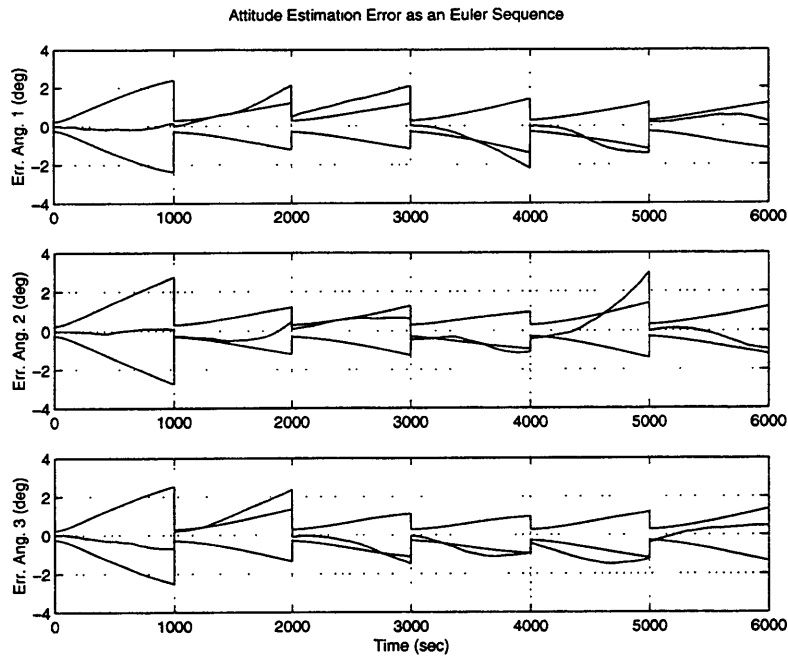


Figure 4-13: Nonmodel Filter Attitude Error During Tumbling - Low Frequency GPS

total performance over all three axes is superior as well. These results demonstrate that even in the event of GPS outage (or reduced data rate), a vehicle dynamics filter with 10% errors can still provide plant information useful for attitude tracking.

After the periodic GPS updates, all three filters' attitude error covariances typically fall around 0.3 degrees per axis. Since each estimator's attitude uncertainty grows significantly between external updates, the algorithms tend to discount their *a priori* attitude estimates in favor of the comparatively small error GPS data. However, during the ensuing gyro-only period of operation, the attitude uncertainty in the nonmodel filter generally grows more rapidly.

Figures 4-16 and 4-17 show the core reason for the model-based filter's superior attitude performance. With knowledge of vehicle inertial dynamics comes greater observability into the gyro bias, the primary driver of filter divergence in navigation settings. Note that the nonmodel filter's bias estimate tends to

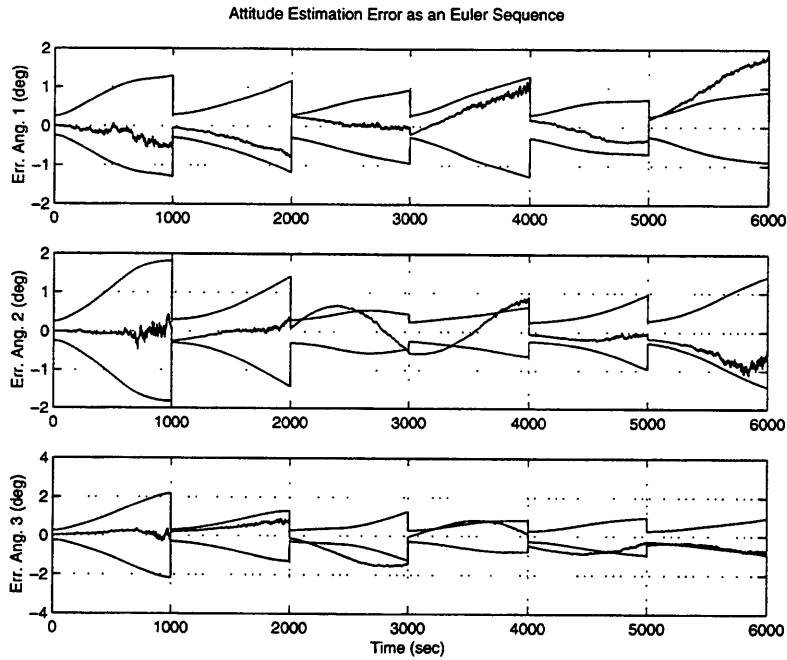


Figure 4-14: Model Filter Attitude Error During Tumbling - Low Frequency GPS

Axis	Mean (deg)	Std. Dev. (deg)	Mean Err. Mag. (deg)	68.2%-tile (deg)
Nonmodel Filter				
1	0.15	0.90	0.69	0.95
2	-0.01	0.67	0.47	0.52
3	-0.24	0.84	0.69	0.97
Model Filter				
1	0.15	0.55	0.39	0.43
2	-0.06	0.37	0.28	0.36
3	-0.19	0.64	0.55	0.72
Model Filter - 10% Inertia Errors				
1	0.23	0.94	0.74	0.84
2	0.06	0.58	0.39	0.39
3	-0.20	0.72	0.55	0.76

Table 4.9: Attitude Performance Statistics - Tumbling with Infrequent GPS Updating

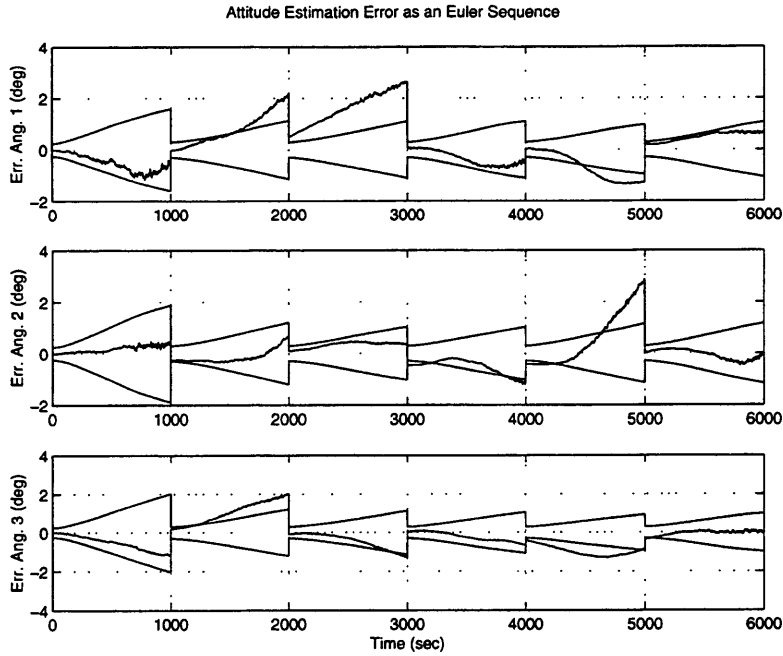


Figure 4-15: Robustified Model Filter Attitude Error During Tumbling - Low Frequency GPS

be high compared to its own perceived error. In contrast, the model filter's bias error typically lies within its slightly tighter $1\text{-}\sigma$ covariance bound.

4.4 Maneuver Performance

The previous two simulation test cases considered naturally LVLH-aligned motion and out of control tumbling motion. Although these scenarios are certainly possible during a given satellite mission, they do not take into account the full range of environmental disturbance torques and the action of an attitude controller. We now compare the model and nonmodel during the execution of a controlled attitude maneuver sequence. Runs are made with mild and worst-case disturbance environment torques. Also, we show the effect of gyro biases on disturbance torque estimation.

The specifics of the test scenario are given in Table 4.10. The rigid body

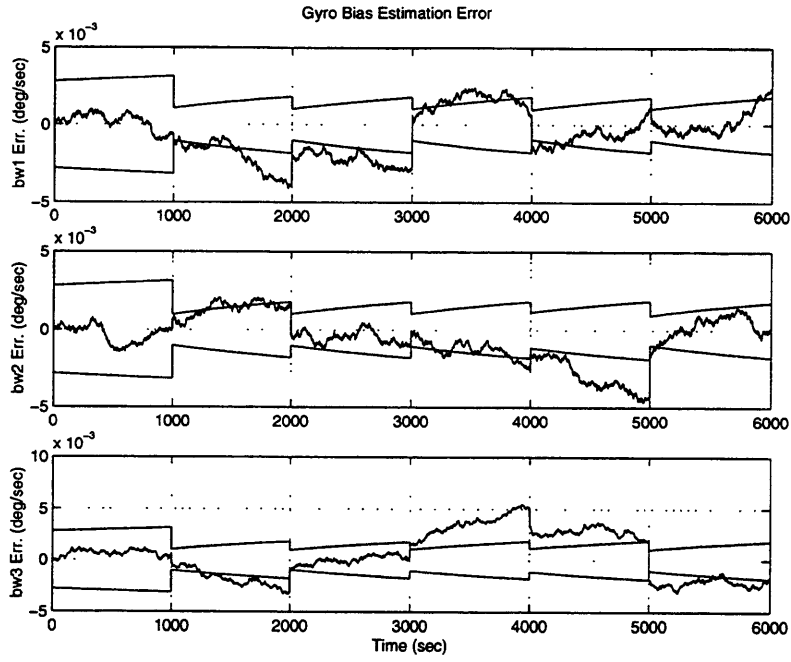


Figure 4-16: Nonmodel Filter Gyro Bias Error During Tumbling

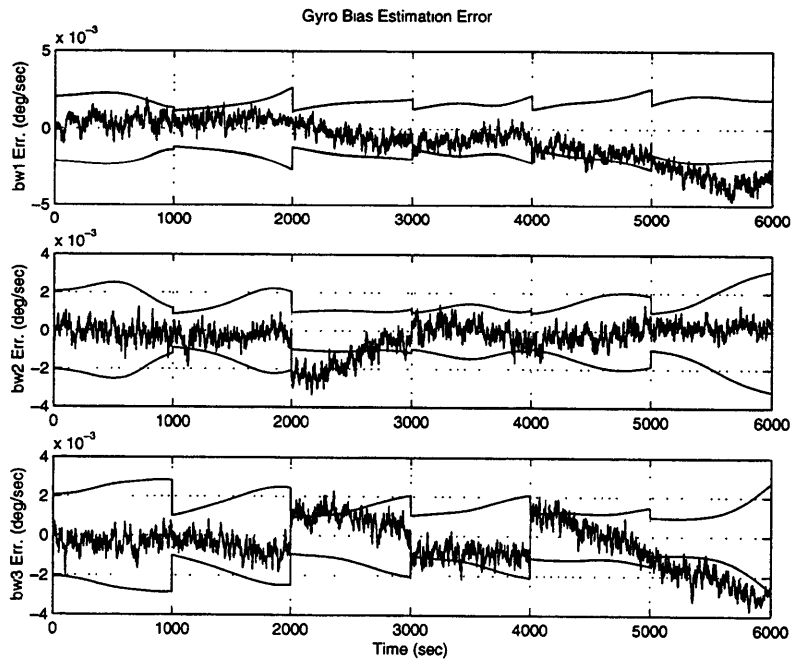


Figure 4-17: Model Filter Gyro Bias Error During Tumbling

Inertia	$I = \begin{bmatrix} 300 & 10 & -20 \\ 10 & 500 & 40 \\ -20 & 40 & 400 \end{bmatrix} \quad kg * m^2$
Initial body rate	$\omega_{bl}(0) = 0_{3x1}$
Initial attitude	$\phi(0) = 0^\circ, \theta(0) = 0^\circ, \psi(0) = 0^\circ$
Gyro update	Every second
Bias parameter	$A_g = -1 * 10^{-5} \text{ sec}^{-1}$
Bias parameter	$G_g = 8.23 * 10^{-7} \text{ rad/sec}^{3/2}$
Angle random walk	$ARW = 0.1 \text{ deg}/\sqrt{hr}$
GPS update	Every 1,000 seconds.
Multipath parameter	$A_{GPS} = -3.7 * 10^{-4} \text{ sec}^{-1}$
Multipath parameter	$G_{GPS} = 1.3 * 10^{-4} \text{ rad/sec}^{1/2}$
GPS white error	0.3 deg 1- σ per axis
Disturbance environment	Grav.-grad.; First case: stochastic disturbance at 100% of worst-case magnitude. Second case: stochastic disturbance at 20% of worst-case magnitude. $T_{solar,rms,worstcase} = 1.8 * 10^{-6} N * m.$ $T_{magnetic,rms,worstcase} = 9.0 * 10^{-6} N * m.$ $T_{aero,rms,worstcase} = 1.9 * 10^{-6} N * m.$
Control	Quaternion feedback to maintain attitude of Figure 4-18.
Control parameter	$\omega_n = 0.1, \zeta = 1$
Control parameter	$D = 2\zeta\omega_n I$
Control parameter	$K = 2\omega_n^2 I$
Orbit altitude	610 km

Table 4.10: System Description for Controller Maneuver Simulation

inertia matrix has been significantly increased to emulate a larger satellite. This change is made simply to demonstrate the model filter applicability to a range of vehicles. The initial conditions indicate an LVLH-aligned body with zero relative rate. Gyro measurements are available every second, with the usual “low” quality error characteristics.

In these runs, the GPS update interval is set at 1,000 seconds. As shown in the previous two sections, the performance difference between the model and nonmodel filters significantly narrowed as the GPS update interval decreased. In the present case of controlled satellite motion with stochastic disturbances, the

model and nonmodel filters were found to perform almost identically with GPS update intervals of less than 100 seconds. Since the model-based filter's benefits are most felt when periods of gyro-only operation are long, we present here runs with a 1,000 second update interval to continue highlighting the differences between the two estimator designs.

GPS white *and* multipath effects are both present. The latter is less relevant when the attitude measurements come in infrequently. However, we include this time-correlated error to fully tax the attitude estimators.

We give results for two different cases. In both, the full array of disturbance torques are included: deterministic gravity gradient and stochastic solar, magnetic, and aerodynamic effects. In the first pair of runs, the stochastic torques are set to their worst case values at an orbit altitude of 610 km. The the second pair, only twenty percent of the worst case values are used. Both are presented since the performance gap between the two filters varies substantially with the tenacity of the orbital environment. The lower the disturbance rms value, the greater the benefits of dynamic modeling in filter design. In general, the actual disturbance magnitude behavior depends significantly on the specific satellite design.

During the run, the attitude controller acts to achieve the attitude profile shown in Figure 4-18. Beginning at 500 seconds into the run and continuing every 1,000 seconds thereafter, the satellite executes an maneuver to a new LVLH-stationary orientation. Between the maneuvers, the controller acts as a regulator, maintaining the given orientation and countering the effects of environmental disturbances. This control profile allows a more interesting test case than the preceding sections and demonstrates the model filter's applicability to both moving and stationary satellites.

To emulate a closed-loop system, the controller acts on estimates of truth quantities. Since it is well suited for both large angle maneuvering *and* regulation, the quaternion and rate feedback controller of Section 2.2.1 is employed. The compensator gains are listed in Table 4.10. In this context, I refers to the

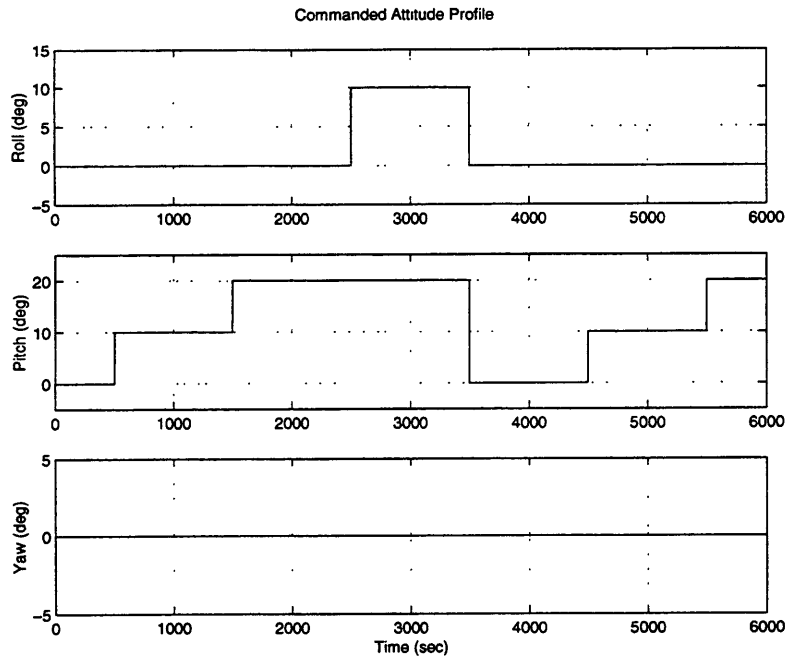


Figure 4-18: Commanded Attitude Profile for Maneuver, Expressed as a Local to Body Transformation

satellite inertia matrix, not the identity $I_{3 \times 3}$.

Worst Case Disturbance Environment

We begin by examining estimation and closed-loop performance with the truth environmental disturbance torques set at their worst case rms magnitudes. The addition of control and environmental disturbance torques should not effect the nonmodel filter design in any way. Since that filter model consists entirely of instrument error parameters, we will obtain best performance by simply matching the truth and filter parameter values.

The attitude estimation error achieved with the nonmodel design is shown in Figure 4-19. The filter covariances show the characteristic “sawtooth” behavior associated with growing gyro bias uncertainty remedied by occasional GPS updating. Note that the filter covariances generally give an accurate measure the actual performance level.

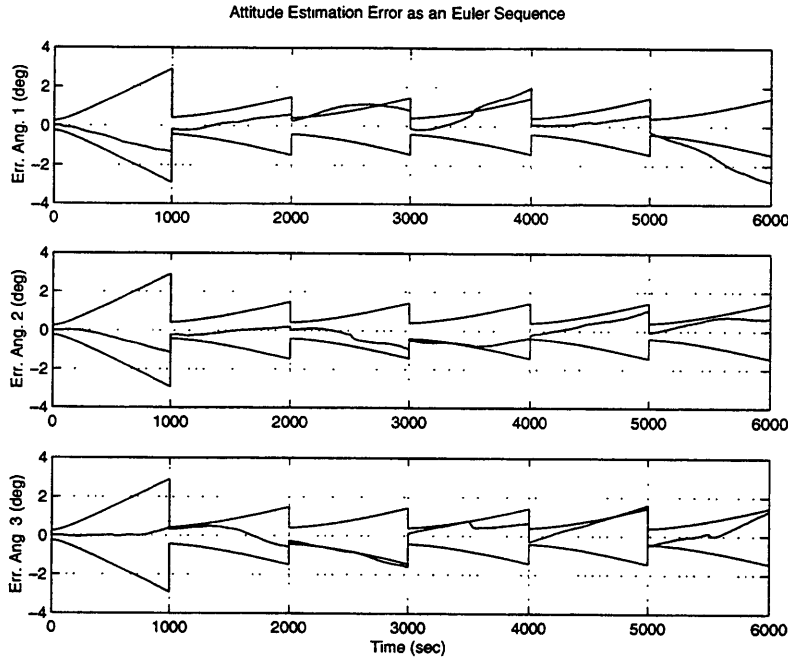


Figure 4-19: Nonmodel Filter - Attitude Estimation Error During Maneuver - Worst Case Torque

In contrast, the model filter design is complicated by the fact that the true environmental torques are generated from higher-order low and bandpass filters as described in Sections 2.2.3, 2.2.4, 2.2.5. It is not feasible to bog down the estimator design with identically complex models for torque estimation. Not only would we require the algorithm to track many fictitious and weakly observable states, but the higher order covariance propagation and matrix inversions would excessively load any available computing resources. Instead, we resort to the first order Gauss-Markov (FOGM) state model described in Section 3.1.2 for disturbance torque estimation. In this scheme, we add in an additional FOGM bandlimited state on each body axis. The design is tuned with a torque cut-off frequency ten percent *above* the orbital frequency and with a steady-state magnitude fifty percent higher than the true disturbance rms value. Additionally, the rate noise covariance Q_{dist} is set to one-tenth the worst case value for additional conservatism. Observability checks indicate that even with gyro bi-

ases and multipath effects present, the disturbance torques are observable when GPS updates are made. Alternatively, one may refrain from adding disturbance torque filter states and simply adjust upward the filter body rate design covariance Q_{dist} . Both of these filter design techniques were implemented; the ensuing performance difference appeared negligible.

Figure 4-20 shows attitude estimation performance achieved while employing the augmented torque state scheme to mitigate disturbance effects. Truth control torques are directly fed to the filter since actuator signals are assumed available for estimation purposes. Like the nonmodel filter covariances in Figure 4-19, the error uncertainty grows significantly between GPS updates since the model filter cannot perfectly estimate the severe environmental disturbances. The filter must inject the remaining torque uncertainty into the rate states to account for any unanticipated vehicle movement. The enlarged rate covariances feed the angle state, producing the sawtooth pattern seen in the figure.

Although difficult to eyeball off of Figures 4-19 and 4-20, which are scaled differently, the model filter covariances grow more slowly between GPS updates. Just prior to the attitude measurement, the model filter attitude uncertainties are around 0.8 deg. while those for the kinematic nonmodel filter fall around 1.4 deg.

Table 4.11 gives quantitative insight into the attitude error behavior by listing the simulation sample statistics. The model provides the most significant gains on the first and second error axes. Not that although third axis numbers are actually higher than the those of the nonmodel filter, the total *combined* error across all three axes, whether computed with a 1- or 2-norm is generally less with the model filter.

Another way to judge the attitude filters' relative performance is to compare the operation of the overall closed-loop system. Since the objective of the attitude controller is to execute a predetermined set of rotational maneuvers and holds, one should examine the degree to which the satellite follows the desired attitude profile of Figure 4-18. If the controller is not given sufficiently accurate

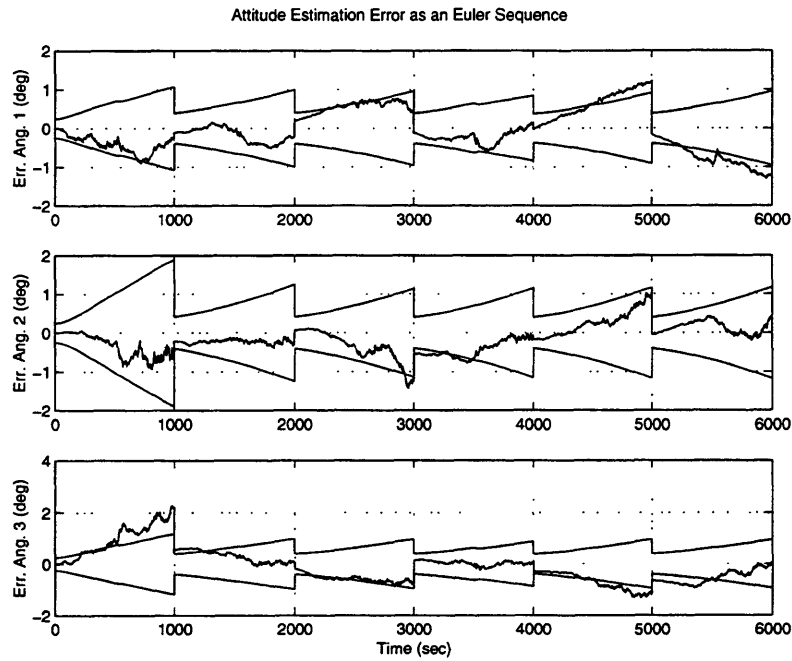


Figure 4-20: Model Filter - Attitude Estimation Error During Maneuver - Worst Case Torque

Axis	Mean (deg)	Std. Dev. (deg)	Mean Err. Mag. (deg)	68.2%-tile (deg)
Nonmodel Filter				
1	-0.03	0.96	0.72	0.96
2	-0.09	0.49	0.41	0.62
3	0.11	0.61	0.47	0.55
Model Filter				
1	-0.07	0.55	0.46	0.59
2	-0.16	0.37	0.31	0.37
3	0.09	0.68	0.52	0.63

Table 4.11: Attitude Estimation Error During Maneuver - Worst Case Torque

information, then it certainly cannot achieve the desired pointing objectives.

Figure 4-21 plots the total angular error between the commanded and actual attitude trajectories when the closed-loop attitude control system included both the nonmodel and model-based filters. The heavier 'x' line tracks the nonmodel performance; the thinner solid line shows the model filter loop. The spikes midway between the GPS updates reflect the suddenly changing control objectives in Figure 4-18.

The nonmodel loop consistently drifts away from the commanded attitude during the regulation intervals. Since the quaternion feedback controller of Section 2.2.1 requires both an attitude and body rate input, it must rely on the *unfiltered* gyro output for rate knowledge. Recall that the nonmodel approach contains only attitude as a filter state, not body rate. Thus, as the gyro bias adds fictitious rate signals to the gyro output, the nonmodel loop will steadily rotate away from the desired orientation.

On the other hand, the model filter estimates both attitude and rate and therefore provides the feedback controller a more accurate depiction of true system behavior. As seen in Figure 4-21, the model filter loop, after undergoing an initial transient period during which the state partitions of body rate, gyro bias, and disturbance torque are sorted, behaves no worse than the nonmodel filter loop. While the latter continues to drift away from the desired behavior, the model filter occasionally provides pointing performance several degrees superior, despite that fact that the estimator was designed with simplified torque models.

Mild Disturbance Environment

The preceding set of figures illustrated model and nonmodel performance when the stochastic disturbances occurred at their worst possible magnitudes for a given satellite mass distribution and orbit altitude. Through careful vehicle design and orbit selection, the disturbance torques can be significantly reduced [27]. We consider now the same control scenario, but with disturbance torque

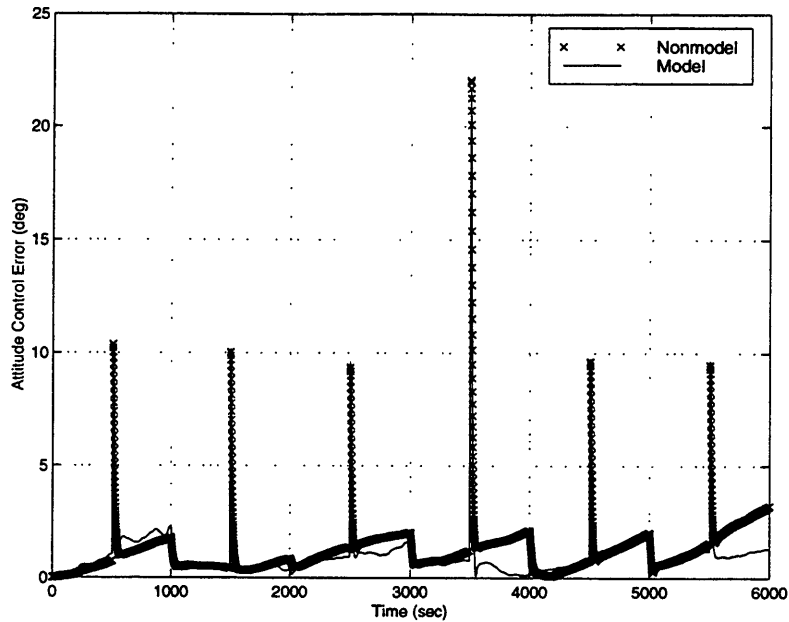


Figure 4-21: Nonmodel & Model Filters - Attitude Control Error During Maneuver - Worst Case Torque

magnitudes reduced to only twenty percent of their worst case rms values.

Table 4.12 shows the attitude estimation error sample statistics for both estimator designs. Referring back to Table 4.11, which gave the analogous results for the worst case environment, we see the nonmodel numbers have not changed. Since the instrument array is the same and the true attitude profile is similar, there is no reason to suspect a significant difference. Examining the first and second axes we see that the gap between the two filters has grown slightly; the model-based method provides improved performance when the exogenous inputs are more benign. As the disturbance environment weakens, the vehicle model should portray more accurately the true system dynamics. The third axis shows a notable degradation in performance and is actually worse than the nonmodel error.

However, Figure 4-22 shows that the performance slip on the third axis, which is likely due to the unavoidable mismatch between real and design distur-

Axis	Mean (deg)	Std. Dev. (deg)	Mean Err. Mag. (deg)	68.2%-tile (deg)
Nonmodel Filter				
1	-0.03	0.96	0.72	0.96
2	-0.09	0.49	0.41	0.62
3	0.11	0.61	0.47	0.55
Model Filter				
1	-0.06	0.39	0.33	0.42
2	-0.22	0.26	0.25	0.26
3	0.08	0.77	0.61	0.73

Table 4.12: Attitude Estimation Error During Maneuver - Mild Torque

bance models, is compensated with significantly improved closed-loop system behavior. Where the nonmodel loop continues to diverge from the commanded attitude, the model-based loop maintains consistently improved pointing behavior, after the initial transient period is passed. The model loop error remains constant around 1 degree while the competing design experiences consistently growing error. Compared to the runs featuring worst case environment behavior, we see that the model filter approach has benefited significantly from the more benign plant torquing.

Disturbance Torque Estimation

In the previous two sections on controlled performance, the model filter mitigated the ill effects of the stochastic environment torques by attempting to estimate them. Since the torque itself does not feed directly into either the attitude or rate measurements, its value must be inferred indirectly from the behavior of other plant states. Section 3.1.2 gave a detailed discussion on how to incorporate disturbance torque estimates into the model filter methodology.

Obviously, the quality of torque estimation depends significantly on the presence of measurement errors. A large gyro bias would naturally tend to obscure the observability of these exogenous system inputs. As the gyro bias level diminishes, the quality of torque estimation should increase since its effect on the

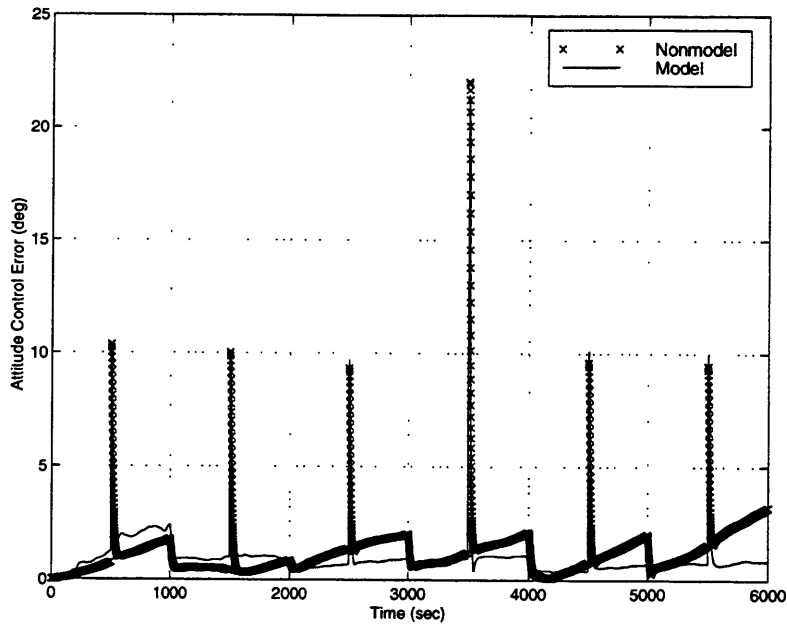


Figure 4-22: Nonmodel & Model Filters - Attitude Control Error During Maneuver - Mild Torque

satellite body rate becomes more apparent. Here, we briefly give quantitative data to support the notion that gyro biases tend to degrade our ability to track external torques.

Figure 4-23 depicts a truth model stochastic environment disturbance torque tuned to the worst case values of Table 4.10. The system measurements, which consisted of gyro data every 1 second and GPS updates every 100 seconds, were fed to a model-based filter. The controller was deactivated and the satellite was allowed to slowly tumble.

Figure 4-24 shows the disturbance torque state estimates when the usual strong bias typical of a low quality gyro was added to the rate measurements. Because of the 100 second GPS updating, the model filter had observability into all system states, included the body rates, gyro biases, and disturbance torques. However, compared to the true torque signals, the estimates seem somewhat erratic. The torque estimation error sample statistics are given in Table 4.13.

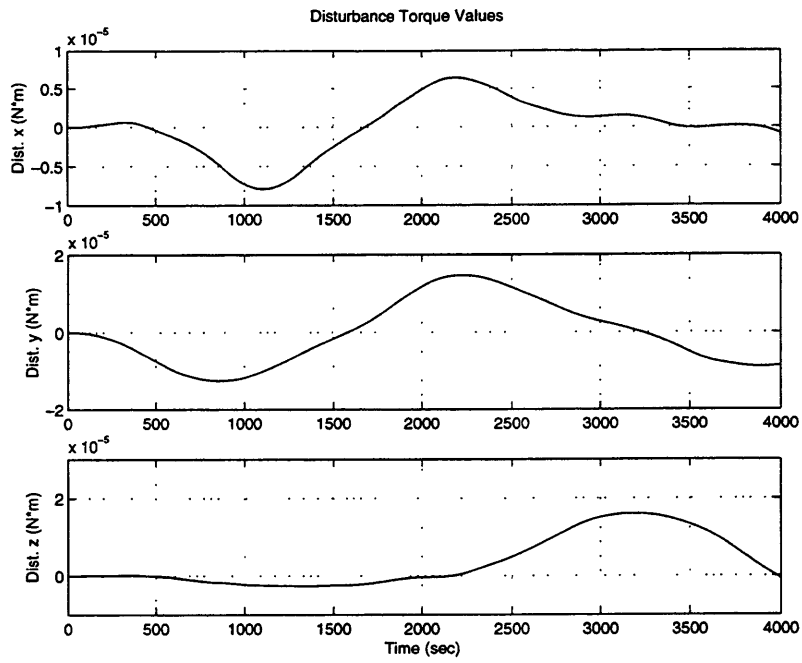


Figure 4-23: True Total Disturbance Torques

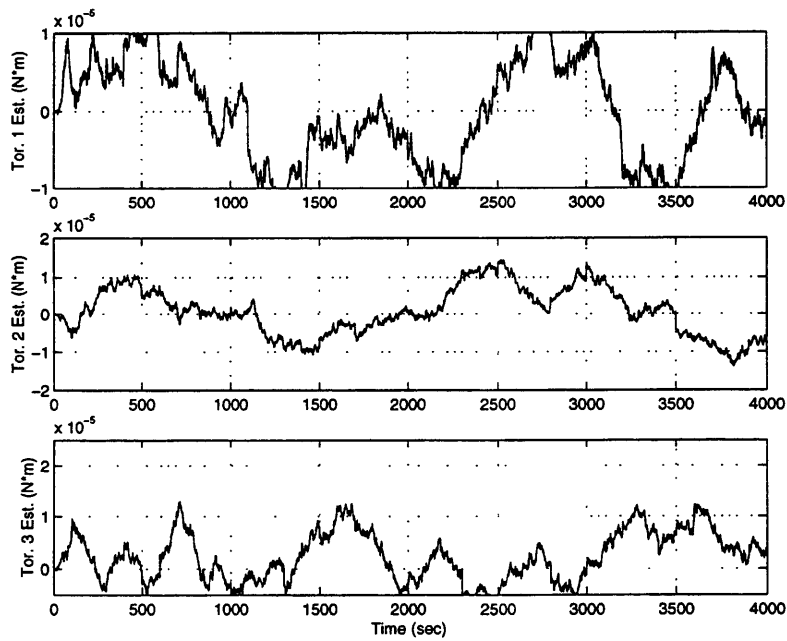


Figure 4-24: Disturbance Torque Estimates With Gyro Biases Present, Model Filter

Figure 4-25 displays the corresponding torque estimates in the case of zero gyro bias. The estimated signals now follow the true torque much more closely, achieving the significantly improved level of performance seen in Table 4.13. Consistent with the intuition that cleaner rate measurements should allow greater insight into the system inputs, the additional effort to implement the algorithm of Section 3.1.2 is rewarded most when the gyro bias is small.

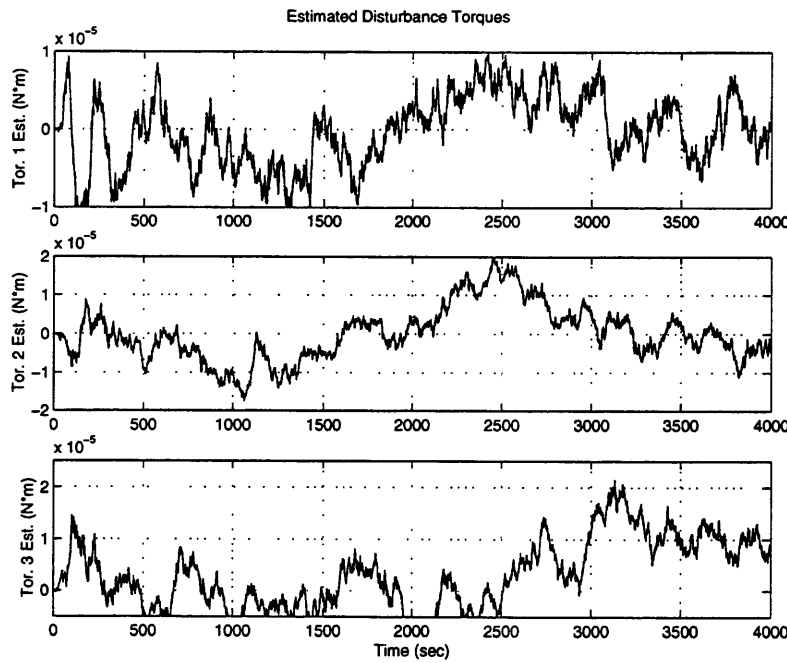


Figure 4-25: Disturbance Torque Estimates With Bias-Free Gyros, Model Filter

However, in the previous two sections on model vs. nonmodel performance in the controlled maneuver case, we saw that even with the severe bias in place and including the torques as a filter state, the model-based methodology still provided superior steady-state performance. This example validates the techniques of Section 3.1.2 and indicates under what conditions the disturbance torques can be best estimated. Clearly, if one is attempting to use disturbance torque estimation for actuator and vehicle health monitoring, then any decision logic that uses torque levels to isolate system failures should consider the effects to instrument biases on the quality of state tracking.

Axis	Mean	Std. Dev.	Mean Err. Mag.	68.2%-tile
Nonmodel Filter				
1	1.86	71.6	59.4	92.6
2	-12.4	79.0	63.8	77.5
3	13.1	71.8	57.0	78.8
Model Filter				
1	2.47	31.6	26.0	32.9
2	-5.20	51.7	43.2	50.3
3	9.96	41.0	33.7	44.1

Table 4.13: Disturbance Torque Estimation Error - All Units 10^{-7} N*m

4.5 Gyro-Free Operation

So far, the thrust of the filter simulations has been on examining the merits of including vehicle dynamics models when gyro quality is low. The guiding principle is to enhance the state propagation between measurements by providing the estimator with better insight into how the system naturally behaves. If the gyro quality were to degrade further, a sufficiently accurate dynamics model would become even more necessary to maintain acceptable attitude performance.

This section examines the role of vehicle modeling when gyro information is totally unavailable. Gyro-free operation may occur under several circumstances. The INS may be deactivated for power savings, the satellite may not even carry inertial equipment, or the INS might fail on-orbit or degrade to the point where rate measurements are no longer useful.

Previous research into gyro-free attitude filter design in the absence of rate gyros has generally focused on dynamic model inclusion. Just as in the low quality INS case, the vehicle model offers useful plant information not obtainable with mere kinematics-based filtering. Motivated by the possibility of gyro omission in system design or an undesirable on-orbit INS failure, Crassidis and Markley devised a predictive model-based filtering scheme to propagate rate and quaternion states between attitude measurements [14]. This method is based on a nonlinear predictive method developed for control design in the pre-

sense of model uncertainty and/or complex dynamics. However, filter designs are possible that do not consider satellite rate dynamics. Responding to a real INS degradation on the Midcourse Space Experiment, Sharer, et. al. modified their attitude determination filter to propagate attitude based only on the most recent INS rate estimate [38].

Here, we examine the relative performance of the nonmodel and model filters when GPS provides the only system measurement. In addition, the negative consequences of taking the GPS attitude output as truth are also demonstrated. We will find that even when inertia terms errors exist, the model filter provides superior attitude tracking and maintains closed-loop stability while competing attitude schemes induce undesirable controller behavior.

Truth System and Filter Redesign

The simulation description is given in Table 4.14. Note that although the satellite begins the simulation in an LVLH-aligned orientation with zero relative body rate, the stochastic disturbances (solar radiation, magnetic dipole, and atmospheric drag) will push the system out of this initial alignment. To maintain an arbitrary nadir-direction pointing mission requirement, a bang-bang controller will exert a 0.5 milli-Newton meter-torque on any axis that exceeds 5 degree attitude perturbation from nominal LVLH. In order to maintain control loop stability, the attitude filter must provide sufficiently accurate state estimates. If the attitude estimation error becomes excessively large, the thrusters may fire unnecessarily a push the satellite away from its desired orientation.

The GPS multipath parameters in the table correspond to a 0.28 deg steady-state error with a time constant of around half an orbit period.

When operating in a gyro-free mode, the nonmodel filter must maintain a constant q_{bl} estimate between GPS updates. As seen in Equation (3.58), propagation of the quaternion state requires a gyro output. If the gyro is inoperative or malfunctioning, then we must assume $\dot{q}_{bl} = 0_{4 \times 1}$ as no other data source is available. Of course, the satellite still continues to move, even while \hat{q}_{bl} is

Inertia	$I = \begin{bmatrix} 40 & 1 & -4 \\ 1 & 20 & 3 \\ -4 & 3 & 30 \end{bmatrix} \quad kg * m^2$
Initial body rate	$\omega_{bl}(0) = 0_{3x1}$
Initial attitude	$\phi(0) = 0^\circ, \theta(0) = 0^\circ, \psi(0) = 0^\circ$
Gyro update	None
GPS update	First case: 10 sec; second case: 100 sec.
Multipath parameter	$A_{GPS} = -3.7 * 10^{-4} \text{ sec}^{-1}$
Multipath parameter	$G_{GPS} = 1.3 * 10^{-4} \text{ rad/sec}^{1/2}$
GPS white error	0.3 deg 1- σ per axis
Disturbance environment	Grav.-grad. + envirn. dist. at 10% of worst-case mag. $T_{solar,rms,worstcase} = 1.8 * 10^{-6} N * m.$ $T_{magnetic,rms,worstcase} = 8.3 * 10^{-6} N * m.$ $T_{aero,rms,worstcase} = 2.8 * 10^{-7} N * m.$
Control	Bang-bang to maintain ± 5 deg nadir pointing per axis.
Orbit altitude	800 km

Table 4.14: System Description for Gyro-Free Simulation

held constant. To account for the attitude uncertainty accumulated during this unobservable vehicle motion, the now-fictitious angle random walk term, R_g in Equation (3.64), is increased in a manner consistent with the expected motion of the system. During simulations, several values were used, all producing very similar performance results. For the run in the next section, this parameter was set to $(50 \text{ deg}/\sqrt{hr})^2 * I_{3x3}$ indicating that satellite might move as much as 50 degrees on each axis over a one hour period. The method of estimating GPS multipath errors is unchanged from the nominal nonmodel estimator design.

The model filter design is quite straightforward. The relations of Section 3.1 still apply exactly; we simply will not perform any gyro updating. However, since only attitude measurements are available, we cannot estimate disturbance torque. Because of system observability constraints, we are limited to estimating the attitude, body rates, and multipath errors. Therefore, the filter rate white noise design term Q_{dist} is set to ten times the *actual* disturbance torque variance to account for the unknown time-correlated environmental influences on satellite

motion. In addition, we tune the GPS multipath steady-state variance to twice its truth value to balance the high Q_{dist} setting.

As an alternative to filtering entirely, one may take the GPS receiver output as truth. This signal is merely the true attitude corrupted by time-correlated multipath and white errors as described in Section 2.3. Between measurements, we must hold the most recent output as our attitude estimate until the next signal becomes available. Obviously, this method of state “estimation” works well only when the GPS update rate is high and the corrupting errors are small.

Frequent GPS

When a GPS array-equipped satellite is near its nominal orientation and a sufficient number of GPS emitter satellites are visible, attitude measurements should be available fairly often. Here, we consider gyro-free operation with GPS data available every 10 seconds. The attitude error for the nonmodel filter during a 4,000 second run is shown in Figure 4-26. Every 10 seconds, the filter combines its *a priori* estimate of q_B with the GPS output. The new estimate is held constant for 10 seconds until another measurement is available. This gyro-free operation produces a very jagged looking attitude error plot since the the estimator is now at the mercy of a single noisy sensor.

As the real environmental disturbances push the satellite about, the control system compares the estimated attitude with the ± 5 degree per axis deadband limits. As the thrusters fire, the vehicle accelerates in the opposite direction until the limit is again exceeded. As seen by comparing Figure 4-26 with Figure 4-27, which shows the corresponding true vehicle attitude and the 5 degree control limits for the same run, the attitude error accumulates as the true body rates become greater and greater. Eventually, holding a single attitude estimate over a 10 second interval is insufficient to grasp the true system behavior. The error grows substantially and the controller acts on less and less accurate data, eventually leading the true satellite attitude to diverge from the desired orientation.

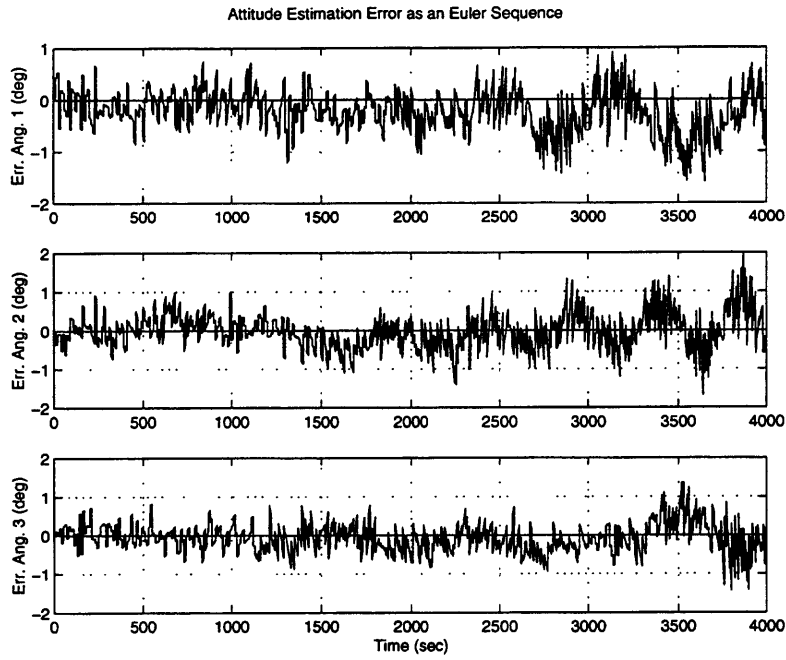


Figure 4-26: Nonmodel Filter - Attitude Error Without Gyros

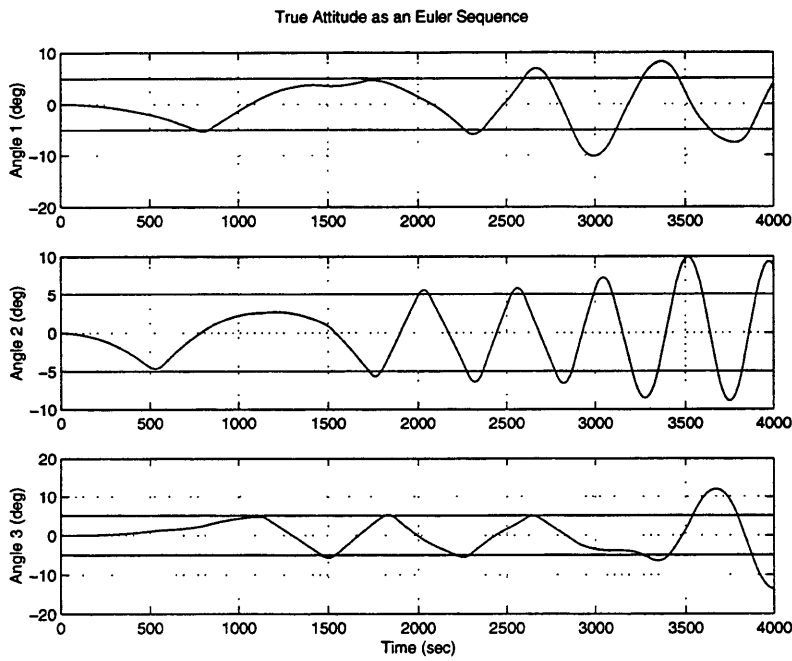


Figure 4-27: Nonmodel Filter - True Attitude Without Gyros

In contrast, the model filter's vehicle rate dynamics considerations preclude attitude solution divergence, as depicted in Figure 4-28. (Note that the axis scaling is different from Figure 4-26). After an initial transient period, the estimation error begins to reconverge to values sufficiently small to maintain closed-loop system stability, indicated by the proper enforcement of the 5 degree deadband in Figure 4-29.

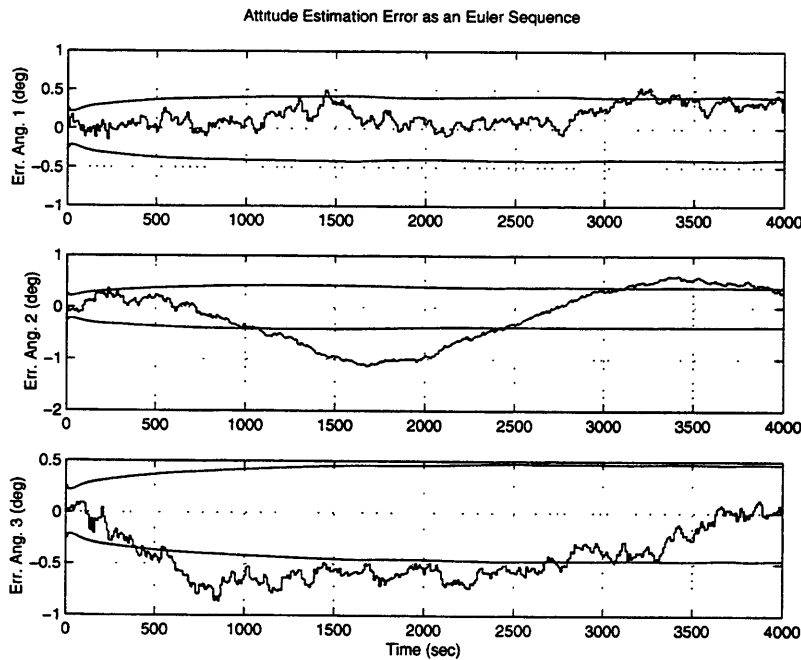


Figure 4-28: Model Filter - Attitude Error Without Gyros

Figure 4-30 strengthens the model-based result by showing that even in the presence of inertia matrix modeling error, the filter and can still maintain an attitude fix sufficient to maintain closed-loop stability for an extended period. Here, the true and filter design inertia matrices were perturbed by an arbitrary 5 percent in every element as shown in Table 4.15. The design process noise variable Q_{dist} was increased by a factor of three to compensate. As the deadband control objective is still satisfied in the figure, we see that a mildly perturbed system model can still provide adequate rate information to propagate q_{bl} effectively.

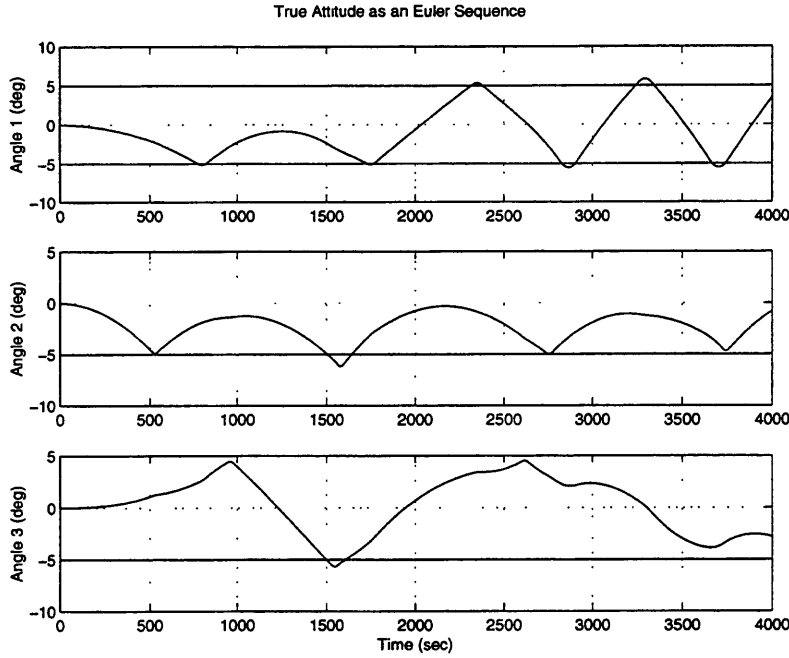


Figure 4-29: Model Filter - True Attitude Without Gyros

$I_{truth} = \begin{bmatrix} 40 & 1 & -4 \\ 1 & 20 & 3 \\ -4 & 3 & 30 \end{bmatrix} \quad kg * m^2$	$I_{filt} = \begin{bmatrix} 38 & 1.05 & -3.8 \\ 1.05 & 21.0 & 2.85 \\ -3.8 & 2.85 & 31.5 \end{bmatrix} \quad kg * m^2$
$\lambda_{i,truth} = 19.0, 29.6, 41.4$	$\lambda_{i,filt} = 20.1, 30, 6, 39.8$
$v_{i,truth} = \begin{bmatrix} -0.10 \\ 0.95 \\ -0.29 \end{bmatrix}, \begin{bmatrix} 0.32 \\ 0.31 \\ 0.90 \end{bmatrix}, \begin{bmatrix} -0.94 \\ 0.00 \\ 0.33 \end{bmatrix}$	$v_{i,filt} = \begin{bmatrix} -0.11 \\ 0.95 \\ -0.28 \end{bmatrix}, \begin{bmatrix} 0.41 \\ 0.30 \\ 0.86 \end{bmatrix}, \begin{bmatrix} -0.91 \\ 0.01 \\ 0.42 \end{bmatrix}$

Table 4.15: Truth and Erroneous Filter Satellite Inertia Matrices and Their Eigenproperties - Gyro-Free Scenario

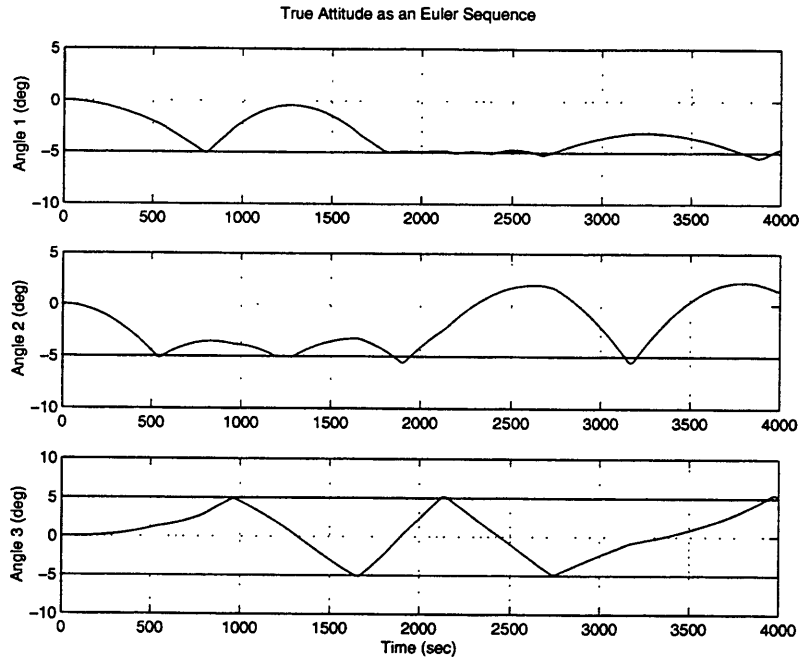


Figure 4-30: Robustified Model Filter - Attitude Error Without Gyros

Seeking an easy alternative to attitude filtering in general, one might ask the question, “How would closed-loop performance compare if we were to take the GPS output as truth, and completely avoid the extended Kalman filter algorithm?”. Figure 4-31 indicates that the closed-loop system would behave similarly to when the nonmodel filter was implemented. Very quickly, the time-correlated multipath errors and disturbance torquing induce considerable error in the attitude solution, accelerating the system into unstable closed-loop behavior. The estimation error grows rapidly as the 10 second data hold becomes inadequate to discretize the true satellite motion.

Table 4.16 presents the simulation sample error statistics for the four preceding runs. Note that the numbers can be misleading. The initial transient errors in the model filter performance elevate the second and third axis numbers above their nonmodel counterparts. However, an examination of the closed-loop attitude behavior with regard to the deadband limits indicates that the model and robustified model filters indeed provide superior performance.

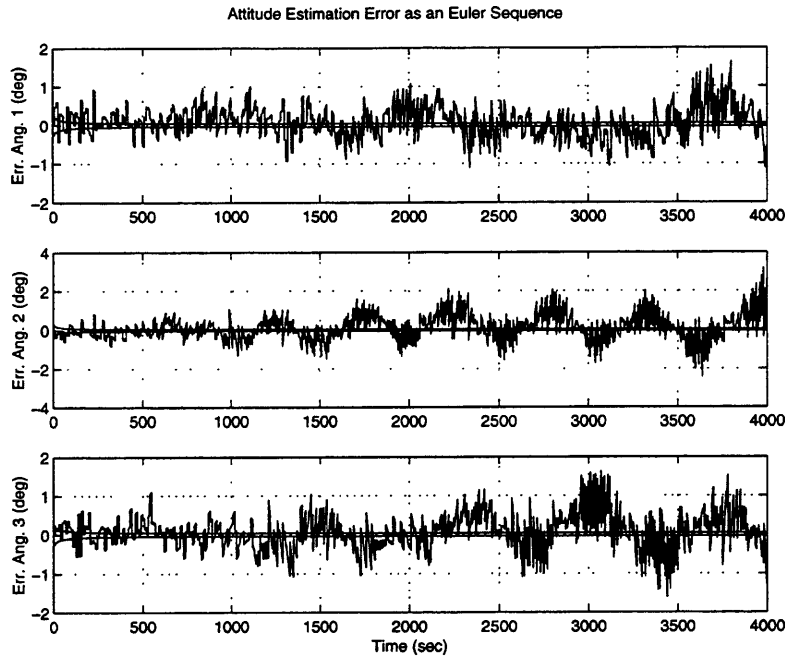


Figure 4-31: GPS Receiver Solution - Attitude Error Without Gyros

Axis	Mean (deg)	Std. Dev. (deg)	Mean Err. Mag. (deg)	68.2%-tile (deg)
Nonmodel Filter				
1	-0.23	0.40	0.36	0.44
2	-0.02	0.45	0.35	0.43
3	-0.07	0.37	0.30	0.36
Model Filter				
1	0.17	0.15	0.18	0.24
2	-0.16	0.53	0.46	0.55
3	-0.43	0.24	0.44	0.58
Robustified Model Filter With 5% Inertia Errors				
1	-0.17	0.30	0.26	0.35
2	-0.30	0.22	0.32	0.46
3	0.08	0.24	0.20	0.26
GPS Receiver Output				
1	0.06	0.39	0.32	0.39
2	0.12	0.62	0.48	0.57
3	0.07	0.44	0.34	0.41

Table 4.16: Attitude Error Performance - No Gyros and Frequent GPS

Sparse GPS

The previous discussion indicated that the model filter methodology was sufficient to keep attitude estimation error small enough for stable closed-loop performance when attitude updates were frequently available. But what if the GPS interval was increased from 10 seconds to 100 seconds? Clearly, we must rely more on the vehicle dynamic information during the more lengthy inter-measurement propagation periods.

Figures 4-32 and 4-33, which plot the attitude estimation error and the closed-loop system attitude, show that the model filter methodology, when given an exact representation of the satellite inertia terms, still provides adequate estimation quality for stable closed-loop control operation. The true system is still driven by stochastic, time-correlated environmental disturbances modeled in the filter only as a white noise input on the rate states. As in the 10 second update simulation, the filter model noise intensity is equal to 10 times the actual combined disturbance root mean square value.

In the case of a 10 second update period, the attitude estimates obtained through both nonmodel filtering and taking the GPS measurement as truth were shown to quickly degrade as the system continued to move. The inadequacy of this $\dot{\hat{q}}_{bl} = 0_{4 \times 1}$ propagation is even more apparent when the GPS sample interval grows to 100 seconds. Figure 4-34 shows that the unfiltered attitude solution taken directly from the GPS receiver quickly diverges from truth. The nonmodel filter was found to diverge similarly; recall that it could not maintain closed-loop stability even at a higher GPS output rate. Clearly, this level of performance is inadequate for control purposes and further justifies vehicle model inclusion in the absence of rate gyros.

Table 4.17 summarizes the filter runs depicted in Figures 4-32 through 4-34. For the model filter, the error standard deviation remains small, on the order of 1 degree or less. For the GPS point-by-point solution, the statistics indicate rapid estimate divergence.

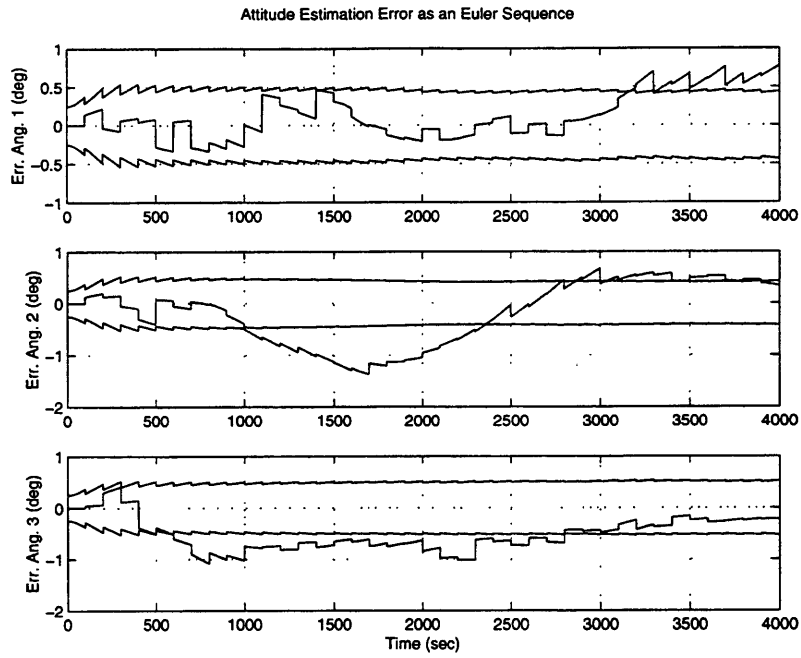


Figure 4-32: Model Filter - Attitude Error Without Gyros

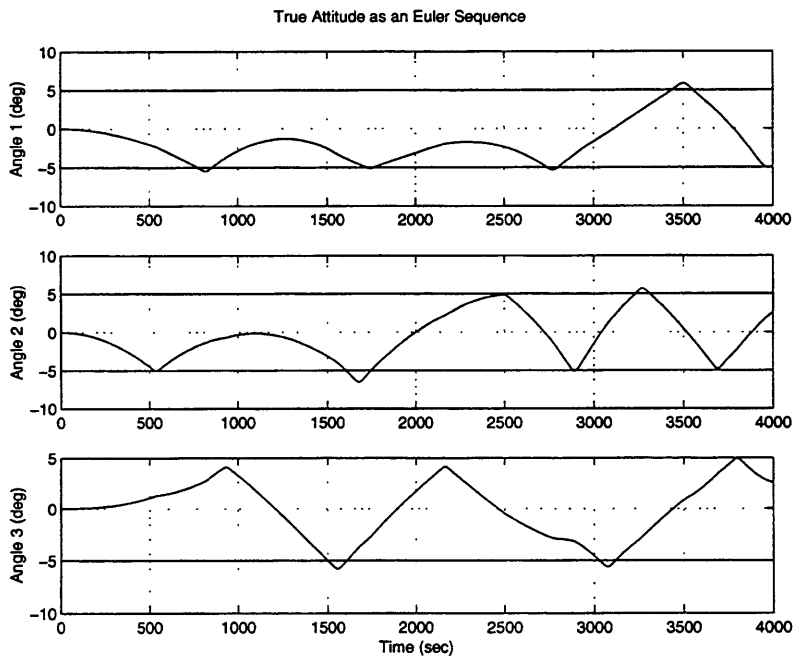


Figure 4-33: Model Filter - True Attitude Without Gyros

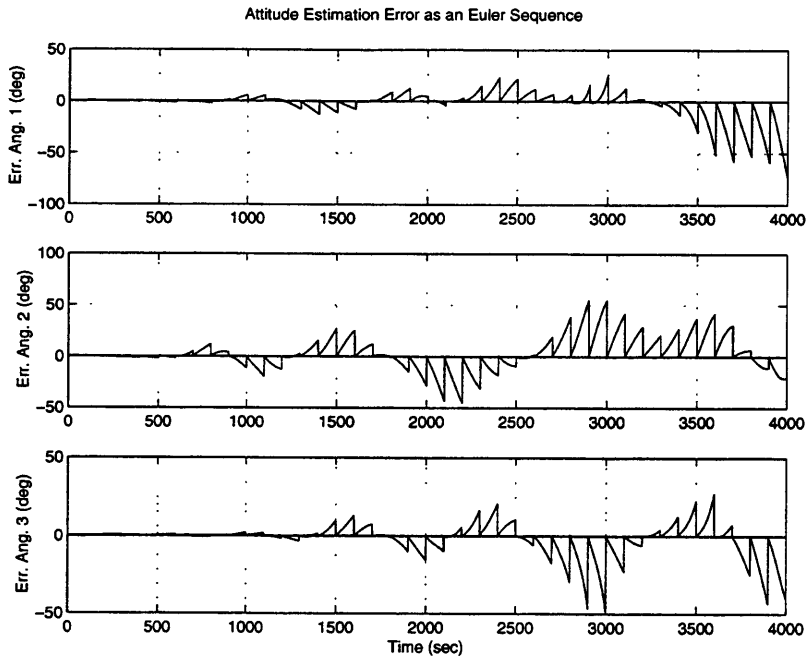


Figure 4-34: GPS Receiver Solution - Attitude Error Without Gyros

Axis	Mean (deg)	Std. Dev. (deg)	Mean Err. Mag. (deg)	68.2%-tile (deg)
Model Filter				
1	0.13	0.29	0.24	0.30
2	-0.19	0.60	0.51	0.58
3	-0.52	0.32	0.55	0.70
GPS Receiver Output				
1	-2.53	12.41	6.4	5.1
2	3.08	14.82	10	12.0
3	-1.96	9.55	5.5	5.6

Table 4.17: Attitude Error Performance - No Gyros and Infrequent GPS

4.6 Summary

This chapter has given specific test cases supporting the hypothesis that model-based filtering can provide superior attitude estimation performance when compared to traditional kinematic, or nonmodel, filter designs. We have generally found that the specific performance improvement depends on several factors which include, but are not limited to, the specific satellite operation mode, the frequency of external GPS updating, and the severity of environmental disturbances. An additional consideration is modeling error in the form of moment of inertia perturbations.

The chapter began with the definition of four error sample measures. These metrics are intended to provide additional insight beyond the attitude error vs. time plots and the behavior of the closed-loop system. It went on to compare performance for marginally stable LVLH-aligned motion, out of control tumbling, controlled attitude maneuvers, and bang-bang nadir-pointing regulation. These examples progressed in complexity, gradually adding in GPS multipath error considerations, additional disturbances, and two differing control implementations.

Chapter 5

Conclusions

This thesis has examined the role of vehicle dynamics modeling for enhanced satellite attitude determination. In contrast to the traditional philosophy of including only kinematic relations in filter design, the estimator has been expanded to include both kinematic and dynamic information, thus aiding the rate gyro in propagating attitude estimates between external measurements. Since the first order differential equations governing quaternion and body rate propagation are both nonlinear, this thesis employed a modified extended Kalman filter (EKF) algorithm for state filtering.

The advent of small, low cost inertial sensors, particularly strapdown gyroscopes which typically contain large output error components motivated this investigation. Since it is reasonable to expect periods of satellite operation when external global positioning system (GPS) or other attitude updates are unavailable, we must introduce additional plant dynamics information, in the form of Euler coupling relations, to slow the divergence of filter attitude solutions. GPS measurements could become inaccessible for a number of reasons. Out of control tumbling may require periods of wavelength integer ambiguity resolution. Portions of the satellite orbit might actually lie above the reach of GPS satellite communication. Further, the GPS attitude receiver may be deactivated for power savings.

Chapter 1 began the thesis by discussing the differences between kinematic-

(“nonmodel”) and dynamics-based (“model-based”) filtering. Discussions of an inertial navigation system (INS) - GPS instrument suite and methods of satellite control were presented. The next chapter gave a detailed discussion of a satellite truth model, comprised of rigid body dynamics, moving reference frame definitions, environmental disturbance effects, and measurement models. Chapter 3 continued by fully expounding both the nonmodel and model-based attitude determination filters. Finally, Chapter 4 examined the performance of both estimators in four simulation test cases. These simulation scenarios are intended to capture a reasonable range of on-orbit operating conditions while highlighting key differences between the two filter methodologies. In addition, two of the simulations indicate that even in the presense of inertia term uncertainty, the model filter can still provide enhanced estimation performance.

5.1 Conclusions

The fundamental conclusion of this thesis, obtained by comparing the simulation results to the initial objectives, is that vehicle dynamic modeling can significantly enhance satellite attitude determination. The strength of the model-based approach lies in its more realistic method of propagating system states. Since the EKF algorithm entails considerable coupling between state estimates, covariance propagation, and measurement incorporation, the specific improvement offered depends critically on the prevailing GPS measurement intervals, disturbance environment intensity, and vehicle mass distribution. Naturally, the results presented here apply to the case of low quality gyro error characteristics. If the strapdown inertial sensors are of sufficiently high quality, then the additional benefits of model inclusion are negligible.

The first, second, and fourth simulations, which featured local vertical-local horizontal (LVLH) aligned motion, out of control tumbling, and gyro-free operation, respectively, indicate that performance gains obtained through vehicle modeling increase with GPS update interval. (Conceptually, the GPS sensor

could be replaced with any external attitude measurement). When the attitude measurement period is large, on the order of 1,000 seconds or more, the model filter outperforms the nonmodel filter on the order of several tenths of degrees per axis. Thus, the model enhances the vehicle's autonomy from external aiding. However, in the complete absence of GPS signals, even the model filter attitude solution will slowly diverge, although typically at a rate less than that with nonmodel implementation. As the EKF covariance propagation is state dependent, the specific divergence rate improvement depends on the current mode of satellite motion (stable, tumbling, etc.).

The marginal gains in autonomy from external aiding can play a key role in maintaining closed-loop control performance. In the simulations on attitude maneuvering and bang-bang regulation, we saw that when GPS data is sparse, model-based filtering improves pointing performance on the order of several degrees when gyros are present and actually prevents closed-loop instability gyro data becomes unavailable. The maneuvering test case indicated that rate feedback for control usage is inadvisable when gyro quality is low, unless vehicle model information is included. This particular simulation also showed that disturbance torque estimation is difficult when gyro bias drift is large. In these situations, it may be desirable to inflate the filter design covariances, rather than add extra torque states and thereby increase the algorithm's computational load.

The tumbling and gyro-free runs also indicate that even when the attitude update interval is large, the model filter can tolerate moderate plant uncertainty in the form of inertia term errors and still provide performance superior to competing nonmodel designs. In these situations, the tracking performance is on the order a few tenths of a degree across all three body axes. When GPS information is frequently available, the error statistics are comparable for the two designs.

Finally, we must note that while the kinematic, or nonmodel, approach is filter design is essentially straightforward once the instrument error models are

sufficiently understood, the model-based design can require considerable filter “tuning”. The set of design covariance variables that provides optimum attitude tracking may be somewhat skewed from the actual truth conditions. As such, to maintain estimation error stability and superior tracking, a model-based filter may require differing sets of design parameters, depending on the current mode of vehicle operation.

5.2 Directions for Continued Investigation and Implementation

This thesis has focused on the design and performance differences between the kinematic and dynamic approaches to attitude filtering. We have performed several simulation examples that demonstrate the potential benefits of model-based state estimation. However to take this methodology closer to on-orbit implementation and to expand the formal research knowledge in this field, there are several further steps which must be taken. Specifics include the following.

- This investigation isolated the satellite translational and rotational dynamics, focusing only on the latter. This separation was motivated our interest in low cost micromechanical gyros which tend to introduce significant error signals into rate measurements. Since a satellite mission seeking to reduce weight and cost in its sensor suite would likely carry micromechanical accelerometers in addition to gyros, a complete navigation filtering study should be performed. Here, the truth and filter state vectors would expand to include quantities such as position, velocity, altitude, and the various orbit elements. An assessment of the navigation quality possible through micromechanical sensors would be one of the primary research objectives.
- The simulations in the previous chapter show that the performance improvement possible through model-based filtering depends on the mission

scenario (tumbling, maneuvering, etc.), the availability of data from other sensors (like GPS), *and* on the satellite inertial distribution. The filter design variables that allowed the gains in attitude estimation quality were generally different case to case. Therefore, if one is to get the most realistic feel for the benefits of model-based filtering in a specific setting, simulations emulating the expected situation should be run repeatedly and analyzed.

- The dominant motivation for bothering to include vehicle dynamics models in the attitude filter was the fear of large gyro error components inducing estimator divergence. As such, we employed “typical” low quality gyro bias and white noise parameters from [9]. These numerical values were not only useful as they gave a starting point for investigation with historically meaningful data, but they also made up for the fact that specific micromechanical gyro performance behavior are unavailable. The state of the technology is constantly improving and a study performed with today’s error parameters may be made obsolete by the technology advances of the next few months. Therefore, when planning a satellite mission with specific instrumentation in mind, the preceding simulations should be run with the most recent gyro error specifications.
- To demonstrate the robustness of the model-based approach to inertia term errors, we generally cranked up the design variables Q_{dist} and G_g to limit the filter’s confidence in its plant knowledge. Further, to mitigate the effects of complexly behaved environmental disturbance torques we similarly tuned Q_{dist} and added a disturbance state partition to the estimator design. Since much of a satellite’s operation occurs in benign settings where meaningful linearization of the system dynamics is possible, we should be able to take advantage of the voluminous research on robust state estimation, including sources [3] and [29]. These works detail formal methodologies for minimax and \mathcal{H}_∞ disturbance rejection, which

could prove particularly useful in warding off the ill effects of GPS multipath errors and disturbance torques. In addition, several previous works have already demonstrated the success of model-based filtering in the face of plant uncertainty [2], [22], [31]. These studies employed both conventional and formal robust estimation methodologies. Typically, these works enable robustness to plant modeling error through consideration of structured uncertainty and state weighting matrices. These measures could provide additional performance improvements far beyond the simple minded Q_{dist} -hiking employed here.

- As an additional avenue to curtailing the effects of plant uncertainty, techniques of system identification should be applied to refine the satellite dynamic model on-line. With the availability of control actuators and sufficient measurement data comes the opportunity to determine on-orbit the vehicle mass distribution, flexible modes, and other dynamic effects. The system information thus obtained could augment experimental and analytic estimates of plant parameters and allow the filter greater confidence in its propagation model.
- Satellite dynamics are often more complex than simple rigid body Euler coupling models. There are typically appendages and arrays that induce flexibility. As a strapdown gyro collects rate data, it will naturally be reading a combination of rigid body and modal effects. If one is interested distinguishing between these two behaviors, then additional oscillatory filter states should be introduced, or a prefilter capable of identifying modal signal components should be placed between the sensors and the attitude filter. Investigation of the best ways to implement these algorithms will likely be a rewarding area of research.

Appendix A

First Order Gauss-Markov Stochastic Processes

In the satellite attitude determination problem, there are many appearances of the white noise-driven system $\dot{x} = Fx + Gw$. Its form occurs in everything from truth models of environmental disturbance torques to truth and filter models of gyro and GPS measurement errors. Its usefulness derives from several factors. By changing the numerical values of f and/or g one can capture processes with vastly different frequency content and steady-state behavior. It has also been shown to reasonably approximate higher order, more complex stochastic processes. This property makes it especially useful in estimation, where true process dynamics may be difficult or impossible to model. Of course, the first order form also makes it very easy to deal with analytically. This Appendix derives some useful relations for the scalar, time-invariant form of this process. It then continues with a discussion of numerical simulation issues. The final section relates $\dot{x} = Fx + Gw$ to the two most basic gyroscope error sources: angle random walk and time-varying biases.

A.1 Continuous Scalar Processes

Many error processes are described by a single state continuous time (CT) linear time-invariant (LTI) white noise-driven system:

$$\dot{x}(t) = fx(t) + gw(t), \quad (\text{A.1})$$

where $x(t)$ is the continuous error process, $w(t)$ is continuous time white noise, and f and g are constant parameters. Various names describe process (A.1); “exponentially-correlated random variable” (ECRV) and “first order Gauss-Markov process” (FOGM) are frequently used. The latter label is appropriate when the process $w(t)$ has a Gaussian, or normal, distribution at every instant in time. An important special case of (A.1) occurs when $f = 0$:

$$\dot{x}(t) = gw(t). \quad (\text{A.2})$$

This process has its own accompanying vocabulary: (A.2) is known as a “Weiner process” and $x(t)$ is said to experience “Brownian motion” or “random walk” (RW) behavior [40].

In Equations (A.1) and (A.2), $w(t)$ represents a continuous time white noise process. This random excitation drives the system and has its own associated statistics. Specifically, $w(t)$ has zero mean:

$$E(w(t)) = 0 \quad (\text{A.3})$$

and infinite variance with intensity q . The infinite variance and intensity of $w(t)$ are expressed simultaneously in the autocorrelation function:

$$E(w(t)w(\tau)) = q\delta(t - \tau). \quad (\text{A.4})$$

Strictly speaking, as a consequence being driven by the CT white noise term $w(t)$, the dynamic variable $x(t)$ is continuous everywhere but differentiable

nowhere. As such, Equation (A.1) is an abuse of notation since it gives a differential expression involving $x(t)$. To properly express the time behavior of x , one should employ stochastic differentials and Ito calculus. Equation (A.1) is more accurately expressed as

$$dx = fxdt + gdw. \quad (\text{A.5})$$

Note that dw is present, not $w dt$. This term accounts for the differential action of the driving white noise and is proportional to the square root of the independent variable, which is time in this setting [1], [35]. In the remainder of this section we will continue the aforementioned abuse of notation, as it does not hinder the development of useful analytical expressions. However, this differential distinction *will* become relevant in Section A.3, when we discuss gyro error model terminology.

Now given (A.1) or (A.5), the mean and variance of $x(t)$ naturally are of interest. The mean $\bar{x}(t) \equiv E(x(t))$ can be found by taking expectations on both sides of (A.1):

$$\begin{aligned} E(\dot{x}(t)) &= E(fx(t) + gw(t)) \\ \dot{E}(x(t)) &= fE(x(t)) + gE(w(t)) \\ \dot{E}(x(t)) &= fE(x(t)), \end{aligned}$$

so

$$\bar{x}(t) = E(x(t)) = \bar{x}(0)e^{ft} \quad (\text{A.6})$$

describes the state mean as a function of time. Note that expectation and differentiation switched order, thanks to the interchangeability of integration and differentiation, and that $E(w(t)) = 0$ led to a nice simplification. However, in most situations, we consider the *initial* error to have zero mean so that $\bar{x}(0) = 0$ and consequently

$$\bar{x}(t) = 0 \quad \forall t. \quad (\text{A.7})$$

Going back to (A.6) and considering the pure random walk case ($f = 0$), we have

$$\bar{x}(t) = \bar{x}(0) \quad (\text{A.8})$$

which is again equal to zero for *all* time if $\bar{x}(0) = 0$.

The variance can be shown to obey its own first order relation:

$$\dot{P}(t) = 2fP(t) + g^2q, \quad (\text{A.9})$$

where

$$P(t) \equiv \text{Var}(x(t)) \equiv E(x(t)x(t))$$

and the zero mean assumption is implicit. Note that Equation (A.9) is a special case of the matrix Riccati equation $\dot{P} = AP + PA^T + GQG^T$. In the first order Gauss-Markov case ($f \neq 0$), Equation (A.9) has the closed-form solution

$$P(t) = P(0)e^{2ft} + \frac{1}{2f}g^2q(e^{2ft} - 1) \quad (\text{A.10})$$

whereas in the pure random walk case ($f = 0$) the solution is

$$P(t) = P(0) + g^2qt. \quad (\text{A.11})$$

If the state $x(t)$ had zero *initial* variance, then $P(0) = 0$ and the simplifications to Equations (A.10) and (A.11) are immediate.

If we are fortunate enough to have zero mean errors, then the variance is identical to the “mean square” value of the process. This terminology follows from the stochastic identity

$$\text{Var}(x) = E((x - E(x))^2) = E(x^2) - (E(x))^2.$$

In such cases, one usually speaks of the process “rms” value, which is simply $\sqrt{P(t)}$. The square root of the variance is also known as the “one sigma” or

“one standard deviation” value.

So if $\bar{x}(t) = 0$ and $P(0) = 0$ (the typical assumptions) then Equations (A.10) and (A.11) simplify, respectively, to:

$$\sigma(t) = \sqrt{P(t)} = |g| \sqrt{\frac{1}{2f} q (e^{2ft} - 1)} \quad (\text{A.12})$$

and

$$\sigma(t) = \sqrt{P(t)} = |g| \sqrt{qt} \quad (\text{A.13})$$

Equation (A.12) shows that if $f < 0$, then $\sigma(t)$ reaches a steady-state value equal to

$$\sigma_{\infty} = |g| \sqrt{\frac{-q}{2f}} \quad (\text{A.14})$$

with a ninety percent settling time of about $-0.83/f$. Actually, looking back to Equation (A.10), we see that the same steady-state value is reached *regardless* of the initial variance. In contrast, the random walk rms value, given in Equation (A.13), grows unboundedly as the square root of time and does not reach a steady-state value.

We see in Equations (A.12) and (A.13) that g and q always appear together as $g^2 q$ to some power; they never appear separately. Therefore, multiplicative changes in q could be accomplished just as easily by equivalent rescalings of g and vice versa. Hence, we fix $q = 1$, making $w(t)$ a *unit* intensity white noise process and use g exclusively to scale the combined $g^2 q$ term. Again, the simplifications to (A.12) through (A.14) are immediate.

After fixing $q = 1$, the first order Gauss-Markov process is completely characterized by two parameters, f and g , and the random walk process is characterized by the single parameter g . Many engineers prefer to express the FOGM signal by two equivalent parameters: the time constant τ and the steady-state rms value σ_{∞} . This latter parameter is identical to the quantity in Equation (A.14). The time constant is simply the negative inverse of f : $\tau = -1/f$.

Rearranging (A.14) and substituting $-1/\tau$ for f gives

$$g = \pm \sqrt{\frac{2\sigma_\infty^2}{\tau}}. \quad (\text{A.15})$$

With these new parameters in place, the rms history of the Gauss-Markov process can be expressed alternatively as:

$$\sigma(t) = \sigma_\infty \sqrt{1 - e^{-2t/\tau}}. \quad (\text{A.16})$$

If $x(t)$ had a nonzero initial variance, then this expression expands to:

$$\sigma(t) = \sqrt{P(0)e^{-2t/\tau} + \sigma_\infty^2(1 - e^{-2t/\tau})}. \quad (\text{A.17})$$

Thus when working with first order Gauss-Markov processes, one can describe the stochastic signal using f and g , τ and σ_∞ , f and σ_∞ , etc. All are equivalent and can be related with the above equations.

Changes in the values of these parameters shape the behavior of the process $x(t)$ that is molded out of the input $w(t)$. For example, consider the τ , σ_∞ parameterization of the first order system. If the steady-state standard deviation σ_∞ is held fixed, then changes in the free parameter τ can be interpreted in several ways. As τ increases, $f = -1/\tau$ decreases and the linear system becomes less stable. The process takes longer to reach steady state as seen in Equation (A.16). If we define the autocorrelation function as

$$\psi_{xx}(\delta) \equiv E(x(t)x(t + \delta)),$$

then for the τ , σ_∞ parameterization,

$$\psi_{xx}(\delta) = \sigma_\infty^2 e^{-|\delta|/\tau}.$$

Hence, for fixed σ_∞ , as τ increases the process values become more and more

correlated over a fixed interval δ . There are frequency domain interpretations as well. If the process power spectral density is defined according to

$$\phi_{xx}(\omega) \equiv \int_{-\infty}^{+\infty} \phi_{xx}(\tau) e^{-j\omega\tau} d\tau$$

then for the τ, σ_∞ parameterization,

$$\phi_{xx}(\omega) = \frac{2\sigma_\infty^2\tau}{1 + \omega^2\tau^2},$$

meaning that with increasing τ , $x(t)$ contains greater low frequency content and rolls off earlier.

A.2 Simulation Considerations

When simulating either a first order Gauss-Markov or random walk stochastic signal, extra caution must be taken in generating the driving CT white noise signal. Our first instinct might be to use the following Matlab statements:

```
t = 0:deltat:tfinal;
u = randn(size(t));
[y,x,timevec] = lsim(f,g,1,0,u,t,x0);
```

But the elements of the u vector, which represent values of the driving CT white noise process, must be scaled according to the time step “deltat”. Recall that CT white noise had infinite variance so we expect the scaling of the u vector to become large as Δt becomes small. The key to finding the proper scaling is to look again at Equation (A.1):

$$\dot{x}(t) = fx(t) + gw(t)$$

During simulation, the process is integrated over a series of time steps of length Δt :

$$x(t + \Delta t) = x(t) + \int_t^{t+\Delta t} fx(t)dt + \int_t^{t+\Delta t} gw(t)dt \quad (\text{A.18})$$

The $\int f x dt$ term is handled by the simulation subroutine using a state transition matrix of the form $\phi = e^{f\Delta t}$. The $\int g w dt$ term is problematic since the process values of $w(t)$ are available *only* at times t and $t + \Delta t$, not throughout the interval $(t, t + \Delta t)$. Hence, the simulation assumes a zero-order hold and takes

$$w(\tau) = \text{const} \quad \forall \tau \in (t, t + \Delta t)$$

However, note that the $\int g w dt$ term represents pure integrated white noise and is therefore a random variable governed by *random walk*. Since we can't drive the simulation with continuous white noise, we instead drive it with a *discrete* sequence that represents many random walks of duration Δt . With the zero-order hold assumption, the simulation subroutine will actually propagate $x(t)$ as follows:

$$x(t + \Delta t) = x(t) + \phi x(t) + g u_t \Delta t, \quad (\text{A.19})$$

where u_t is the appropriate member of the discrete driving disturbance. Of course, $g u_t \Delta t$ has variance $g^2 \Delta t^2 \text{Var}(u_t)$. From Equation (A.13) the $\int g w dt$ term *should* have variance $g^2 \Delta t$ so we need $\text{Var}(u_t) = 1/\Delta t$. This is accomplished by with the following Matlab statements:

```
t = 0:deltat:tfinal;
u = inv(sqrt(deltat))*randn(size(t));
[y,x,timevec] = lsim(f,g,1,0,u,t,x0);
```

Now each term in the discrete white noise input has a coefficient of $1/\sqrt{\Delta t}$ and its variance is $1/\Delta t$, as desired. Note that as Δt becomes small, the discrete input sequence is more dense in time and each member has a greater variance. As $\Delta t \rightarrow 0$, $1/\sqrt{\Delta t} \rightarrow \infty$ so the input sequence looks more and more like pure CT white noise as the integration step size gets smaller and smaller.

A.3 Classical Gyro Error Modeling

Now that the generic mathematical description of first order Gauss-Markov and random walk processes is in place, we can apply the expressions in Section A.1 to gyro error modeling. The classic gyro error model is:

$$\omega_m(t) = \omega_t(t) + b(t) + g_v v_1(t) \quad (\text{A.20})$$

$$\dot{b}(t) = a_b b(t) + g_b v_2(t). \quad (\text{A.21})$$

Equation (A.20) says that the measured angular rate $\omega_m(t)$ is given by the true angular rate $\omega_t(t)$ plus a time varying “bias” error $b(t)$ plus a continuous time white noise error $g_v v_1(t)$. (In the following, we assume that the bias and measurement processes are all in *continuous time*). Equation (A.21) describes the dynamics of the time varying bias. It is simply a first order Gauss-Markov model after (A.1). Alternatively, the bias dynamics may be given by a simpler random walk model:

$$\dot{b}(t) = g_b v_2(t) \quad (\text{A.22})$$

The variables ω_m , ω_t , and b naturally have the units of angular rate, say degrees per hour (deg/hr). Since it is equal to the inverse time constant, a_b has units 1 over hour (1/hr). The units of g and v are a little more subtle. The key lies in the stochastic differentials described by Ito calculus [1], [35]. The ω_m term on the left hand side of Equation (A.20) is an angle derivative with respect to time so (A.20) is in fact a stochastic differential equation:

$$\omega_m(t) = \frac{d\theta}{dt} = \omega_t(t) + b(t) + g_v v_1(t) \quad (\text{A.23})$$

In differential form, it becomes:

$$d\theta = \omega_t dt + b dt + g_v dv_1. \quad (\text{A.24})$$

Ito calculus dictates the use of the differential white noise term dv_1 instead of $v_1 dt$ and indicates that dv_1 is proportional to \sqrt{dt} . In Equation (A.24), all terms

must have units of angle, including the $g_v dv_1$ term. Since dv_1 has units of the square root of time, g_v must have units of angle per root time. Typically, g_v is given the units degree per root hour (deg/root-hr). In fact, g_v has the special name “gyro angle random walk” since the form of Equation (A.23) shows that the $g_v v_1(t)$ white noise integrates into *random walk* in the computed angle.

As shown in Equation (A.13) this angle random walk is responsible for an uncertainty in the computed angle whose rms value grows as the square root of time. Note that if the process intensity q on the white noise term v_1 is considered dimensionless, then the angle/root-time dimensions of g_v comport with Equation (A.13).

In a similar manner, Equation (A.21) can be placed in differential form:

$$db = a_b b dt + g_b dv_2. \quad (\text{A.25})$$

Since bias has dimension angle/time, so must every term here. Again, dv_2 has dimension root-time forcing g_b to have units angle/time^{3/2}. These units are consistent with earlier expressions such as (A.15). This discussion does not change if the bias model were given by (A.22) instead of (A.21); the $a_b b(t)$ term has no effect on the units of the white noise term.

The following numerical example demonstrates the use of Section A.1 equations in the context of Section A.3 terminology. Suppose one is given the following fictitious gyro error specifications:

Angle random walk: 0.01 deg/root-hr

Bias steady-state value: 10 deg/hr

Bias standard deviation at 1 hour: 5 deg/hr.

with the task of correctly tuning the relevant coefficients in the error model of Equations (A.20) and (A.21) to a radians-seconds system. In this example we assume *unit* intensity white noises $v_1(t)$ and $v_2(t)$ and zero *initial* process variance ($\sigma(0) = 0$). Basically, there are three numerical values to compute: g_v , a_b , and g_b . The easiest calculation is for the angle random walk coefficient g_v .

All we need to do is convert the given 0.01 deg/root-hr to rad/root-sec:

$$g_v = 0.01 \frac{\text{deg}}{\sqrt{\text{hr}}} \left(\frac{\pi \text{ radians}}{180 \text{ deg}} \right) \left(\frac{\sqrt{1 \text{ hour}}}{\sqrt{3600 \text{ seconds}}} \right) \simeq 2.9(10^{-6}) \frac{\text{rad}}{\sqrt{\text{sec}}}.$$

To compute the bias model parameters a_b and g_b , we employ Equations (A.15) and (A.16). Rearranging the latter reveals a_b :

$$a_b = \frac{-1}{\tau} = \frac{1}{2t} \ln \left(1 - \left(\frac{\sigma(t)}{\sigma_\infty} \right)^2 \right),$$

or with the current example's specifications:

$$a_b = \frac{1}{2(1 \text{ hour})} \ln \left(1 - \left(\frac{5 \text{ deg/hr}}{10 \text{ deg/hr}} \right)^2 \right)$$

$$a_b \simeq -0.14 \text{ hr}^{-1} \simeq -4.0(10^{-5}) \text{ sec}^{-1}.$$

Now Equation (A.15) gives g_b :

$$g_b = \sqrt{\frac{2\sigma_\infty^2}{\tau}} = \sqrt{-2a_b\sigma_\infty^2},$$

so with actual numbers:

$$g_b = \sqrt{(-2)(-4.0(10^{-5}) \text{ sec}^{-1}) \left(10 \left(\frac{\pi}{180} \right) \left(\frac{1}{3600} \right) \frac{\text{rad}}{\text{sec}} \right)^2},$$

$$g_b \simeq 4.3(10^{-7}) \frac{\text{rad}}{\text{sec}^{3/2}}.$$

Now with the numerical values of g_v , a_b , and g_b , we can obtain realizations of the stochastic error process, model the process in an observer, or covert the parameters to their discrete time equivalents. Although the discrete equivalents are commonly used in simulations on digital computers, the continuous error process values are somewhat easier to compute and lend themselves to convenient steady-state analysis.

Appendix B

Attitude Representations

This thesis is concerned with the problem of satellite attitude determination. Since attitude is synonymous with orientation, or rotation, of a rigid body, it is important to mention three important devices for characterizing a rigid body rotation mathematically. Of course, when mentioning a “rigid body rotation”, we equivalently mean a rotation of rigid orthogonal axes fixed to the body. As the rotations are unconstrained, there are up to three degrees of freedom available. Euler angles, direction cosine matrices (DCM’s), and quaternions are discussed briefly below. Our goal here is to describe each attitude representation and give the main relations for their integration and interconversion. Detailed derivations and discussions are available in the literature.

B.1 A Generic Rotation

Suppose there is a set of rigid right-handed orthogonal axes X , Y , and Z with origin O that define a coordinate frame A . While keeping the origin fixed in space, the axes are allowed to rotate freely about O to some new orientation. During this rotation, the axes must remain orthogonal. At the new orientation, we rename the axes x , y , and z and call the resulting coordinate frame B . Figure B-1 shows the frames A and B .

The attitude representations covered in this appendix describe the relative

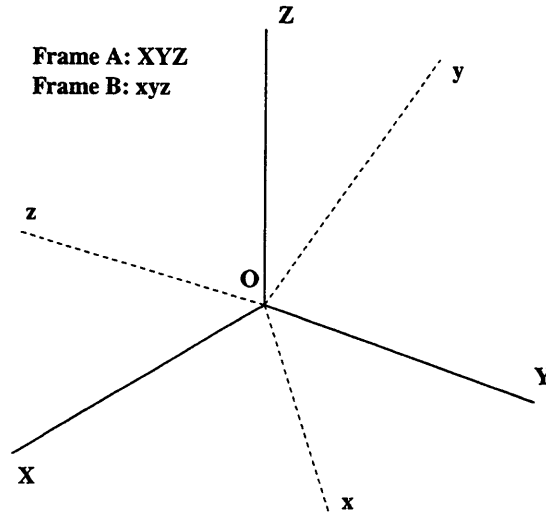


Figure B-1: Generic Frame Transformation from A to B

orientation of these frames *without* regard to the specific rotation that took place. That is, in themselves, Euler angles, DCM's, and quaternions do not capture any details of coordinate frame motion; they describe only relative position. If we wish to detail precisely how B moves relative to A (we consider B to be free while A is fixed in space), then an angular velocity vector ω is necessary. Possibly time-varying, ω gives the angular motion of B *relative* to A. Unless otherwise specified, ω is assumed to be instantaneously expressed in the coordinates of frame B. That is, $\omega = (\omega_x, \omega_y, \omega_z)^T$.

B.2 Euler Angles

Euler angles are an intuitively simple series of three rotations that take frame A to frame B's orientation. Each rotation in the series corresponds to motion about a specific axis in the frame A. For example, an Euler angle sequence might be described verbally as “first rotate about the A frame Z axis; now rotate about the new location of the X axis; finally revolve around the new Y axis; the net effect is the current orientation of the x, y, and z axes in the B frame”. However, since the direction of rotation and choice of axis sequence is somewhat

arbitrary, one must carefully define the physical meaning of an Euler sequence. In this document, we name the X/x axis the “roll” axis, the Y/y axis the “pitch” axis, and the Z/z axis the “yaw” axis. Our Euler sequence is a roll-pitch-yaw sequence as follows:

1. Rotate in a right-handed fashion about the roll axis an amount ϕ , then
2. Rotate in a right-handed fashion about the new pitch axis an amount θ , then
3. Rotate in a right-handed fashion about the new yaw axis an amount ψ .

With this angle sequence (ϕ, θ, ψ) , we can start at A and achieve any possible attitude for B. Note that this characterization is not without ambiguity since sequences $(\phi = 0, \theta = \pi, \psi = 0)$ (units in radians) and $(\phi = \pi, \theta = 0, \psi = \pi)$ achieve the same net rotation although the sequence elements are different. (It is important to think of Euler angles as a physical sequence, or process, not as elements of some vector quantity).

In addition to possible sequence ambiguity, Euler angles are difficult to compose. That is, given a rotation sequence from frame A to B, $(\phi_{BA}, \theta_{BA}, \psi_{BA})$, and a *subsequent* rotation Euler sequence $(\phi_{CB}, \theta_{CB}, \psi_{CB})$ from frame B to a third frame C, it is difficult to find the overall rotation sequence $(\phi_{CA}, \theta_{CA}, \psi_{CA})$. Certainly, the total rotation is *not* given by the arithmetic sum of the sequence elements: $(\phi_{CB} + \phi_{BA}, \theta_{CB} + \theta_{BA}, \psi_{CB} + \psi_{BA})$. The reader should fashion examples to illustrate this non-additive property.

However, if we know the initial orientation of B relative to A and the angular velocity vector $(\omega_x(t), \omega_y(t), \omega_z(t))^T$ that describes subsequent motion of B with respect to A, then we can continuously calculate the time evolution of the “A to B” Euler sequence. The propagation equations are

$$\begin{pmatrix} \dot{\phi} \\ \dot{\theta} \\ \dot{\psi} \end{pmatrix} = \frac{1}{\cos\theta} \begin{pmatrix} \cos\psi & -\sin\psi & 0 \\ \cos\theta\sin\psi & \cos\theta\cos\psi & 0 \\ -\sin\theta\cos\psi & \sin\theta\sin\psi & \cos\theta \end{pmatrix} \begin{pmatrix} \omega_x \\ \omega_y \\ \omega_z \end{pmatrix}. \quad (\text{B.1})$$

Note that a $\cos\theta = 0$ condition upsets the Euler angle propagation. This singularity corresponds to mathematical coincidence of the roll and yaw axes. When the axes overlay in this manner, roll rotations become instantaneously indistinguishable from yaw rotations and mathematical ambiguity results. Unfortunately, this “gimbal lock” phenomenon appears in every Euler sequence propagation equation, regardless of the sequence definition. Unavoidable singularities like this one limit the usefulness of the Euler angle attitude representation scheme.

B.3 Direction Cosine Matrices

The direction cosine matrix (DCM) attitude representation overcomes several flaws of the Euler angle scheme. There is no need to explicitly define a sequence of rotations. The time propagation equations are singularity free, and where Euler angles were difficult to compose, DCM composition is straightforward. A disadvantage of the DCM is the requirement of nine parameters where Euler angles sufficed with only three.

At its root, the DCM attitude representation is about projections. Consider Figure B-2 which shows the two coordinate frames A and B and a common vector v .

Although there is only one vector, its components can be resolved into either frame A or B. That is, there is a frame A representation: $v^A = (v_x, v_y, v_z)^T$, and a frame B representation: $v^B = (v_x, v_y, v_z)^T$. The superscripts indicate which frame is used in the resolution. A DCM T_{BA} is simply a 3x3 matrix that transforms the A frame resolution of v to the B frame resolution:

$$v^B = T_{BA}v^A. \tag{B.2}$$

Note that that unlike Euler angles, the DCM does not give any information on how to actually rotate frame A into frame B; it is just a transformation tool

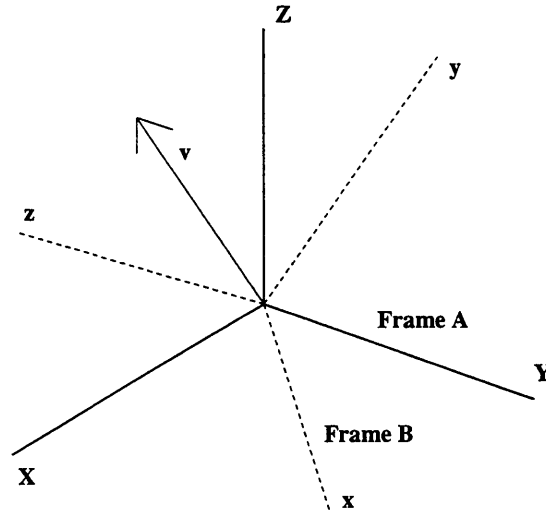


Figure B-2: Vector v Expressible In Two Frames

based on the relative orientation. The first subscript of T gives the destination frame; the second subscript gives the origin frame. With this notation in mind, we can express the inverse transformation with

$$v^A = T_{AB}v^B \quad (\text{B.3})$$

It can be shown that the “forward” DCM, T_{BA} , and the “reverse” DCM, T_{AB} , are related through inversion. Further, since the columns of any DCM can be shown to be *orthonormal*, the matrix inversion is accomplished by a simple matrix transposition:

$$T_{AB} = T_{BA}^{-1} = T_{BA}^T \quad (\text{B.4})$$

Where rotation composition was difficult with Euler angles, DCM composition is as easy as matrix multiplication. If T_{BA} captures the first rotation from A to B and T_{CB} captures the second rotation from B to C, then

$$T_{CA} = T_{CB}T_{BA}. \quad (\text{B.5})$$

This composition rule follows trivially from repeated application of Equation

(B.2).

Just as Euler angles can be propagated in time if $\omega(t) = \omega^B(t)$ is known, one can also propagate the DCM given the same rate information. The following differential expression is given in [28]

$$\dot{T} = [\omega(t)]_X T, \quad (\text{B.6})$$

where $[\omega(t)]_X$ is the “cross-product matrix”

$$[\omega(t)]_X = \begin{pmatrix} 0 & \omega_z & -\omega_y \\ -\omega_z & 0 & \omega_x \\ \omega_y & -\omega_x & 0 \end{pmatrix}. \quad (\text{B.7})$$

Equation (B.6) is perfectly analogous to Equation (B.1).

Of course, there are times when given a roll, pitch, yaw sequence (ϕ, θ, ψ) one needs to find the corresponding DCM. By treating each of the yaw, pitch, and roll motions separately and then applying Equation (B.5) to the individual rotations, one can derive the following Euler angle to DCM conversion formula

$$T = \begin{pmatrix} c\theta c\psi & s\phi s\theta c\psi + c\phi s\psi & -c\phi s\theta c\psi + s\phi s\psi \\ -c\theta s\psi & -s\phi s\theta s\psi + c\phi c\psi & c\phi s\theta s\psi + s\phi c\psi \\ s\theta & -s\phi c\theta & c\phi c\theta \end{pmatrix}, \quad (\text{B.8})$$

where

$$s\alpha \equiv \sin\alpha$$

$$c\alpha \equiv \cos\alpha.$$

The inverse problem is somewhat harder. Given a DCM, what is the corresponding roll, pitch, yaw sequence? Reference [39] gives the following conversion expressions. All angles are expressed in radians.

$$\theta = \sin^{-1}(T_{31})$$

$$\begin{aligned} \cos\theta \neq 0 &\Rightarrow \begin{cases} \phi = \tan_2^{-1}(-T_{32}, T_{33}) \\ \psi = \tan_2^{-1}(-T_{21}, T_{11}) \end{cases} \\ \cos\theta = 0 &\Rightarrow \begin{cases} \phi = \tan_2^{-1}(T_{23}, T_{22}) \\ \psi = 0. \end{cases} \end{aligned} \quad (\text{B.9})$$

The first argument to \tan_2^{-1} is a y-axis component; the second argument is an x-axis component. That is, use $\tan_2^{-1}(y, x)$. In the above, T_{ij} is the (i, j) element of the matrix T .

B.4 Quaternions

A third alternative to Euler angles and DCM's exists. It is the four-element quaternion. It captures the essence of Euler's Theorem which states that any rigid rotation (such as that in Section B.1) can be achieved by a *single* rotation about a *single* axis. Such an axis is referred to as an "Euler axis" or "eigenaxis". Figure B-3 illustrates the axis and rotation angle idea.

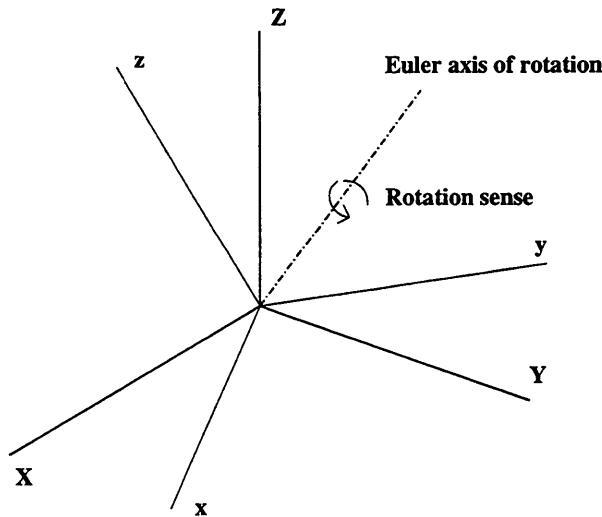


Figure B-3: Euler Axis Rotation From XYZ to xyz

From the theorem, if one knows the Euler axis and the magnitude of the rotation, then there is enough information to characterize the transformation.

Quaternions, developed in the 1860's by Hamilton [19], are simply four element vectors that describe the eigenaxis and rotation angle. Three of the elements are grouped into a single three component vector v and called the “vector part”. The remaining fourth single element is termed the “scalar part”. Unfortunately, there is not universal agreement about whether the vector or scalar part should be listed first in the quaternion. In *this* document, the vector portion occupies the upper three elements of the quaternion; the scalar part is the bottom element. Equation (B.10) illustrates this vector-scalar block structure.

$$\mathbf{q} = \begin{pmatrix} v \\ q_4 \end{pmatrix} \quad \text{where} \quad v = \begin{pmatrix} q_1 \\ q_2 \\ q_3 \end{pmatrix} \quad (\text{B.10})$$

The vector-scalar subdivision is related to Euler's theorem. The vector portion v is simply the product of the *unit* vector \hat{n} pointing along the rotation axis and the sine of *half* the rotation angle. Here, the rotation angle sign is related to \hat{n} by the right-handed convention. The remaining scalar element of the quaternion is the cosine of half the rotation angle. Equation (B.11) summarizes.

$$\mathbf{q} = \begin{pmatrix} \sin(\frac{\theta}{2})\hat{n} \\ \cos(\frac{\theta}{2}) \end{pmatrix} \Rightarrow v = \sin\left(\frac{\theta}{2}\right)\hat{n}; \quad q_4 = \cos\left(\frac{\theta}{2}\right). \quad (\text{B.11})$$

Thanks to the unit length of \hat{n} and trigonometric identities, every quaternion has a unit norm property:

$$\|\mathbf{q}\|^2 = \mathbf{q}^T \mathbf{q} = 1. \quad (\text{B.12})$$

To invert a single axis rotation, one would naturally just use the same axis but pivot in the opposite direction. Mathematically, this corresponds to replacing θ with $-\theta$ in Equation (B.11). Since the sine function is odd and the cosine function even, the consequence is a sign reversal for the vector portion of

the quaternion. Equation (B.13) expresses quaternion inversion.

$$\mathbf{q}_{AB} = \mathbf{q}_{BA}^{-1} = \begin{pmatrix} -v_{BA} \\ q_4 \end{pmatrix}. \quad (\text{B.13})$$

Just as with DCM composition, quaternion composition is very straightforward. However, since the mathematics of the composition does not involve the two arguments *as* quaternions but instead as a matrix and a vector, we define a special operator \otimes . When written out, as in Equation (B.14), the second sequential rotation appears as the first “factor” and the first rotation appears as the second “factor”. This the same order the objects appeared in Equation (B.5).

$$\mathbf{q}_{CA} = \mathbf{q}_{CB} \otimes \mathbf{q}_{BA}. \quad (\text{B.14})$$

Equations (B.15) and (B.16) give two different but completely equivalent expressions for quaternion composition [28]. Obviously, these matrix-vector products should themselves be quaternions satisfying the unit norm property.

$$\mathbf{q}_A \otimes \mathbf{q}_B = \begin{pmatrix} q_4 & q_3 & -q_2 & q_1 \\ -q_3 & q_4 & q_1 & q_2 \\ q_2 & -q_1 & q_4 & q_3 \\ -q_1 & -q_2 & -q_3 & q_4 \end{pmatrix}_A \begin{pmatrix} q_1 \\ q_2 \\ q_3 \\ q_4 \end{pmatrix}_B. \quad (\text{B.15})$$

$$\mathbf{q}_A \otimes \mathbf{q}_B = \begin{pmatrix} q_4 & -q_3 & q_2 & q_1 \\ q_3 & q_4 & -q_1 & q_2 \\ -q_2 & q_1 & q_4 & q_3 \\ -q_1 & -q_2 & -q_3 & q_4 \end{pmatrix}_B \begin{pmatrix} q_1 \\ q_2 \\ q_3 \\ q_4 \end{pmatrix}_A. \quad (\text{B.16})$$

Equations (B.1) and (B.6) showed the propagation of Euler angles and DCM’s given the angular rate vector of the B frame relative to the A frame

expressed in the B frame. The analogous expression for quaternions is

$$\dot{\mathbf{q}} = \frac{1}{2}\Omega(\boldsymbol{\omega})\mathbf{q}, \quad (\text{B.17})$$

where

$$\Omega(\boldsymbol{\omega}) = \begin{pmatrix} 0 & \omega_z & -\omega_y & \omega_x \\ -\omega_z & 0 & \omega_x & \omega_y \\ \omega_y & -\omega_x & 0 & \omega_z \\ -\omega_x & -\omega_y & -\omega_z & 0 \end{pmatrix}. \quad (\text{B.18})$$

Of course, we wish to be able to convert between the three forms of attitude representation reviewed here: Euler angles, direction cosine matrices, and quaternions. The relations connecting Euler angles and DCM's were given in Equations (B.8) and (B.9). Given a roll, pitch, yaw sequence, construction of the corresponding quaternion is simple. Recalling Euler's theorem and the meaning of \hat{n} and θ in Equation (B.11), then one can treat the Euler sequence (ϕ, θ, ψ) as three independent rotations and employ quaternion composition:

$$\mathbf{q} = \begin{pmatrix} 0 \\ 0 \\ \sin(\frac{\psi}{2}) \\ \cos(\frac{\psi}{2}) \end{pmatrix} \otimes \begin{pmatrix} 0 \\ \sin(\frac{\theta}{2}) \\ 0 \\ \cos(\frac{\theta}{2}) \end{pmatrix} \otimes \begin{pmatrix} \sin(\frac{\phi}{2}) \\ 0 \\ 0 \\ \cos(\frac{\phi}{2}) \end{pmatrix} \quad (\text{B.19})$$

Extraction of a roll, pitch, yaw sequence from a quaternion is less straightforward and we rely on [39] for an expression:

$$\begin{aligned} \theta &= \sin^{-1}(2(q_4q_2 + q_3q_1)) \\ \cos\theta \neq 0 &\Rightarrow \begin{cases} \phi = \tan_2^{-1}(q_1 + q_3, q_4 + q_2) + \\ \quad \tan_2^{-1}(q_1 - q_3, q_4 - q_2) \\ \psi = \tan_2^{-1}(q_1 + q_3, q_4 + q_2) - \\ \quad \tan_2^{-1}(q_1 - q_3, q_4 - q_2) \end{cases} \end{aligned} \quad (\text{B.20})$$

$$\cos\theta = 0 \Rightarrow \begin{cases} \phi = \tan_2^{-1}(q_1 + q_3, q_4 + q_2) & \text{if } \theta = \frac{\pi}{2} \\ \phi = \tan_2^{-1}(q_1 - q_3, q_4 - q_2) & \text{if } \theta = -\frac{\pi}{2} \\ \psi = 0. \end{cases}$$

Reference also [39] gives a procedure to extract a quaternion from a DCM. Equations (B.21) through (B.25) comprise the algorithm. First compute the following four quantities:

$$\begin{aligned} \alpha_1 &= 1 + T_{11} + T_{22} + T_{33} \\ \alpha_2 &= 1 + T_{11} - T_{22} - T_{33} \\ \alpha_3 &= 1 - T_{11} + T_{22} - T_{33} \\ \alpha_4 &= 1 - T_{11} - T_{22} + T_{33}. \end{aligned} \tag{B.21}$$

Now compute the four quaternion elements based on which of the α_i was greatest:

$$\begin{aligned} \text{If } \alpha_1 &= \max(\alpha_i), \text{ then} \\ q_4 &= \pm \frac{1}{2} \sqrt{1 + T_{11} + T_{22} + T_{33}} \\ q_1 &= \frac{1}{4q_4} (T_{23} - T_{32}) \\ q_2 &= \frac{1}{4q_4} (T_{31} - T_{13}) \\ q_3 &= \frac{1}{4q_4} (T_{12} - T_{21}) \end{aligned} \tag{B.22}$$

$$\begin{aligned} \text{If } \alpha_2 &= \max(\alpha_i), \text{ then} \\ q_1 &= \pm \frac{1}{2} \sqrt{1 + T_{11} - T_{22} - T_{33}} \\ q_2 &= \frac{1}{4q_1} (T_{12} + T_{21}) \\ q_3 &= \frac{1}{4q_1} (T_{13} + T_{31}) \\ q_4 &= \frac{1}{4q_1} (T_{23} - T_{32}) \end{aligned} \tag{B.23}$$

$$\begin{aligned}
\text{If } \alpha_3 &= \max(\alpha_i), \quad \text{then} \\
q_2 &= \pm \frac{1}{2} \sqrt{1 - T_{11} + T_{22} - T_{33}} \\
q_1 &= \frac{1}{4q_2} (T_{21} + T_{12}) \\
q_3 &= \frac{1}{4q_2} (T_{23} + T_{32}) \\
q_4 &= \frac{1}{4q_2} (T_{31} - T_{13})
\end{aligned} \tag{B.24}$$

$$\begin{aligned}
\text{If } \alpha_4 &= \max(\alpha_i), \quad \text{then} \\
q_3 &= \pm \frac{1}{2} \sqrt{1 - T_{11} - T_{22} + T_{33}} \\
q_1 &= \frac{1}{4q_3} (T_{31} + T_{13}) \\
q_2 &= \frac{1}{4q_3} (T_{32} + T_{23}) \\
q_4 &= \frac{1}{4q_3} (T_{12} - T_{21}).
\end{aligned} \tag{B.25}$$

After any computation that produces a quaternion, it is a good idea to renormalize the four element vector to have unity norm. All of the above equations should produce unit norm outputs but numerical issues could cause slight deviations.

Fortunately, the computation of a DCM from a quaternion is much easier than the reverse. The quaternion to DCM transformation is expressed compactly as [28]

$$T = (q_4^2 - |v|^2)I_{3 \times 3} + 2vv^T + 2q_4[v]_X, \tag{B.26}$$

where the cross product matrix of Equation (B.7) is employed again.

For additional discussion of the above three attitude representation schemes *and* others, consult references [8], [39], and [43].

Appendix C

Kalman and Extended Kalman Filtering

This thesis is essentially an application of the extended Kalman filtering algorithm to a satellite navigation problem. The extended Kalman filter (EKF) is a suboptimal but implementable method of addressing nonlinear estimation problems. As its name suggests, the EKF contains the standard linear Kalman filter as a special case. This appendix presents the basic EKF algorithm, the main engine of this research, and the Kalman filter, the most widely used technique in modern estimation work. The latter is presented first since it is the historically older algorithm and contains the seed of virtually all current estimation practice.

C.1 The Kalman Filter

The Kalman filter (KF) is a well understood and widely used method of tracking stochastic dynamic systems. Developed in the early 1960's, the KF algorithm is the gift of Rudolph Kalman and Richard Bucy. Those seeking original writing on the filter are referred to [24]. Additional derivation and discussion is available in [9], [17], and [23]. This section presents the basic KF algorithm for continuous systems with discrete measurements and mentions some of its properties.

Consider a vector-valued process $x(t)$ driven by the linear stochastic dynamic system

$$\dot{x}(t) = A(t)x(t) + G(t)w(t). \quad (\text{C.1})$$

The system has a certain, possibly unknown, initial condition

$$x(0) = x_0 \quad (\text{C.2})$$

and $w(t)$ is a driving continuous time white noise signal with zero mean and intensity $Q(t)$ which we express by

$$E[w(t)] = 0 \quad E[w(t)w^T(\tau)] = Q(t)\delta(t - \tau). \quad (\text{C.3})$$

At times t_k , discrete linear noisy measurements y_k are available of the current state vector $x(t_k)$

$$y_k = C_k x(t_k) + v_k. \quad (\text{C.4})$$

Here, v_k is a discrete white noise vector with zero mean and covariance R_k . It is also assumed that the process noise $w(t)$ is uncorrelated with the measurement noise. These three conditions are expressed by

$$E[v_k] = 0 \quad E[v_k v_j^T] = R_k \delta_{kj} \quad E[w(t) v_k^T] = 0. \quad (\text{C.5})$$

The Kalman filter's job is to provide a continuously available estimate $\hat{x}(t)$ of the state vector. The KF is the solution of an optimization problem whose objective criterion depends on the estimation error $\tilde{x}(t)$, defined as

$$\tilde{x}(t) \equiv x(t) - \hat{x}(t). \quad (\text{C.6})$$

Since both terms of Equation (C.6) are stochastic processes, the estimation error $\tilde{x}(t)$ is itself a random variable. Hence, its covariance $P(t)$ is given as follows

(assuming $E[\tilde{x}(t)] = 0$):

$$P(t) \equiv E[\tilde{x}(t)\tilde{x}^T(t)]. \quad (\text{C.7})$$

Now, with the estimation error and its covariance defined, we ask the Kalman filter to provide estimates which minimize the trace of the error covariance matrix. That is,

$$\hat{x}(t) = \arg \min_{\hat{x}(t)} \text{trace}(P(t)). \quad (\text{C.8})$$

Put another way, the KF provides estimates that minimize the sum of the error *variances* for all the system states. This objective is apparent by considering the meaning of $P(t)$'s diagonal elements or through the identity

$$\text{trace}(P(t)) = E[\tilde{x}^T(t)\tilde{x}(t)].$$

The filter that solves this optimization problem turns out to be another continuous-discrete dynamic system. Its derivation is omitted here but can be found in virtually any text concerning optimal and applied estimation.

To execute the filter, one first begins with an initial estimate \hat{x}_0 and initial error covariance matrix P_0 :

$$\hat{x}(0) = \hat{x}_0 \quad P(0) = P_0. \quad (\text{C.9})$$

Then the state is propagated assuming noise-free system dynamics. The error covariance matrix is computed considering the system model and the amount of uncertainty $w(t)$ injects into the system. These propagations take the form of first order multidimensional ODE's that continuously maintain the criterion specified in (C.8):

$$\begin{aligned} \dot{\hat{x}}(t) &= A(t)\hat{x}(t) \\ \dot{P}(t) &= A(t)P(t) + P(t)A^T(t) + G(t)Q(t)G(t). \end{aligned} \quad (\text{C.10})$$

For any random variable, dynamic or not, the minimum error covariance esti-

mate is identical to the conditional mean. That is,

$$\hat{x}(t) = \arg \min_{\hat{x}(t)} \text{trace}(P(t)) = E[x(t)|\text{available information}]. \quad (\text{C.11})$$

Between measurements, the state estimate evolves according to Equation (C.10) so

$$\hat{x}(t) = E[x(t)|\text{all prior measurements}].$$

The filter computes $\hat{x}(t)$ in this manner until time t_k when measurement y_k becomes available. Before we actually incorporate y_k , our estimate is the best possible accounting for previous measurements. We give this estimate the symbol \hat{x}_k^- , term it the *a priori* estimate, and represent it mathematically as

$$\hat{x}_k^- = E[x(t_k)|y_0, \dots, y_{k-1}]. \quad (\text{C.12})$$

The filter then combines \hat{x}_k^- with y_k to produce an *a posteriori* estimate \hat{x}_k^+ whose probabilistic description is

$$\hat{x}_k^+ = E[x(t_k)|y_0, \dots, y_k]. \quad (\text{C.13})$$

In the filter derivation, the combination of \hat{x}_k^- and y_k is assumed to be linear. By enforcing condition (C.8) on the linear combination, we arrive at the measurement update relations for the state estimate and error covariance. The covariance must be adjusted at this time since our confidence in the state estimate depends on the metric of measurement quality, R_k . The update relations are:

$$\begin{aligned} \hat{x}_k^+ &= \hat{x}_k^- + K_k(y_k - C_k \hat{x}_k^-) \\ &= (I - K_k C_k) \hat{x}_k^- + K_k y_k \\ P_k^+ &= (I - K_k C_k) P_k^- (I - K_k C_k)^T + K_k R_k K_k^T, \end{aligned} \quad (\text{C.14})$$

where K_k is the Kalman gain matrix given by

$$K_k = P_k^- C_k^T (C_k P_k^- C_k^T + R_k)^{-1}, \quad (\text{C.15})$$

assuming the parenthetical expression is invertible. Like the corresponding state estimates \hat{x}_k^- and \hat{x}_k^+ , P_k^- and P_k^+ denote the error covariance matrices before and after measurement update, respectively.

Thanks to the derivation of the Kalman filter, the estimation error has zero mean both before and after measurement update. That is, Equations (C.12) and (C.13) illustrate that the *a priori* and *a posteriori* estimates have the true states as their expectations. In this sense, the KF is said to be an “unbiased” estimator.

It should be noted that we assumed nothing about the statistical distribution of the process and sensor noises (Eqns. (C.3) and (C.5)), only that they have certain means and variances. For all the filter knows, the probability density functions of these disturbances could be uniform, ramp shaped, or almost anything. It turns out that the Kalman filter is endowed with additional properties if the disturbances are *gaussian* distributed. For example, since the system states are necessarily gaussian as are the state estimates, the estimation error, defined in Equation (C.6), is also gaussian distributed. Hence, the zero error mean and covariance matrix $P(t)$ give a complete description of the error statistics, since a mean and variance are necessary and sufficient to specify a complete normal density. Further, in the gaussian disturbance case, the Kalman filter becomes the minimum error variance estimator *of any kind*. In contrast, if the error is not normally distributed, then the KF is merely the *linear* minimum variance estimator. Although this distinction seems academic, the implication is that in the normal disturbance case, the linear form of the Kalman filter does not have to be assumed *a priori*. See reference [29] for further discussion.

Note also that if the truth system is stabilizable from the process noise and detectable through the outputs, then the error dynamics are guaranteed stable.

For completeness, the continuous dynamics-continuous measurement Kalman filter equations are also given. Here, the filter operation is much cleaner since the measurements feed directly into the estimate propagation equation. The continuous measurements eliminate the need to define *a priori* and *a posteriori* estimates.

Assume the plant and measurement equations are given by

$$\begin{aligned}\dot{x}(t) &= A(t)x(t) + G(t)w(t) \\ y(t) &= C(t)x(t) + v(t).\end{aligned}\tag{C.16}$$

Then the filter, consisting of state estimate, error covariance, and gain, is given by

$$\begin{aligned}\dot{\hat{x}}(t) &= A(t)\hat{x}(t) + K(t)(y(t) - C(t)\hat{x}(t)) \\ &= (A(t) - K(t)C(t))\hat{x}(t) + K(t)y(t) \\ \dot{P}(t) &= A(t)P(t) + P(t)A^T(t) + G(t)Q(t)G^T(t) - P(t)C^T(t)R^{-1}(t)C(t)P(t) \\ K(t) &= P(t)C^T(t)R^{-1}(t).\end{aligned}\tag{C.17}$$

Conditions (C.2) and (C.3) still hold but (C.5) is replaced with

$$\begin{aligned}E[v(t)] &= 0 \\ E[v(t)v^T(\tau)] &= R(t)\delta(t - \tau) \\ E[w(t)v^T(\tau)] &= 0.\end{aligned}\tag{C.18}$$

C.2 The Extended Kalman Filter

We now change the problem statement a little. Instead of a linear truth system as in (C.1), we consider the following nonlinear state dynamics,

$$\dot{x}(t) = f(x(t), t) + w(t).\tag{C.19}$$

Note the the process noise is still assumed to enter in a linear fashion. Gelb discusses how nonlinear process inputs can be approximated with this representation [17]. As before, the system must have an initial state

$$x(0) = x_0 \tag{C.20}$$

and quantifiable process noise statistics:

$$E[w(t)] = 0 \quad E[w(t)w^T(\tau)] = Q(t)\delta(t - \tau). \tag{C.21}$$

Further, the state measurements may now take the more general nonlinear form

$$y_k = h_k(x(t_k)) + v_k \tag{C.22}$$

instead of that seen in Equation (C.4). The additive measurement error v_k is a discrete white sequence with familiar statistics and is uncorrelated with the continuous process disturbance $w(t)$:

$$E[v_k] = 0 \quad E[v_k v_j^T] = R_k \delta_{kj} \quad E[w(t)v_k^T] = 0. \tag{C.23}$$

Although the previous section omitted the details of the Kalman filter derivation, it was critical to obtain expressions for the state expectation and covariance as a function of time, especially for the period between measurement updates. Since linear systems driven by stochastic inputs are well understood, these mean and covariance formulae were obtainable and given in Equation (C.10). However, for nonlinear systems, the propagation expressions for any statistical moment are much more complex and descend from the recursive, partial-differential expression known as the Fokker-Planck equation [16]. On-line use of the Fokker-Planck equation is analytically and computationally prohibitive; thus, we make use of *approximate* expressions to propagate the state vector mean and covariance.

For the mean, we simply discard the process noise in (C.19) and perform a nonlinear state integration:

$$\dot{\hat{x}}(t) = f(\hat{x}(t), t). \quad (\text{C.24})$$

For the covariance, we propagate based on a Taylor series expansion and truncation of all second order terms and higher. The result is a matrix differential equation similar in spirit to (C.10):

$$\dot{P}(t) = F(\hat{x}(t), t)P(t) + P(t)F^T(\hat{x}(t), t) + Q(t) \quad (\text{C.25})$$

where $A(t)$ is replaced by the state dynamics jacobian matrix,

$$F(\hat{x}(t), t) = \left. \frac{\partial f(x(t), t)}{\partial x(t)} \right|_{x(t)=\hat{x}(t)}. \quad (\text{C.26})$$

There are already several departures from the standard linear Kalman filter of the previous section. First, since we are now computing the state estimate according to the approximate expression (C.24), the estimation error no longer has zero mean. That is, the error is now biased. We also see that whereas the state and covariance propagations were independent in Equations (C.10), they are now coupled since the Jacobian in (C.26) is a linearization of the state dynamics about the *current estimate*. This coupling prevents us from precomputing and storing the covariances as was possible with the standard KF algorithm, where the independence of the moments allowed significant savings in on-line computation.

Of course, the $P(t)$ matrix in (C.25) is actually not a covariance at all, but an estimate of it. This expression arose as the Taylor series truncation neglected important higher order terms. Therefore, filter covariance statistics can no longer be taken as absolute truth, even if there is no plant-filter model mismatch. Filter performance should now be judged by considering both this pseudo-covariance and the error sample statistics from Monte-Carlo runs.

It is also worth mentioning that the approximations present in (C.24) and (C.25) are valid only if the true state and state estimates are sufficiently close for the Taylor series truncations to remain valid. For this reason, filter divergence is a greater hazard for the EKF than for standard linear Kalman filter.

With these caveats in mind, we proceed to the measurement update. As in the previous section, the definitions of *a priori* and *a posteriori* quantities still apply. In fact, the form of the update exactly echoes that in Equations (C.14) and (C.15):

$$\begin{aligned}
\hat{x}_k^+ &= \hat{x}_k^- + K_k(y_k - h_k(\hat{x}_k^-)) \\
&= (I - K_k h_k(\hat{x}_k^-)) \hat{x}_k^- + K_k y_k \\
P_k^+ &= (I - K_k H_k(\hat{x}_k^-)) P_k^- (I - K_k H_k(\hat{x}_k^-))^T + K_k R_k K_k^T \\
K_k &= P_k^- H_k^T(\hat{x}_k^-) (H_k(\hat{x}_k^-) P_k^- H_k^T(\hat{x}_k^-) + R_k)^{-1}
\end{aligned} \tag{C.27}$$

with the following definition of H_k ,

$$H_k(\hat{x}_k^-) = \left. \frac{\partial h_k(x(t_k))}{\partial x(t_k)} \right|_{x(t_k)=\hat{x}_k^-}. \tag{C.28}$$

Note that like $F(\hat{x}(t), t)$, H_k is an estimate-dependent Jacobian matrix.

The extended Kalman filtering algorithm of Equations (C.24), (C.25), and (C.27) is one of several possible approaches to the nonlinear estimation problem posed by (C.19) and (C.22). It does have the virtue of being similar in nature to the standard Kalman filter. As might be expected, the EKF reduces identically to the KF if the filter model happens to be linear.

However, we must be careful in making too great an association between these two algorithms. The Kalman filter is the optimal, linear minimum variance estimator for linear plants. The extended Kalman filter is not necessarily the optimal, nonlinear minimum variance estimator for nonlinear plants. An optimal filter would make full use of all the true statistical moments; the EKF only approximates two of them. It is not the true covariance whose trace is

minimized; it is the approximate error covariance $P(t)$ that is treated.

Complete derivations and discussions of the EKF and nonlinear estimation are available in [9], [16], [17], and [29].

Again, for completeness, we give the fully continuous version of the algorithm. As with the continuous KF, the continuous EKF is spared the “-” and “+” notation since there are no discrete “hiccups” for state and error covariance updating. The following equations and notation are borrowed from [17].

Assume nonlinear continuous plant and measurement equations as follows:

$$\begin{aligned}\dot{x}(t) &= f(x(t), t) + w(t) \\ y(t) &= h(x(t), t) + v(t).\end{aligned}\tag{C.29}$$

Naturally, the plant has a certain initial condition $x(0) = x_0$. The process and measurement noises possess the usual properties:

$$\begin{aligned}E[w(t)] &= 0 \\ E[w(t)w^T(\tau)] &= Q(t)\delta(t - \tau) \\ E[v(t)] &= 0 \\ E[v(t)v^T(\tau)] &= R(t)\delta(t - \tau) \\ E[w(t)v^T] &= 0.\end{aligned}\tag{C.30}$$

The filter state estimate, error covariance, and gain equations exactly mirror those of the Kalman filter, as seen in Equations (C.17):

$$\begin{aligned}\dot{\hat{x}}(t) &= f(\hat{x}(t), t) + K(t)(y(t) - h(\hat{x}(t), t)) \\ &= (f(\hat{x}(t), t) - K(t)h(\hat{x}(t), t)) + K(t)y(t) \\ \dot{P}(t) &= F(\hat{x}(t), t)P(t) + P(t)F^T(\hat{x}(t), t) + Q(t) \\ &\quad - P(t)H^T(\hat{x}(t), t)R^{-1}(t)H(\hat{x}(t), t)P(t) \\ K(t) &= P(t)H^T(\hat{x}(t), t)R^{-1}(t).\end{aligned}\tag{C.31}$$

The estimate dependent matrices $F(\hat{x}(t), t)$ and $H(\hat{x}(t), t)$ are the Jacobians of the nonlinear state functions $f(x(t), t)$ and $h(x(t), t)$:

$$\begin{aligned} F(\hat{x}(t), t) &= \left. \frac{\partial f(x(t), t)}{\partial x(t)} \right|_{x(t)=\hat{x}(t)} \\ H(\hat{x}(t), t) &= \left. \frac{\partial h(x(t), t)}{\partial x(t)} \right|_{x(t)=\hat{x}(t)}. \end{aligned} \tag{C.32}$$

Bibliography

- [1] Adomain, George, *Stochastic Systems*. Academic Press, Inc., New York, 1983.
- [2] Agustin, Ramses M. *Robust Estimation and Failure Detection for Reentry Vehicle Attitude Control Systems*, Masters Thesis, Massachusetts Institute of Technology, Department of Mechanical Engineering, (C.S Draper Laboratory CSDL-T-1301), Jun. 1998.
- [3] Appleby, Brent D., *Robust Estimator Design Using the \mathcal{H}_∞ Norm and μ Synthesis*, Ph.D. Thesis, Massachusetts Institute of Technology, Department of Aeronautics and Astronautics, (C.S. Draper Laboratory CSDL-T-1065), Feb. 1990.
- [4] Azor, Ruth, Itzhack Y. Bar-Itzhack, and Richard R. Harman, "Satellite Angular Rate Estimation from Vector Measurements", AIAA-96-375.
- [5] Axelrad, Penina, and Charles P. Behre, "Attitude Estimation Algorithms for Spinning Satellites Using Global Positioning System Phase Data", *Journal of Guidance, Control, and Dynamics*, Vol. 20, No. 1, Jan.-Feb., 1997.
- [6] Axelrad, Penina, and Lisa M. Ward, "Spacecraft Attitude Estimation Using the Global Positioning System: Methodology and Results for RADCAL", *Journal of Guidance, Control, and Dynamics*, Vol. 19, No. 6, Nov.-Dec., 1996.
- [7] Axelrad, Penina. Personal conversations.

- [8] Battin, Richard H., *An Introduction to the Mathematics and Methods of Astrodynamics*. American Institute of Aeronautics and Astronautics, Inc., New York, 1987.
- [9] Brown, Grover B. and Patrick Y.C. Hwang, *Introduction to Random Signals and Applied Optimal Estimation*, 3rd ed., John Wiley & Sons, New York, 1977.
- [10] Bryson, Arthur E., Jr., *Control of Spacecraft and Aircraft*, Princeton University Press, Princeton NJ, 1994.
- [11] Carpenter, Russell, and Roger Hain, "Precise Evaluation of Orbital GPS Attitude Determination on the STS-77 GPS Attitude and Navigation Experiment (GANE)", Proceedings of the National Technical Meeting, The Institute of Navigation, 1997.
- [12] Chesley, Bruce Carl, *An Integrated Attitude Determination System for Small Satellites*, Ph.D. Thesis, University of Colorado, Department of Aerospace Engineering Sciences, University of Colorado, 1995.
- [13] Crandall, Stephen H., Dean C. Karnopp, Edward F. Kurtz, Jr., and David C. Pridmore-Brown, *Dynamics of Mechanical and Electromechanical Systems*, Krieger Publishing Company, Malabar, FL, 1968.
- [14] Crassidis, John L., and F. Landis Markley, "Predictive Filtering for Attitude Estimation Without Rate Sensors," *Journal of Guidance, Control, and Dynamics*, Vol. 20, No. 3, May-Jun. 1997, pp. 522-527.
- [15] Draper, Charles S., Walter Wrigley, and John Hovorka, *Inertial Guidance*, Pergamon Press, Oxford, 1960.
- [16] Draper, Stark C., *Learning Augmented Recursive Estimation For Uncertain Nonlinear Dynamics Systems*, Masters Thesis, Massachusetts Institute of Technology, Department of Electrical Engineering and Computer Science, (C.S. Draper Laboratory CSDL-T-1267), Jun. 1996.

- [17] Gelb, Arthur (Ed.), *Applied Optimal Estimation*, MIT Press, Cambridge, MA, 1974.
- [18] Giustino, Antonio, 2 LT, *Interferometric GPS Micro-mechanical Gyro Attitude Determination System: A Study Into The Integration Issues*, Masters Thesis, Massachusetts Institute of Technology, Department of Aeronautics and Astronautics, (C.S. Draper Laboratory CSDL-T-1307), Jun. 1998.
- [19] Hamilton, Sir W.R., *Elements of Quaternions*. London: Longmans, Green, and Co., 1866.
- [20] Hayes, Brian, "The Way the Ball Bounces", *American Scientist*, Vol. 84, No. 4, pp. 331-336.
- [21] Hofmann-Wellenhof, B., H. Lichtenegger, and J. Collins, *Global Positioning System Theory and Practice*, Third revised edition, Springer-Verlag, Wien, 1992.
- [22] Jacquemont, C., *Aircraft Attitude Determination Using Robust Estimation*, Masters Thesis, Massachusetts Institute of Technology, Department of Aeronautics and Astronautics, Aug. 1997.
- [23] Kailath, Thomas, "A View of Three Decades of Linear Filtering Theory," *IEEE Transactions on Information Theory*, Vol. 20, No. 2, Mar. 1974, pp. 146-181.
- [24] Kalman, Rudolph E., "A New Approach to Linear Filtering and Prediction Problems," *Transaction of the ASME Journal of Basic Engineering*, Vol. 82D, Mar. 1960, pp. 35-45.
- [25] Koifman, M., and S.J. Merhav, "Autonomously Aided Strapdown Attitude Reference Scheme," *Journal of Guidance, Control, and Dynamics*, Vol. 14, No. 6, pp. 1164-1172.

- [26] Kourepenis, A., J. Borenstein, J. Connelly, P. Ward, and M. Weinberg, "Performance of Small Low Cost Rate Sensors for Military and Commercial Applications," Presented at the *Twenty-third Joint Services Data Exchange for Guidance, Navigation, and Control*, Nov. 96.
- [27] Larson, W.J., and J.R. Wertz (Ed.), *Space Mission Analysis and Design*, Torrance, California, and Kluwer Academic Publishers, Dordrecht, The Netherlands, 1992.
- [28] Lefferts, E.J., F.L. Markley, and M.D. Shuster, "Kalman Filtering for Spacecraft Attitude Estimation," *Journal of Guidance, Control, and Dynamics*, Vol. 5, No. 5, Sep.-Oct. 1982, pp. 417-429.
- [29] Mangoubi, Rami S., *Robust Estimation and Failure Detection: A Concise Treatment*, Springer-Verlag, 1998.
- [30] Maybeck, Peter S., *Stochastic Models, Estimation, and Control, Volume I*, Academic Press, Inc., 1979.
- [31] Merhav, Shmuel, *Aerospace Sensor Systems and Applications*, Springer-Verlag, New York, 1996.
- [32] Meriam, J.L., and L.G. Kraige, *Dynamics*, 3rd ed., John Wiley & Sons, New York, 1992.
- [33] Montgomery, P.Y., *Carrier Phase Differential GPS as a Sensor for Automatic Control*, Ph.D. Dissertation, Leland Stanford University, Department of Aeronautics and Astronautics, Jun. 1996.
- [34] Norton, Harry N., *Handbook of Transducers*, Prentice-Hall, Inc., Englewood Cliffs, NJ, 1989.
- [35] Poor, H. Vincent, *An Introduction to Signal Detection and Estimation*, Springer-Verlag, New York, 1988.

- [36] Puri, Varun, 2 LT, *Tightly Coupled GPS-Gyro Integration for Spacecraft Attitude Determination*, Masters Thesis, Massachusetts Institute of Technology, Department of Aeronautics and Astronautics, (C.S. Draper Laboratory CSDL-T-1289), Jun. 1997.
- [37] Puri, Varun, 2 LT, Personal conversations.
- [38] Sharer, P.J., T.E. Strikwerda, D.R. Haley, J.C. Ray, and D.A. Ossing, "Midcourse Space Experiment Attitude System Performance For Gyro Disabled Operations", AIAA-98-4389, AIAA/AAS Astrodynamics Specialist Conference, Boston, 1998.
- [39] Shuster, Malcolm D., "A Survey of Attitude Representations," *The Journal of the Astronautical Sciences*, Vol. 41, No. 4, Oct.-Dec. 1993, pp. 439-517.
- [40] Slade, Gordon, "Random Walks", *American Scientist*, Vol. 84, No. 2, pp. 146-153.
- [41] Ward, Lisa Marie, *Spacecraft Attitude Estimation Using GPS: Methodology and Results*, Ph.D. Thesis, University of Colorado, Department of Aerospace Engineering Sciences, 1996.
- [42] Weinberger, Marc, "Statistics for Spacecraft Pointing and Measurement Error Budgets", *Journal of Guidance, Control, and Dynamics*, Vol. 17, No. 1, pp. 55-61.
- [43] Wertz, J.R. (Ed.), *Spacecraft Attitude Determination and Control*, D. Reidel Publishing Company, Dordrecht, Holland, 1978.
- [44] Wie, B., H. Weiss, and A. Arapostathis, "Quaternion Feedback Regulator for Spacecraft Eigenaxis Rotations," *Journal of Guidance, Control and Dynamics*, Vol. 12, No. 3, May-Jun. 1989, pp. 375-380.

Index

- angle random walk
 - in gyro error models, 139
 - definition of, 131
 - in numerical simulations, 137
 - units of, 139
- angular velocity, 142
- attitude representations, 141
- controllers (attitude), 29, 40
 - bang-bang, 44, 115
 - proportional feedback, 41
 - quaternion feedback, 43, 103
- direction cosine matrices, 144
 - conversion from quaternion, 152
 - conversion from RPY, 146
 - conversion to quaternion, 151
 - conversion to RPY, 146
 - propagation of, 146
- disturbance torques, 40, 102, 110, 116
 - atmospheric drag, 48
 - estimation of, 67
 - gravity gradient, 45
 - magnetic dipole, 47
 - solar radiation, 46
- Draper Laboratory, 27, 28
- Euler angles, 142
 - definition of RPY sequence, 143
 - propagation for RPY sequence, 143
 - RPY conversion from DCM, 146
 - RPY conversion from quaternion, 150
 - RPY conversion to DCM, 146
 - RPY conversion to quaternion, 150
- Euler's equation, 36
- extended Kalman filter, 158
 - mixed continuous-discrete form, 161
 - properties of, 161
 - pure continuous form, 162
- failure detection, 71
- Fokker-Planck equation, 159
- Gauss-Markov processes, 131
 - autocorrelation of, 135
 - covariance at steady-state, 134
 - covariance propagation, 133
 - for gyro error modeling, 138

- parameterizations of, 135
- PSD of, 136
- simulation of, 136
- global positioning system (GPS), 27
 - error modeling, 29, 50
 - in measurement updating, 63, 75
 - interferometry, 27
- gyros, 23
 - error modeling, 25, 138
 - for state propagation, 73
 - in measurement updating, 62
 - types of, 24
- inertial navigation systems (INS), 23
- Kalman filter, 18, 153
 - mixed continuous-discrete form, 156
 - properties of, 157
 - pure continuous form, 157
- model filter, 20, 55
 - dynamics, 56
 - measurement updating, 61
 - states, 55
- nonmodel filter, 20
 - dynamics, 73
 - measurement updating, 75
 - states, 72
- observability considerations, 71
- quaternions, 147
- composition of, 149
- conversion from DCM, 151
- conversion from RPY, 150
- conversion to DCM, 152
- conversion to RPY, 150
- in attitude filtering, 56
- in reduced order filtering, 58
- propagation of, 150
- reference frames
 - body and inertial, 35
 - orbital/LVLH, 36
- simulations
 - controlled maneuver, 100
 - gyro-free operation, 114
 - LVLH-aligned, 80
 - tumbling, 88
 - white noise generation for, 136
- thrusters, 29, 42

§ 7.2.4.1